

2

AD-A150 745

THE NUCLEATION
OF
CAVITATION IN AQUEOUS
MEDIA

DTIC FILE COPY



THE UNIVERSITY OF MISSISSIPPI
PHYSICAL ACOUSTICS RESEARCH GROUP
DEPARTMENT OF PHYSICS AND ASTRONOMY

DTIC
ELECTE
FEB 25 1985
A

This document has been approved
for public release and sale; its
distribution is unlimited.

85 02 08 129

Approved for Public Release: Distribution Unlimited

Technical Report for
Office of Naval Research
Contract N00014-84-C-0193

THE NUCLEATION
OF
CAVITATION IN AQUEOUS
MEDIA

by

A. A. Atchley* and L. A. Crum
Physical Acoustics Research Laboratory
Department of Physics and Astronomy
The University of Mississippi
University, MS 38677

DTIC
SELECTED
FEB 25 1985
A

This document has been approved
for public release and unlimited
distribution is authorized.

*Ph.D dissertation directed by L. A. Crum

Reproduction in whole or in part is permitted for any purpose by the U. S.
Government

Unclassified

SECURITY CLASSIFICATION OF THIS PAGE (When Data Entered)

| REPORT DOCUMENTATION PAGE | | READ INSTRUCTIONS BEFORE COMPLETING FORM |
|--|-------------------------------------|--|
| 1. REPORT NUMBER 1-85 | 2. GOVT ACCESSION NO. AD-A150745 | 3. RECIPIENT'S CATALOG NUMBER |
| 4. TITLE (and Subtitle) The Nucleation of Cavitation in Aqueous Media | | 5. TYPE OF REPORT & PERIOD COVERED Technical |
| 7. AUTHOR(s) A. A. Atchley and L. A. Crum | | 6. PERFORMING ORG. REPORT NUMBER |
| 9. PERFORMING ORGANIZATION NAME AND ADDRESS Physical Acoustics Research Laboratory Department of Physics, University of MS University, MS 38677 | | 8. CONTRACT OR GRANT NUMBER(s) N00014-84-C-0193 |
| 11. CONTROLLING OFFICE NAME AND ADDRESS Office of Naval Research, Physics Division Code 412, Arlington, VA 22217 | | 10. PROGRAM ELEMENT, PROJECT, TASK AREA & WORK UNIT NUMBERS |
| 14. MONITORING AGENCY NAME & ADDRESS (if different from Controlling Office) | | 12. REPORT DATE 1-25-85 |
| | | 13. NUMBER OF PAGES 113 |
| | | 15. SECURITY CLASS. (of this report) Unclassified |
| | | 15a. DECLASSIFICATION/DOWNGRADING SCHEDULE |
| 15. DISTRIBUTION STATEMENT (of this Report) Approved for public release; distribution unlimited | | |
| 17. DISTRIBUTION STATEMENT (of the abstract entered in Block 20, if different from Report) | | |
| 18. SUPPLEMENTARY NOTES | | |
| 19. KEY WORDS (Continue on reverse side if necessary and identify by block number) Acoustic cavitation nonlinear oscillation nucleation bubbles <i>disinfection</i> | | |
| 20. ABSTRACT (Continue on reverse side if necessary and identify by block number) The topic of this report is cavitation nucleation and concerns itself with both the cavitation nucleus and the mechanisms by which the nucleus is stabilized. Three different theories of the cavitation nucleus are considered most plausible. They are the crevice model, the surfactant skin model, and the ionic skin model. These hypothesized nuclei are physically | | |

DD FORM 1473

1 JAN 73

EDITION OF 1 NOV 65 IS OBSOLETE

S/N 0102-LF-014-6601

Unclassified

SECURITY CLASSIFICATION OF THIS PAGE (When Data Entered)

different and each has been used to explain separate groups of data. Presented in this report are theoretical and experimental advances made while searching for a unified model of a cavitation nucleus.

The previous crevice model ~~had~~ required that, in order for a vaporous cavity to grow from a crevice nucleus, the liquid-gas interface must reach the receding contact angle. This condition is necessary, but not sufficient. An additional criterion is that the radius of curvature of the interface must be greater than a critical radius, beyond which the cavity is mechanically unstable. Using these nucleation criteria, the model is rederived. The results of the rederivation are quite satisfactory. Both the old and new crevice models predict the cavitation threshold as a function of surface tension and temperature well. However, they ~~models~~ diverge when predictions of the threshold as a function of dissolved gas content are considered. The old crevice model predicts a linear dependence but experiment shows that the threshold increases rapidly with decreasing gas content. This behavior is predicted by the revised model.

In addition to vaporous cavitation, the revised model is applied to diffusion cavitation. It is shown that the model predicts features present in the data previously explained only in terms of the varying-permeability model.

The experimental part of the dissertation consists of a series of experiments performed to measure the acoustic cavitation threshold of water as a function of the dissolved ion concentration. The results indicate that up to about 1 mmol/l, the threshold increases with increasing concentration. This is directly opposite to predictions based on the ionic skin model. However, the results of these experiments are difficult to explain with any of the models in their present state of development.

Accession
100-100000-100000
100-100000-100000
100-100000-100000



ACKNOWLEDGEMENTS

I would like to acknowledge the support and encouragement of my advisor and friend Dr. Larry Crum. I extend my gratitude to Dr. Andrea Prosperetti who suggested that I apply the concept of a critical radius to the crevice model. I would also like to thank my fellow graduate students for many useful discussions and their companionship.

The financial support of the Office of Naval Research and the National Science Foundation that permitted me to work as a research assistant is also gratefully acknowledged.

Finally, I thank my parents and brother for their complete support in my pursuit of this non-traditional career.

TABLE OF CONTENTS

| | Page |
|---|------|
| LIST OF FIGURES. | vii |
| Chapter | |
| 1. INTRODUCTION. | 1 |
| 1-1 Statement of the Problem. | 1 |
| 1-2 Historical Perspective. | 2 |
| 1-3 Review of Stabilization Mechanisms. | 9 |
| 1-3.1 Ionic Skin Model | 10 |
| 1-3.2 Rigid Organic Skin Model | 14 |
| 1-3.3 Varying Permeability Model | 15 |
| 1-3.4 Crevice Model. | 21 |
| 1-4 Final Introductory Remarks. | 25 |
| 2. DERIVATION OF CAVITATION THRESHOLDS USING THE CRITICAL RADIUS APPROACH TO THE CREVICE MODEL | 27 |
| 2-1 Introduction. | 27 |
| 2-2 Critical Radius | 28 |
| 2-2.1 Critical Radius for Growth by Gaseous Diffusion. | 28 |
| 2-2.2 Critical Radius for Growth in the Absence of Diffusion | 31 |
| 2-3 Threshold Derivations | 32 |
| 2-3.1 Acoustic Cavitation Nucleation | 33 |

| Chapter | Page |
|--|------|
| 2-3.2 Diffusion Cavitation Nucleation. | 40 |
| 3. ANALYSIS OF THE CRITICAL RADIUS APPROACH TO THE CREVICE MODEL. | 48 |
| 3-1 Introduction. | 48 |
| 3-2 Application of the Crevice Model to Acoustic Cavitation. | 48 |
| 3-2.1 The Effect of Dissolved Gas Pressure | 48 |
| 3-2.2 The Effect of Surface Tension. | 59 |
| 3-2.3 The Effect of Temperature. | 60 |
| 3-2.4 Comments on Sensitivity. | 67 |
| 3-3 Application of the Crevice Model to Diffusion Cavitation. | 71 |
| 4. OTHER CANDIDATES FOR THE CAVITATION NUCLEUS | 76 |
| 4-1 Introduction. | 76 |
| 4-2 Ionic Skin Model. | 76 |
| 4-3 Varying-Permeability Model. | 80 |
| 5. SUMMARY, CONCLUSIONS AND TOPICS FOR FURTHER STUDY. | 90 |
| 5-1 Summary of the Dissertation | 90 |
| 5-2 Conclusions | 91 |
| 5-3 Topics for Further Study. | 92 |
| REFERENCES | 94 |
| APPENDIX | 98 |
| A-1 Introduction. | 98 |

| Chapter | page |
|--|------|
| A-2 Purpose of the Experiment | 98 |
| A-3 Experimental Apparatus. | 98 |
| A-4 Experimental Procedure. | 103 |
| A-4.1 Procedure for Sample Preparation | 104 |
| A-4.2 Procedure for Data Acquisition | 107 |
| A-5 Results of the Experiment | 108 |
| BIOGRAPHICAL SKETCH OF THE AUTHOR. | 113 |

LIST OF FIGURES

| Figure | Page |
|--|------|
| 1. Threshold versus Dissolved Ion Concentrations | 12 |
| 2. Illustration of a surfactant skin nucleus | 16 |
| 3. Typical pressure schedule for a compression/decompression experiment. | 18 |
| 4. Plot of P_{ss} versus P_{crush} | 20 |
| 5. Diagram of a gas-filled conical crevice embedded in a hydrophobic solid | 22 |
| 6. Illustration of a free bubble surrounded by a liquid | 29 |
| 7. Diagram of a crevice model nucleus. | 34 |
| 8. Illustration of crevice geometry. | 37 |
| 9. Illustration of interfacial motion during the compression phase of a compression/ decompression process | 42 |
| 10a. Theoretical prediction of the cavitation threshold as a function of dissolved gas pressure for a surface tension of 70 dyn/cm | 50 |
| 10b. Theoretical prediction of the cavitation threshold as a function of dissolved gas pressure for a surface tension of 40 dyn/cm | 51 |
| 11a. Graph of threshold versus gas pressure. | 53 |
| 11b. Graph of threshold versus gas pressure for low gas pressures | 54 |
| 12. Graph of Blake threshold versus gas pressure. | 58 |
| 13. Graph of threshold versus surface tension | 61 |
| 14a. Illustration of the polynomial fit used to determine Henry's law constant as a function of temperature | 63 |

| Figure | page |
|---|------|
| 14b. Illustration of the polynomial fit used to determine the surface tension of water as a function of temperature | 64 |
| 15. Graph of threshold versus temperature | 66 |
| 16a. Graph of threshold versus surface tension illustrating the sensitivity of equation (31) | 68 |
| 16b. Graph of threshold versus surface tension illustrating the sensitivity of equation (31) | 69 |
| 16c. Graph of threshold versus surface tension illustrating the sensitivity of equation (31) | 70 |
| 17. Plot of P_{ss} versus P_{crush} illustrating the change in slope at $P_{crush} = P^*$ as predicted by the crevice model | 74 |
| 18a. Graph of normalized cavitation threshold versus the log of the dissolved ion concentration for KI | 78 |
| 18b. Graph of the normalized cavitation threshold versus the log of the dissolved ion concentration for NaI | 79 |
| 19a. Graph of the cavitation threshold versus dissolved gas pressure for a V-P nucleus with $b=1.43$ bar | 85 |
| 19b. Graph of the cavitation threshold versus dissolved gas pressure for a V-P nucleus with $b=1.96$ bar | 86 |
| 19c. Graph of the cavitation threshold versus dissolved gas pressure for a V-P nucleus with $b=1.00$ bar | 87 |
| 20a. Schematic diagram of the sample preparation system | 100 |

| Figure | page |
|---|------|
| 20b. Schematic diagram of the data acquisition system | 101 |
| 21a. Graph of the cavitation threshold versus the log of the dissolved ion concentration for NaI | 110 |
| 21b. Graph of the normalized cavitation threshold versus the log of the dissolved ion concentration for NaI | 111 |

Chapter 1

Introduction

1-1 Statement of the Problem

The topic of this dissertation is stabilization mechanisms for the cavitation nucleus. For the purposes of this dissertation, cavitation may be defined as the formation of vapor cavities or gas bubbles in a liquid through a reduction of the pressure within that liquid. Although the majority of this work will pertain to acoustic cavitation, many types of cavitation are not acoustic in origin. These processes will not be ignored. Cavitation occurs in a wide variety of places, ranging from sterile laboratory systems to dirty beer mugs, from ship propellers to inside biological systems. That cavitation occurs in these vastly different environments can be ascribed to a single common phenomenon: a (microscopic) site exists at a place within the system where conditions are favorable for the formation of a (macroscopic) bubble. This site is called a cavitation nucleus.

The impetus behind this research was to answer the questions: what is the nature of this nucleus? Is a nucleus unique to a given environment, or can a nucleus cause cavitation in more than one environment and under more than one set of circumstances? Indeed, can all cavitation processes be attributed to a single type of nucleus? The answers to these questions have been sought for more than a century and

completely satisfactory answers will not be given here. In a practical sense, it was suspected at the outset of this project that all of the answers would not be found. They were meant to serve as "the carrot in front of the horse". What will be presented here are some theoretical and experimental advances made while seeking the answers. Not only do these results clarify some of the past and present research in this field, they also serve as beacons pointing to new directions that future researchers should pursue.

1-2 Historical Perspective

Perhaps the first type of cavitation observed was the formation of bubbles in liquids supersaturated with gas. This is familiar to all of those who have ever opened or poured a carbonated beverage. Tomlinson¹ discussed a series of twelve experiments performed with soda-water and various solids. He contended that if the solids were "chemically clean", no bubbles would form on them. He went on to point out that if a solid, initially chemically clean, came into contact with a dirty cloth, unclean air, or dust particles, copious bubbles formed on it when immersed in the soda-water. Tomlinson concluded that chemically clean solids are perfectly wetted, whereas dirty solids are not. From this he argued that if a solid were dirty it would have a greater adhesion force for the gas than for the liquid and that it was this asymmetry that caused bubble formation. Although this line of reasoning is incorrect, the results of his extensive experimentation with effervescence support the explanation offered by his contemporary M.

Gernez². Gernez proposed that the outgassing of supersaturated gaseous solutions was caused by gas pockets, embedded in the fissures found on the surface of every solid, regardless of its degree of finish. (It is therefore Gernez who is the initial proponent of the crevice model of the cavitation nucleus - a model to be discussed extensively here.) Effervescence is a form of cavitation which requires gaseous diffusion to "pump up" gas-containing nuclei until they grow large enough to rise to the surface of the liquid. At about the same time that Tomlinson and Gernez were doing their work, another genre of cavitation was being investigated.

This other kind of cavitation has its origin with the conception and development of hydrodynamics. Not until Daniel Bernoulli³ set down the guidelines for this new branch of science in 1738 was it understood that a negative pressure could be produced in a liquid. In the following years Euler and d'Alembert debated over the consequences of negative pressures⁴. Euler believed that the application of a negative pressure could result in a rupture of the liquid while d'Alembert refused to accept this view.

The rise of cavitation as a topic for scientific research began with the development of high-powered, high rpm steam turbines in the mid 1800's. With this came the means of moving an object (such as a propeller) through a fluid rapidly enough so that the object lost contact with the fluid. The most obvious concern to which this new phenomenon drew attention was that the state-of-the-art propeller design

was poor. A second, and as was soon evident, much greater concern was propeller erosion. In fact, this problem was so critical that in 1915 the British Admiralty appointed a special subcommittee to investigate this phenomenon. In 1917, Lord Rayleigh⁵ became involved. His solution of the equations governing vapor cavity dynamics is still quite useful today.

Concurrent to this work the first attempts to measure the tensile strengths of liquids were being undertaken. In about 1850, Berthelot began to measure the tensile strength of water and found it to be on the order of 50 bars (maximum)⁶. His method consisted of heating a liquid, which was sealed in an evacuated glass capillary tube, until the expanding liquid completely filled the tube. The temperature at which the tube was filled was recorded and the liquid was then allowed to cool. Because the liquid adhered to the sides of the tube, this subsequent contraction resulted in the liquid undergoing a tensile stress, eventually ending in the rupture of the liquid. The temperature at which rupture occurred was also recorded. From a knowledge of the filling and rupturing temperatures, along with the thermal expansion coefficient for the liquid being tested, Berthelot was able to calculate a tensile strength. Many other measurements of the tensile strength of water through these static means have been made over the intervening one hundred and thirty-four years, and their results (ranging from as low as about 5 to as high as about 200 bars) are comparable to Berthelot's. A detailed discussion of these works will not be given here. The point is that for the first time investigators

were intentionally putting liquids under stress and considering the consequences. The application of a tensile stress to a liquid is the basis for present day acoustic cavitation studies, which are actually studies of the "dynamic" tensile strength, as opposed to these earlier "static" measurements.

Acoustic cavitation was first observed during the period from 1915 to 1920 by Langevin and his co-workers while he was pioneering the field of ultrasonics⁷. Söllner⁶ was one of the first to observe cavitation in degassed liquids at room temperature and atmospheric pressures (1936). In the 1930's and 1940's a number of other researchers investigated various aspects of ultrasonic cavitation, among them R.W. Boyce⁶, E.N. Harvey⁶, and Kornfeld and Suverov⁸.

The fundamental problem of cavitation was by now well formed. Numerous measurements of the cavitation threshold (tensile strength) of water yielded results in the range of 5-25 bars (using the most careful and painstaking procedures thresholds of up to 300 bars have been obtained⁹, but they are unusual) and yet, theoretical predictions of the homogeneous (pure liquid) threshold of water are thousands of bars.⁶ What accounts for this order-of-magnitude (best case) discrepancy? Failure in solids under tension is usually attributed to an imperfection in the solid. The same logic (i.e., imperfections in the liquid) was applied to the failure of liquids.

In the remainder of this section different types of cavitation will be mentioned in an overview of the field in the last half-century. The

were intentionally putting liquids under stress and considering the consequences. The application of a tensile stress to a liquid is the basis for present day acoustic cavitation studies, which are actually studies of the "dynamic" tensile strength, as opposed to these earlier "static" measurements.

Acoustic cavitation was first observed during the period from 1915 to 1920 by Langevin and his co-workers while he was pioneering the field of ultrasonics⁷. Söllner⁶ was one of the first to observe cavitation in degassed liquids at room temperature and atmospheric pressures (1936). In the 1930's and 1940's a number of other researchers investigated various aspects of ultrasonic cavitation, among them R.W. Bcyce⁶, E.N. Harvey⁶, and Kornfeld and Suvorov⁸.

The fundamental problem of cavitation was by now well formed. Numerous measurements of the cavitation threshold (tensile strength) of water yielded results in the range of 5-25 bars (using the most careful and painstaking procedures thresholds of up to 300 bars have been obtained⁹, but they are unusual) and yet, theoretical predictions of the homogeneous (pure liquid) threshold of water are thousands of bars.⁶ What accounts for this order-of-magnitude (best case) discrepancy? Failure in solids under tension is usually attributed to an imperfection in the solid. The same logic (i.e., imperfections in the liquid) was applied to the failure of liquids.

In the remainder of this section different types of cavitation will be mentioned in an overview of the field in the last half-century. The

investigators of these branches of cavitation research sought these imperfections (cavitation nuclei) to explain the various aspects of the particular cavitation process. Cavitation nucleated by these inhomogeneities is termed heterogeneous cavitation.

In 1944, Dean¹⁰ suggested that vapor cavities form in the center of small vortices produced by turbulent motion of water around solid objects. In the same year, Harvey¹¹ suggested that gas pockets stabilized at the bottom of crevices found on dirt particles accounted for the cavitation found in animals. He had concerned himself mainly with cavitation formed by compression/decompression processes in animals (the "bends"); however, he did discuss his model's application to acoustic cavitation. One of the most careful and extensive experiments of the time was performed by Briggs, Johnson, and Mason¹². They measured cavitation thresholds for a variety of liquids as a function of dissolved gas pressure, viscosity, and pulse length. However, their theoretical explanation of their results was later shown to be incorrect⁶.

The 1950's was a decade of diversification for cavitation research. Perhaps the most important example of this breadth is the invention of the bubble chamber by Glaser. This invention gave rise to the field of radiation-induced cavitation. Seitz¹³ gave an explanation for bubble formation in superheated liquids by charged particles. He concluded that the majority of bubbles were "nucleated by moderately-energetic free electrons produced by the incident particles in Coulomb encounters". The bubble chamber was developed as a tool for elementary

particle physics while radiation-induced cavitation research took a different avenue. Lieberman¹⁴ measured the threshold for acoustic cavitation in pentane and acetone exposed to neutron and beta sources. He concluded that the cavitation was nucleated by the recoil of carbon ions; these results agreed well with Seitz's theory.

In the field of acoustically induced cavitation, a different type of nucleus was suggested in 1954 by Fox and Herzfeld¹⁵. This nucleus consisted of a gas bubble surrounded by a rigid skin of organic molecules. This organic skin model will be discussed further in the next section. An extensive set of measurements was reported by Strasberg¹⁶. He analyzed his results in terms of the nuclei proposed up to that time and found the crevice model offered the best explanation. Other noteworthy papers of the 1950's are by Connolly and Fox¹⁷, and Galloway¹⁸; some of their results will be discussed later.

Sette and Wanderlingh¹⁹ were the first to study acoustic cavitation in water induced by cosmic rays. They concluded that the nuclei were recoiling oxygen atoms and their results agreed well with calculations based on Seitz's theory. The Soviet researcher Akulichev²⁰ proposed another cavitation nucleus based on his measurements of the influence of dissolved ions on cavitation thresholds. His nucleus, similar to that of Fox and Herzfeld, consisted of an ionic skin surrounding a gas bubble. Greenspan and Tschiegg²¹ described a method by which they were able to attain unusually high cavitation thresholds. This method consisted of prolonged filtering and cleaning of the liquids to be

tested in a closed system.

In 1970, Apfel²² developed the crevice model further to include the size of the crevice; he suggested that there existed a "critical" size for the crevice. Cavities larger than and smaller than this critical size exhibit quite different behavior. Apfel published papers on both homogeneous and heterogeneous cavitation. In 1971²³, he modified a theory for homogeneous nucleation of vapor cavities at the interface between a flat solid and a pure liquid to account for nucleation at the interface between two pure liquids. Apfel's crevice model was modified further by Crum²⁴ who considered the variation of contact angles with surface tension. The crevice model in this latest form was successful in explaining a wide variety of data obtained from acoustic cavitation measurements. Winterton²⁵ also modified Apfel's model and used it to explain boiling and non-acoustic cavitation.

At about the same time Yount was developing a different type of nucleus.²⁶ Modifying the organic skin models of Fox and Herzfeld, and Sirotyuk²⁷, Yount considered his nucleus to be a bubble surrounded by polar surfactant molecules. This skin has the property of offering a varying permeability to gas, depending upon the ambient conditions. He has applied his model to compression/decompression processes and has been successful in explaining his data.

And so this was the state of the field when this project was undertaken. Since that time, Yount²⁸ has further developed his model theoretically and experimentally so that there is little doubt that it is plausible. However, the crevice model, with new developments to be

discussed later, explains a very broad set of data. After this brief and sketchy historical review of the field in general, the cavitation nucleation and stabilization mechanisms will be discussed in detail in the following section with emphasis on the organic skin model of Yount and the crevice model as developed by Apfel and Crum.

1-3 Review of Stabilization Mechanisms

The most obvious candidate for the cavitation nucleus is a gas-filled bubble. However, this nucleus is unstable. A bubble will dissolve in an undersaturated solution and the effect of surface tension will cause it to dissolve in a saturated solution. In supersaturated solutions, a bubble can be in equilibrium because the tendency for the bubble to dissolve due to surface tension is opposed by the tendency for the bubble to grow by diffusion of gas into it. However, this equilibrium is unstable; the bubble will grow or dissolve depending on whether the perturbation increases or decreases the bubble's radius relative to its equilibrium radius.^{29,30} Therefore, a liquid would be free of bubbles after a short period of time and cavitation thresholds would quickly approach those for homogeneous nucleation. This does not imply that gas bubbles could not serve as cavitation nuclei. It does imply, however, that in order for gas bubbles to serve as cavitation nuclei, they must be stabilized at a size small enough to prevent their rising to the surface of the liquid, yet large enough so that they will grow when exposed to negative pressure as low as a few bars. In other

words, a stabilization mechanism must exist for a gas bubble before it can act as a cavitation nucleus.

That cavitation nuclei do in fact contain gas has been borne out in numerous experiments.^{11,15-18,24,26} Some measurements show that the cavitation threshold is strongly dependent on dissolved gas pressure, except for extremely clean water.²¹ Also, samples which undergo a compression/ decompression cycle prior to testing show higher thresholds than samples which do not.

Various types of stabilizing skins have been proposed. These skins usually consist of contaminants which somehow deposit themselves on the bubble's surface and counteract the surface tension. The first of these skin models to be discussed is the ionic skin model proposed by Akulichev.²⁰

1-3.1 Ionic Skin Model

Alty³¹ noted that it has been known since the 1860's that liquid-gas interfaces are electrically charged. He experimentally determined that bubbles quickly acquired a charge after being introduced into water and behaved as though they carried a net negative charge. In a later paper³², Alty postulated a charging mechanism by which a bubble became charged by the selective adsorption of ions onto the bubble surface. He noted that the rate at which the bubble dissolved decreased as the charge on the bubble increased--a phenomenon which he attributed to the Coulomb repulsion of the adsorbed charges. The mechanism by which this selective adsorption took place, however, was unclear.

Akulichev postulated that not only could the rate of dissolution of a bubble be decreased, the dissolution could be stopped altogether. He explained the selective adsorption in terms of the type of hydration exhibited by various ions. Those exhibiting positive hydration behave in a hydrophilic manner. They are surrounded by water molecules when dissolved in aqueous solutions. On the other hand, ions exhibiting negative hydration behave in a hydrophobic manner and are not "as" surrounded by water molecules as are hydrophilic ions. Hydrophobic ions, therefore, are more likely to stay on the surface of a bubble once they encounter it than are hydrophilic ions, in other words--selective adsorption. Hydrophilic ions include Na^+ , Li^+ ; examples of hydrophobic ions are Mg^{++} , K^+ , F^- , Cl^- , and I^- .

In order to test these ideas, Akulichev measured the cavitation threshold as a function of dissolved ion concentration. Some of his results are reproduced in figure 1. Figure 1a shows the variation in threshold with concentration for three salts: LiOH , KI , and KBr . Since OH^- is a natural constituent of water, Akulichev argued that it could not affect the bubble. Lithium is hydrophilic. Therefore, the presence of LiOH in the water should have no effect on the threshold. It is seen from figure 1a that the threshold is independent of concentration for LiOH . The ions K^+ , I^- , and Br^- are all hydrophobic so they should all be adsorbed by a bubble. This results in the bubble being charged. Therefore, because of Coulomb repulsion of the ions, the equilibrium radius is larger than for an uncharged bubble. This adsorption should

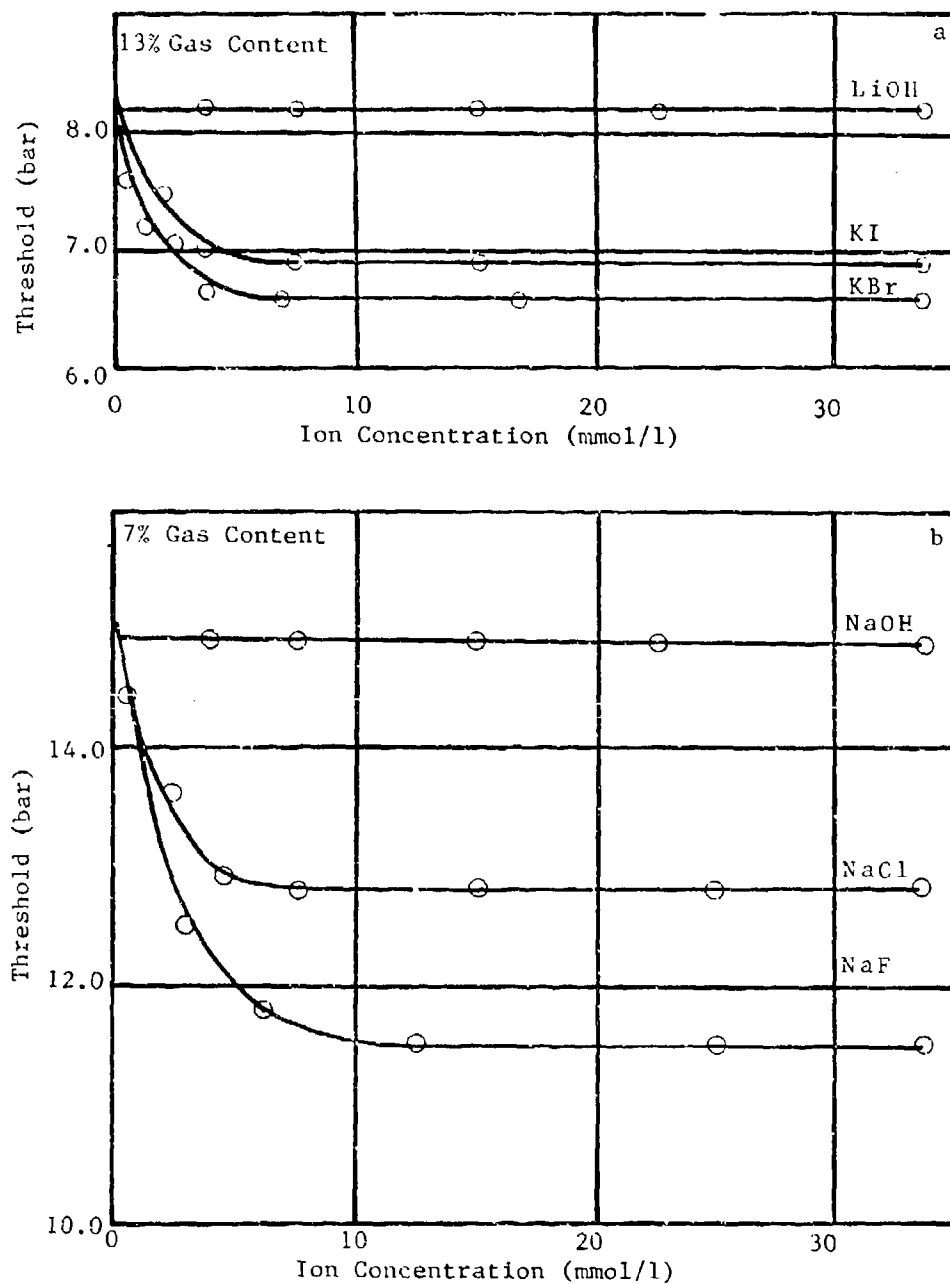


Figure 1. Threshold versus Dissolved Ion Concentration for various compounds and dissolved gas pressures. Reproduced from Akulichev (reference 20).

produce a lower threshold for aqueous solutions of KBr and KI than of LiOH. Notice that the effect tends to saturate at a concentration of about 5 mmol/l. He attributes the slightly lower threshold (about 5% lower) of KBr compared to that of KI to the difference in mobilities of the two ions Br^- and I^- . Figure 1b is a similar graph for the salts NaOH, NaCl, and NaF. In this instance, the positive ion (Na^+) is hydrophilic. The differences in the three curves are, therefore, due to the different natures of OH^- , Cl^- , and F^- . Again, the threshold is lower for solutions of the hydrophobic anions.

Akulichev's model requires that as the ion concentration approaches zero, the thresholds for the various salt solutions approach the threshold of LiOH and NaOH. In other words, the threshold must increase with decreasing ion concentration. It is important to notice two things about Akulichev's data. First, the lines drawn are not theoretical calculations. They are best fit lines to his experimental data. Second, no measurements are made for ion concentrations below about 1 mmol/l. The thresholds at zero concentration are extrapolated from thresholds measured at concentrations greater than about 1 mmol/l. We have extended Akulichev's experimental results to concentrations below 1 mmol/l. These measurements will be discussed in detail in a later chapter.

Akulichev and Alty considered these stabilizing ions to be trace contaminants in their water. It is known that water of all but the purest of samples contains such contaminants. Organic molecules are also found as contaminants in water and they have been employed by

others as stabilizing agents. The first such attempt was by Fox and Herzfeld,¹⁵ and so their model will be the first to be discussed.

1-3.2 Rigid Organic Skin Model

Fox and Herzfeld¹⁵ proposed that surface active organic molecules could form a rigid skin around a gas bubble. This skin would be impermeable to gas diffusion and would be mechanically strong enough to withstand moderate hydrostatic pressures. A nucleus would cavitate when the acoustic pressure reached a (negative) level at which the skin would tear because of the pressure difference between the gas pressure inside and the acoustic pressure outside. According to this model, the skin would have a characteristic crushing pressure. As long as the hydrostatic pressure remained below this crushing pressure, the nucleus would be unaffected by increases in hydrostatic pressure. If the hydrostatic pressure exceeded the crushing pressure, the skin would crumble and the nucleus would dissolve. This would result in an increase in the cavitation threshold since the nuclei would no longer be present. It was this property which forced Herzfeld³³ to later retract his model. Strasberg¹⁶ had found that the threshold does increase with hydrostatic pressure. However, the variation is continuous; there is no lower limit to this variation as predicted by the rigid skin model.

The idea of an organic skin has been developed further by others^{27,28}; the most viable form²⁸ will be discussed next.

1-3.3 Varying Permeability Model

Rather than the rigid skin of organic molecules proposed by Fox and Herzfeld, Yount^{26,28} has developed a stabilization theory in which the dissolution of gas bubbles is halted by a non-rigid organic skin. This skin has mechanical strength against compression, but none against tension. This postulated nucleus is depicted schematically in figure 2.

This nucleus is formed in the following manner. A gas bubble is introduced into a liquid (water, say) and begins to dissolve. While the dissolution takes place, surface active molecules accumulate on the surface. Eventually, within minutes or seconds, the density of these surfactants is such that they resist the collapse of the bubble. This is presumably a Coulomb interaction. These molecules are polar (perhaps even carry a net charge) and align themselves such that their polar "heads" face outward (toward the water) and their tails (typically hydrocarbons) stick inward. Thus, as the density increases, the separation of the heads becomes small enough for dipole fields to become important. Of course, one would expect that if the surfactants were charged, the density at which stabilization occurs would be lower because monopolar fields vary as r^{-2} rather than r^{-3} .

Once the critical density is reached, the radius of the nucleus may change through changes in the number of molecules on the skin. The equilibrium condition for this nucleus is that the electrochemical potentials of the skin and the reservoir must be equal. The reservoir is a thin (perhaps monomolecular) layer of non-aligned surfactants which surrounds the skin of aligned molecules. This equilibrium condition can

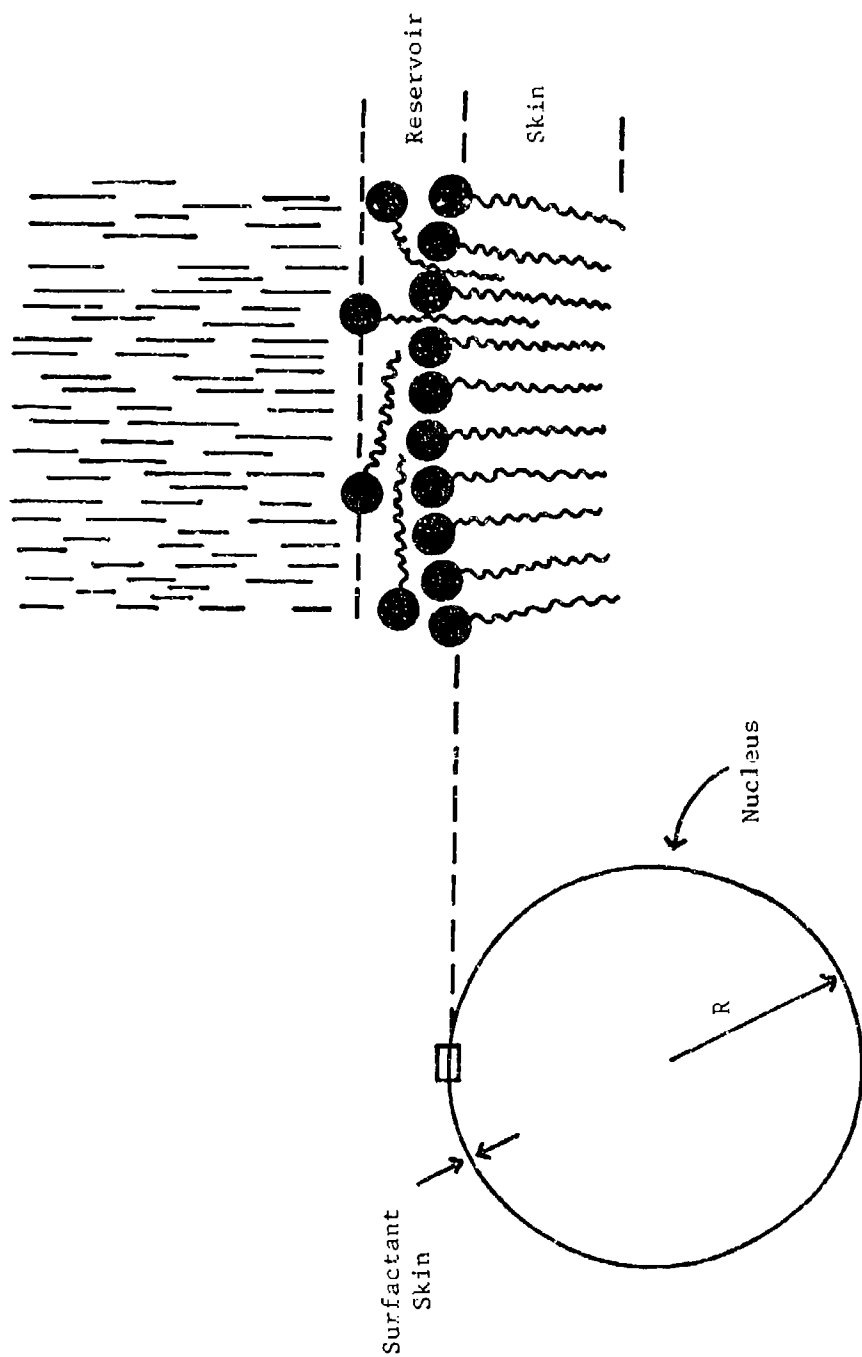


Figure 2. Illustration of a surfactant skin nucleus.
(After Yount, reference 28.)

be satisfied by the accretion or deletion of molecules from the skin (or reservoir), resulting in a "large-scale" change in radius. Having adjusted the radius in this manner, subsequent "small-scale" changes in radius occur. These changes involve only the adjustment of the separation of adjacent skin molecules, not a change in the number of molecules. At equilibrium, the nucleus can be thought of as two concentric shells of negligible thickness--the outer one, the reservoir, is in contact with the liquid and the inner one, the skin, is in contact with the gas. So far, this model has only been used to make predictions about compression/decompression processes during which gas diffusion can play a major role. However, Yount²⁸ has calculated characteristic times in which a skin molecule can be accreted or deleted, due to an inequality of electrochemical potentials, and found them to range from 10^{-3} to 10^{-6} seconds. The shortest times approach the period of acoustic signals used in ultrasonic studies. This would imply that large-scale changes in radius may be able to keep up with the variations in applied pressure associated with acoustic cavitation.

As mentioned above, Yount has performed only long-time scale experiments. A typical experiment will now be described. During the experiment, gelatin samples (surface tension around 50-55 dyn/cm) are subjected to a pressure schedule which is typically like the one shown in figure 3. The sample, about 0.4 ml in volume, initially at a pressure P_o , is rapidly compressed to a pressure P_m . "Rapidly" means that no gas diffuses out of the nucleus during the compression. The sample is held at P_m long enough for the dissolved gas pressure in the

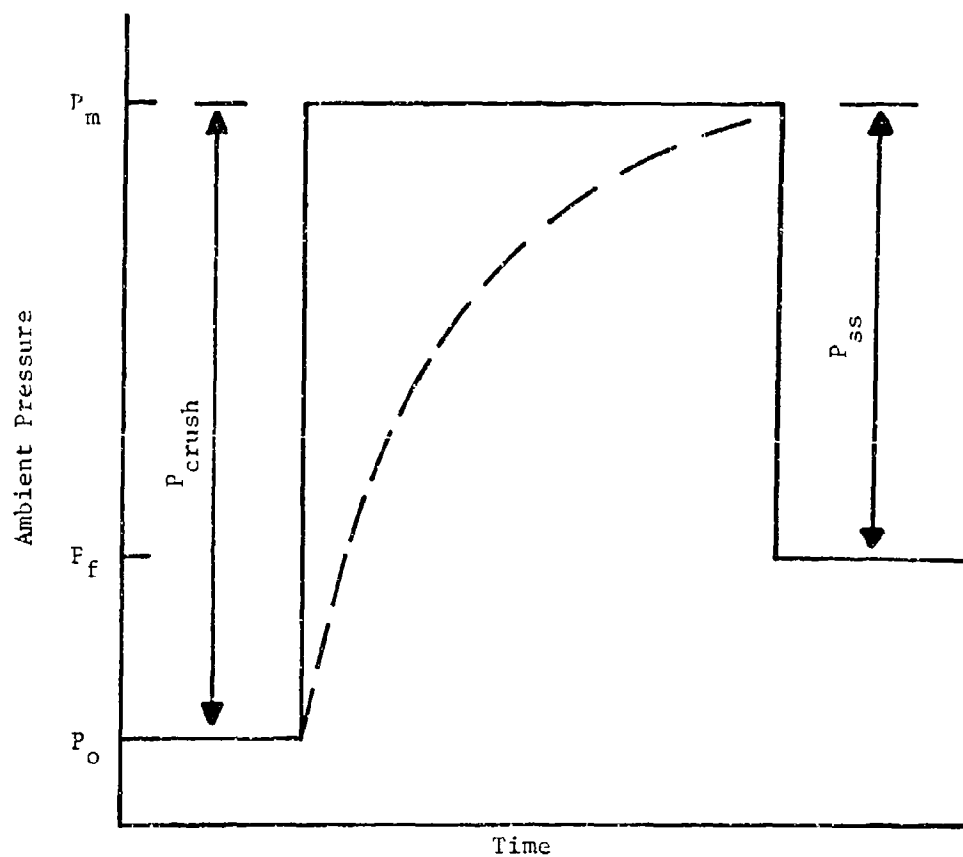


Figure 3. Typical pressure schedule for a compression/decompression experiment. The dashed line depicts the change in the dissolved gas pressure.

sample to come to equilibrium at P_m ; i.e., it becomes saturated. The holding time is typically 5.25 hours. The ambient pressure is then reduced rapidly to P_f resulting in the growth of some of the nuclei. This growth occurs through gas diffusion from the now supersaturated liquid into the nuclei. Several minutes are allowed for the nuclei to grow to visible size. Then the total number of visible bubbles are counted and correlated with the pressure schedule. Yount defines the crushing pressure, P_{crush} , as $P_m - P_o$; and the supersaturation pressure, P_{ss} , as $P_m - P_f$. One manner of data presentation is a graph of P_{ss} vs. P_{crush} for lines of constant number of bubbles. Such a graph is reproduced in figure 4.

The isopleths (lines of constant number of bubbles) in figure 4 show a gradual decrease in slope at $P_{crush} = P^* - P_o$. The segments of the lines on either side of this critical point are more or less linear. This behavior is explained as follows. For modest values of P_{crush} the skin remains permeable to gas diffusion. This enables the gas inside the nucleus to remain in equilibrium with the dissolved gas in the gelatin. However, at a critical ambient pressure, $P^* = P_o + P_{crush}$, the skin molecules become so tightly packed that the skin becomes essentially impermeable to gas diffusion. This prevents the interior and exterior of the bubble from remaining in equilibrium. Therefore, the gas pressure inside the bubble will be less than the gas pressure of the saturated gelatin, resulting in a lower "effective" P_{ss} during decompression. Throughout decompression the skin is always permeable, independent of P_{crush} . This process gives rise to the name "varying-

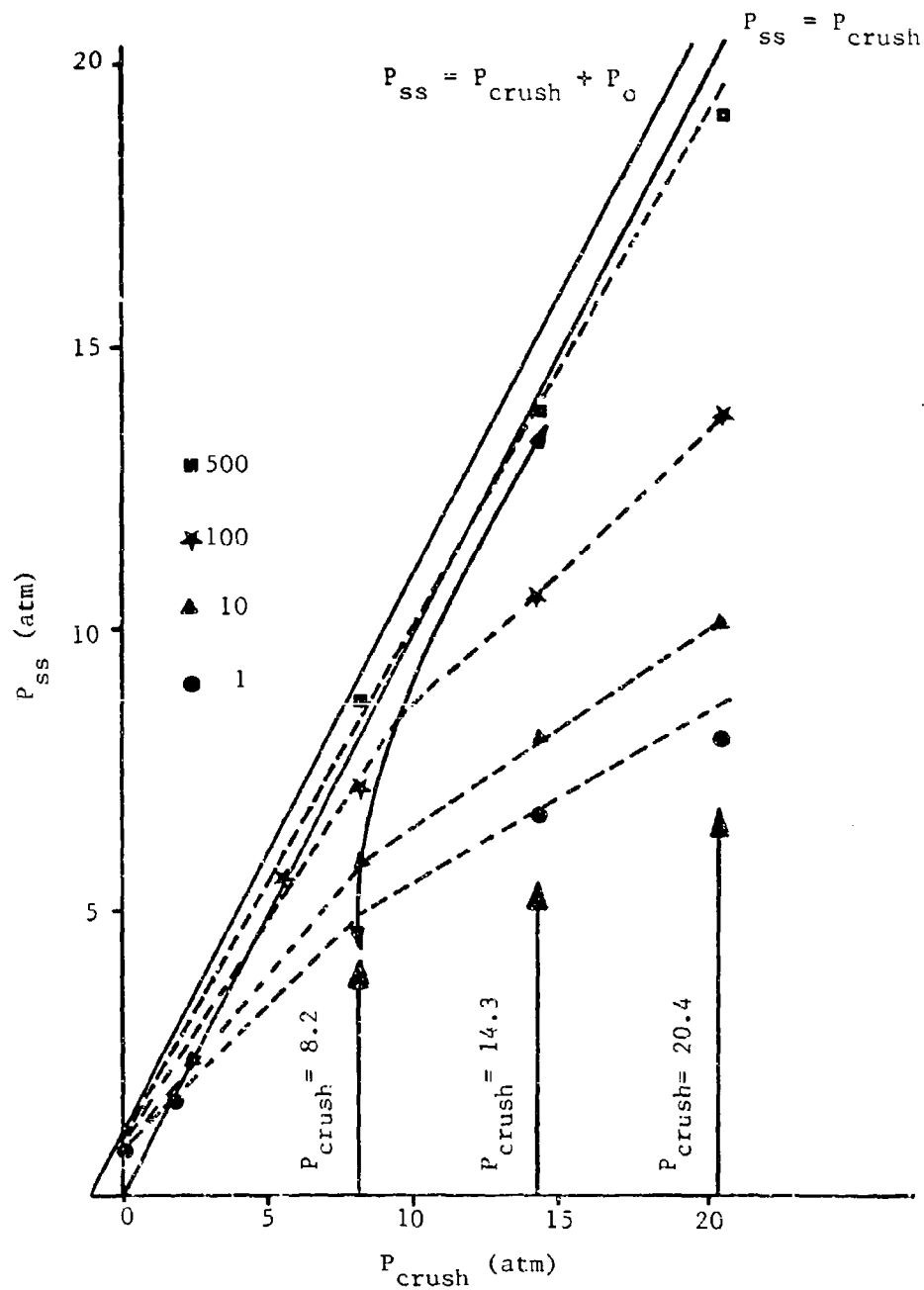


Figure 4. Plot of P_{ss} versus P_{crush} for various numbers of bubbles. (After Yount, reference 26.)

permeability".

Perhaps it is useful to point out that for acoustic processes $P_{\text{crush}} = P_{\text{ss}}$ and that the holding time is usually too short for any significant gas diffusion to occur. Other aspects of this elegant model will be discussed later.

1-3.4 Crevice Model

The crevice model is fundamentally different from the other models discussed. Its stabilization mechanism does not require that surface tension be nullified. Rather, it uses surface tension, combined with geometrical considerations, to stabilize a gas pocket at the bottom of a crevice. It is, perhaps, the most "worked over" of the models. This is partly true because it can account for a wide range of experimental data, whereas the other models can account for only limited sets of data, most often that of the model's proponent. Since the crevice model has undergone several revisions, it would be unreasonable to discuss all of them in detail. Therefore, the model will be discussed briefly in the form reported by Crum³⁴; this model will then be revised in the next chapter.

The crevice model assumes that gas pockets are stabilized at the bottom of conical cracks or crevices found on hydrophobic solid impurities present in the water. The essential features of the model are depicted in figure 5. When the liquid is saturated with gas, the liquid-gas interface is essentially flat. However, when the liquid is degassed, the interface bows toward the apex of the crevice. This

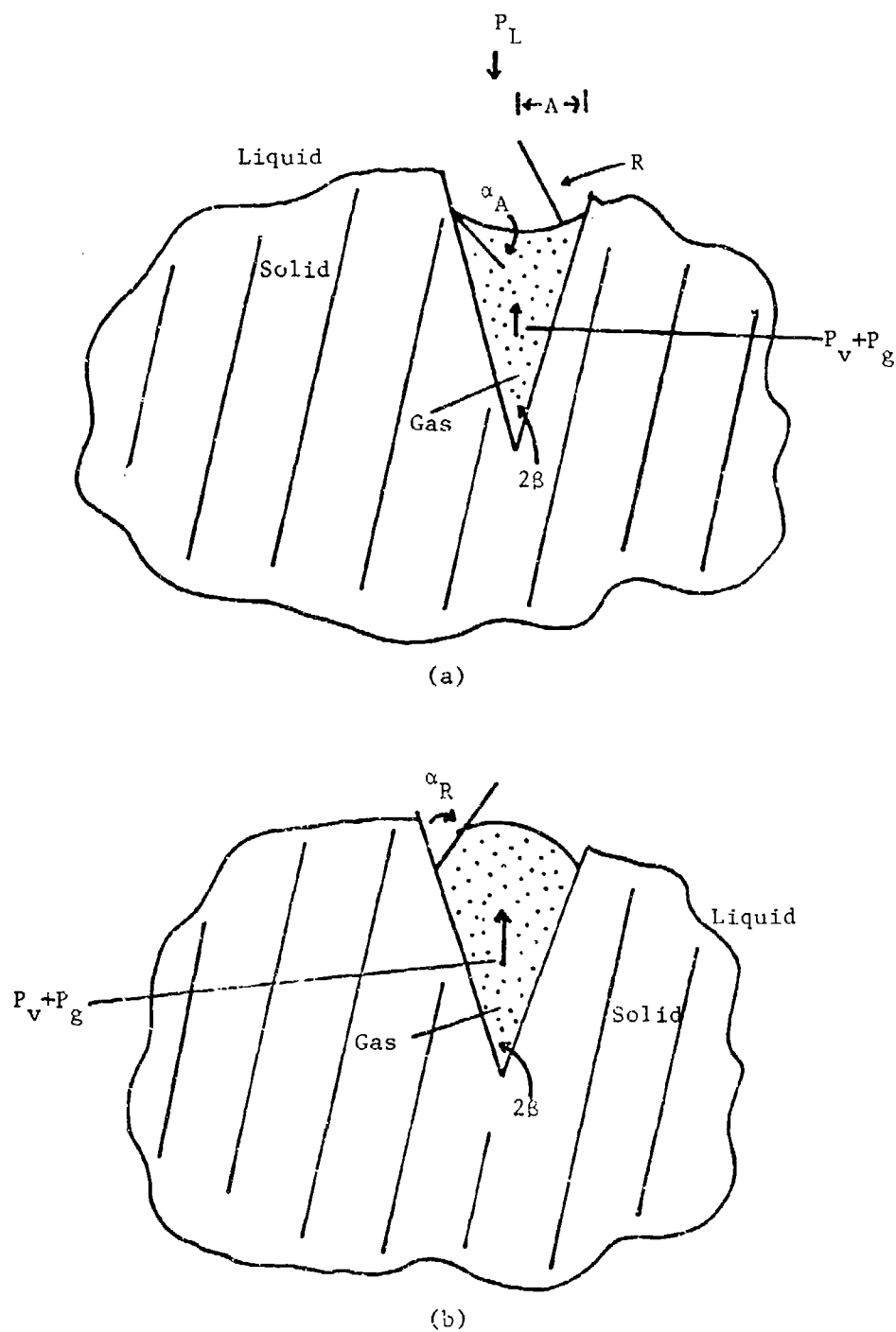


Figure 5. Diagram of a gas-filled conical crevice embedded in a hydrophobic solid a) in the degassed state and b) in the nucleation phase. (After Crum, reference 34).

behavior occurs for the following reason. In a saturated solution, the dissolved gas pressure, P_g , equals the pressure which the liquid exerts on the interface. We call this the liquid pressure, P_L , and define it to be the sum of all the pressures present--hydrostatic and acoustic. Diffusion maintains the gas pressure in the nucleus at the dissolved gas pressure. Assuming that vapor pressure is negligible for the time being, we have $P_L = P_g$ for saturated solutions. Since there is no pressure difference across the interface, it is flat and the Laplace pressure ($2\gamma/r$, where γ = surface tension and r = radius of curvature of the interface) is zero. When the liquid is degassed, P_g is less than P_L and the interface bows toward the apex. This curvature gives rise to a Laplace pressure which exactly equals the difference between P_L and P_g . Since all pressures are now balanced, the nucleus does not dissolve and remains intact.

Suppose we have a degassed liquid and the liquid pressure is increased. In response to this condition, the interface bows inward more, until it reaches the advancing contact angle. At this point any subsequent motion of the interface involves the entire interface advancing as a whole toward the apex. As it advances, the radius of curvature necessarily becomes smaller, since the angle of the interface measured from the crevice wall is now fixed. As the radius of curvature decreases, the Laplace pressure increases, eventually becoming high enough to balance the increased liquid pressure.

If the liquid pressure is now suddenly decreased becoming negative, as during the negative portion of an acoustic cycle, the interface bows

outward and may reach the receding contact angle. If the receding contact angle is reached, any subsequent motion of the interface involves the entire interface receding away from the apex. This recession results in a decrease in the Laplace pressure, since the radius of curvature increases. With the Laplace pressure decreased the gas pressure inside the nucleus is retarded even less. Previous researchers^{16,22,24,25} assumed, therefore, that the criterion for nucleation from a crevice was that the interface must reach the receding contact angle. They argued that once the interface had reached the receding contact angle, any subsequent interfacial motion would increase the radius of curvature, resulting in less Laplace pressure (which was now opposing the growth of the nucleus) and so the growth would be unbounded. (This argument will be opposed in the next chapter.) This unbounded growth would result in a mostly-vapor-filled cavity being emitted from the crevice. This nucleation process must occur within the time frame of an acoustic period.

Using this nucleation criterion to define a cavitation threshold, the threshold can be predicted. Crum has modified previous results to include the effects of surface tension. He finds the threshold to be

$$P_A = (P_L - P_V - P_g) + \frac{P_L - P_V - P_g}{\delta} \{ (\cos\phi) \left(\frac{C}{Y} - 1\right) + (\sin\phi) [1 - \left(\frac{C}{Y} - 1\right)^2]^{1/2} \}$$

where:

P_A = (negative) acoustic pressure

P_L = liquid pressure

P_V = vapor pressure

P_g = gas pressure

$\delta = |\cos(\alpha_A - \beta)|$

$\phi = \alpha_H + \beta$

c = constant = 50 dyn/cm

α_A = advancing contact angle

β = crevice half angle

α_H = hysteresis angle

This equation predicts the threshold as a function of dissolved gas pressure, surface tension, and temperature fairly well. More details of these predictions will be given later.

1-4 Final Introductory Remarks

Each of the models discussed above are stabilization mechanisms; each requires the presence of a gas phase large enough to be stabilized. The origin of the gas phase is not of concern here. None of the models mentioned predict the subsequent growth of a nucleus to an observable size. It is simply assumed that after the bubble is nucleated, it will grow large enough to be detected. This is, of course, a huge assumption and is not always valid. This point will be addressed in a subsequent chapter.

In this dissertation, many different, and sometimes subtle, concepts are introduced and discussed. One way in which these many topics could be handled would be to discuss each in exhaustive detail, the result being a much longer, and perhaps more complete, dissertation. However, in an effort to be as concise as possible, this approach was not taken. This choice may lead to a choppy appearance of the body of the text. In an effort to remedy this appearance, a brief description of the layout of this dissertation will be given.

Two types of cavitation will be dealt with. One type is vaporous

(or transient) cavitation in which the cavity is mostly vapor-filled. The other type of cavitation will be termed "diffusion cavitation" and it is controlled by gaseous diffusion into or out of the bubble. Three different nucleation models will be discussed. Of the three, the crevice model will receive the majority of the attention. The other two models are the ionic skin model and the varying-permeability organic skin model.

Chapter 2 contains the majority of the theoretical derivations that will be presented. The concept of a critical radius will be introduced for both types of cavitation. This concept will then be applied to the crevice model and expressions for both the vaporous and diffusion cavitation thresholds will be derived. In chapter 3, the theoretical thresholds predicted by the crevice model will be compared to experimental results. Chapter 4 is devoted to the other models. The plausibility of the ionic skin model will be discussed in light of the results of measurements of the variation in the acoustic cavitation threshold with the dissolved ion concentration. In addition, the varying-permeability model will be applied to vaporous cavitation. To the author's knowledge, this is the first attempt at such an application. The final chapter will include a summary of the important points presented in the dissertation as well as the conclusions that may be drawn from them.

Chapter 2

Derivation of Cavitation Thresholds Using the Critical Radius Approach to the Crevice Model

2-1 Introduction

In the previous chapter, it was noted that in the current crevice model, a vapor bubble would be nucleated when the liquid-gas interface reached the receding contact angle. In this dissertation, it will be shown that this criterion is indeed necessary but not sufficient. In order for a cavity to be nucleated, it is also necessary that the radius of curvature exceed a critical value determined from a stability criterion, the nature of which depends upon the type of cavitation under investigation. In view of this requirement, an expression for the liquid pressure required to produce such a radius of curvature will be derived.

The discussion will be divided into two cases: one for ambient pressures less than the vapor pressure and the other for ambient pressures greater than the vapor pressure. In the first case the cavity formed will be vapor-filled while in the second case the cavity will be gas-filled, growing by gaseous diffusion. The results of this rederivation will be compared with those of the previous crevice model. It will be shown that predictions of cavitation thresholds based on this revised crevice model agree closely with experimental results. In

addition, the revised model will be applied to situations previously explained only in terms of the varying-permeability model.

2-2 Critical Radius

The concept of a critical radius is not new. Therefore, it is somewhat surprising that this approach to the crevice model has not been taken before. Harvey¹¹ did discuss a critical radius for a nucleus to grow by gaseous diffusion. However, he did not use it in a quantitative way. Blake³⁷ and Prosperetti³⁸ have discussed the critical radius at which a vapor bubble is stable against growth or collapse. Building on these concepts, expressions will be derived for the applied pressure, called the cavitation threshold, required for a bubble to be nucleated from a crevice. (Note: the applied pressure may assume negative values.) Since the spherical geometry of a free bubble lends itself to easier manipulation than the conical geometry of a crevice, the critical radii will be derived for a free bubble. In general, the stability conditions hold for either case; exceptions will be noted when necessary.

2-2.1 Critical Radius for Growth by Gaseous Diffusion

Consider a gas filled bubble of radius R surrounded by a liquid which exerts a pressure P_L on the bubble. The liquid-gas surface tension is σ . The gas pressure inside the bubble is P_g ; the vapor pressure, P_v , is assumed negligible (see figure 6). Assume the bubble is in equilibrium so that the pressure inside (P_g) equals the liquid pressure plus the Laplace pressure due to the surface tension:

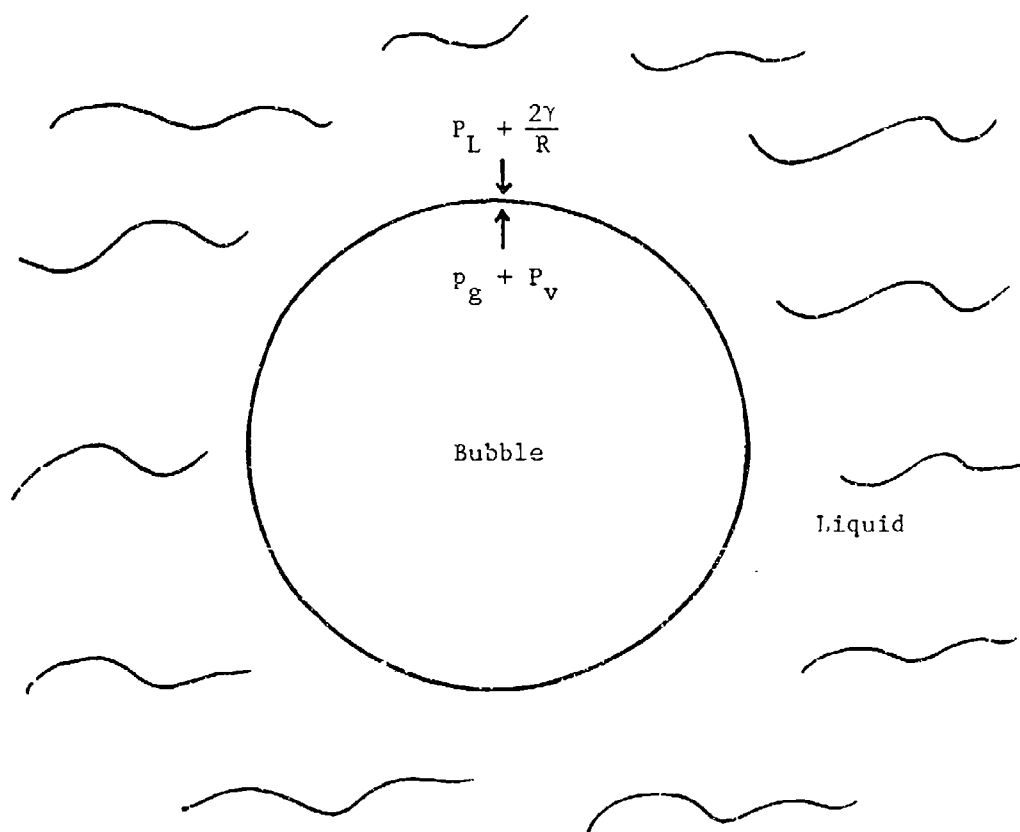


Figure 6. Illustration of a free bubble surrounded by a liquid. The external pressure is the sum of the liquid and Laplace pressures and the internal pressure is the sum of the gas and vapor pressure.

$$P_g = P_L + \frac{2\gamma}{R} . \quad (1)$$

Simultaneously, the system must be in diffusion equilibrium. This requires

$$c_L = a c_i \quad (2)$$

where c_L and c_i refer to the concentrations of gas dissolved in the liquid and present inside the bubble, respectively; "a" is the solubility coefficient of the gas in the liquid. If the gas is ideal then (2) becomes

$$P_g = \frac{B T c_L}{a} \quad (3)$$

where B is the universal gas constant and T is the absolute temperature. Equation (3) is a form of Henry's Law. At equilibrium P_g may be replaced with t, called the gas tension, which is a measure of the partial pressure of the gas dissolved in the liquid. At equilibrium

$$P_g = P_L + \frac{2\gamma}{R} = t \quad (4)$$

or

$$(t - P_L) = \frac{2\gamma}{R} . \quad (5)$$

The critical (equilibrium) radius is, therefore,

$$R_{cg} = \frac{2\gamma}{t - P_L} . \quad (6)$$

The subscript "cg" refers to the critical radius for a bubble to grow by gaseous diffusion. Notice that the radius of curvature is positive only in supersaturated solutions. Since a negative radius is meaningless for free bubbles, stability can occur only in supersaturated solutions.

2-2.2 Critical Radius for Growth in the Absence of Diffusion

The discussion presented in this section is similar to that of the previous one, except now the effect of vapor pressure is included. Again, at equilibrium the following condition holds

$$P_v + P_g = P_L + \frac{2\gamma}{R} \quad (7)$$

The condition given by equation (3) is dropped and the amount of gas inside the bubble is fixed. (In other words, no diffusion of gas takes place. However, the amount of vapor is not fixed.) If the gas is ideal then rearranging (7) gives

$$P_L + \frac{2\gamma}{R} = \frac{3nBT}{4\pi R^3} + P_v \quad (8)$$

where n is the number of moles of the gas inside the bubble. To examine the stability consider the effect of a small increase in R . For the bubble not to grow spontaneously, the effective external pressure, which is given by the left-hand side of equation (8), must increase more than the internal pressure, given by the right-hand side of equation (8). This will always be true if $P_L \geq P_v$, because the gas pressure decreases more with an increase in R than does the Laplace pressure. If, however, $P_L < P_v$ then the situation is different.

The stability criterion can be expressed, in general, as

$$\frac{\partial}{\partial R} \left(P_L + \frac{2\gamma}{R} \right) > \frac{\partial}{\partial R} \left(\frac{3nBT}{4\pi R^3} + P_v \right) \quad (9)$$

Performing the differentiation and solving for R gives

$$R < \frac{4\gamma}{3(P_v - P_L)} \quad (10)$$

In other words, when $P_v > P_L$, the bubble will be stable against

spontaneous growth only if $R < R_{cv}$ where

$$R_{cv} = \frac{4\gamma}{3(P_v - P_L)} \quad (11)$$

Taking the other view, a bubble will grow in a spontaneous unbounded manner when the liquid pressure is less than the vapor pressure only if $R \geq R_{cv}$. A bubble that grows in this way will be mostly vapor-filled. Therefore, the subscript "cv" refers to the critical radius for a vapor bubble to grow from a gas-filled nucleus. The reader is referred to Prosperetti³⁸ for more details.

2-3 Threshold Derivations

In the preceding section, the conditions for the nucleation of both gaseous and vaporous bubbles were developed. Using them, expressions will now be derived for the applied pressures required for nucleation from gas-filled crevices. These are referred to as cavitation thresholds. It should be noted that the applied pressure, P_A , is equal to the liquid pressure minus the ambient static pressure; i.e., $P_A = P_L - P_O$. (P_A experimentally is the applied acoustic pressure.) The discussion which follows will be divided into two different cases: one for $P_L < P_v$ and the other for $P_L \geq P_v$. This division is a natural one; the difference in the restrictions on P_L is in a sense the difference between acoustic cavitation and diffusion cavitation. Acoustic cavitation is produced by negative applied pressures and its nucleation usually involves the growth of vapor-filled bubbles, although not always. On the other hand, diffusion cavitation is usually produced by ambient pressures greater than the vapor pressure and gas diffusion is

the predominant mechanism in its nucleation. Diffusion cavitation should not be confused with gaseous (stable) acoustic cavitation; the two occur in different regions of ambient pressures. Acoustic cavitation will be considered first.

2-3.1 Acoustic Cavitation Nucleation

Assume that a deep crevice, partially filled with gas, exists in a hydrophobic solid surrounded by a gas-saturated liquid. The hydrostatic pressure due to the liquid is negligible and it is exposed to an atmosphere at pressure P_o (refer to figure 7). The liquid-gas interface contacts the crevice wall at a height z above the apex. The crevice angle is 2θ . The system is in equilibrium, so

$$P_o = t = P_g. \quad (12)$$

For temperatures far below the boiling point, $P_v \ll P_o$ and thus the interface is essentially flat.

The liquid is now degassed so that $t < P_o$. Gas will diffuse out of the nucleus causing the interface to bow inward, toward the apex, as shown by the dashed line (b) in figure 7. At equilibrium $P_g = t$ and

$$P_o = P_g + P_v + \frac{2\gamma}{R_o}. \quad (13)$$

The new equilibrium position of the nucleus is shown by the solid line (c) in figure 7. At this position the angle between the interface and the wall is α_A , the advancing contact angle.

At this point, an acoustic field of pressure amplitude P_A is applied such that the liquid pressure exerted on the interface is $P_o + P_A$.

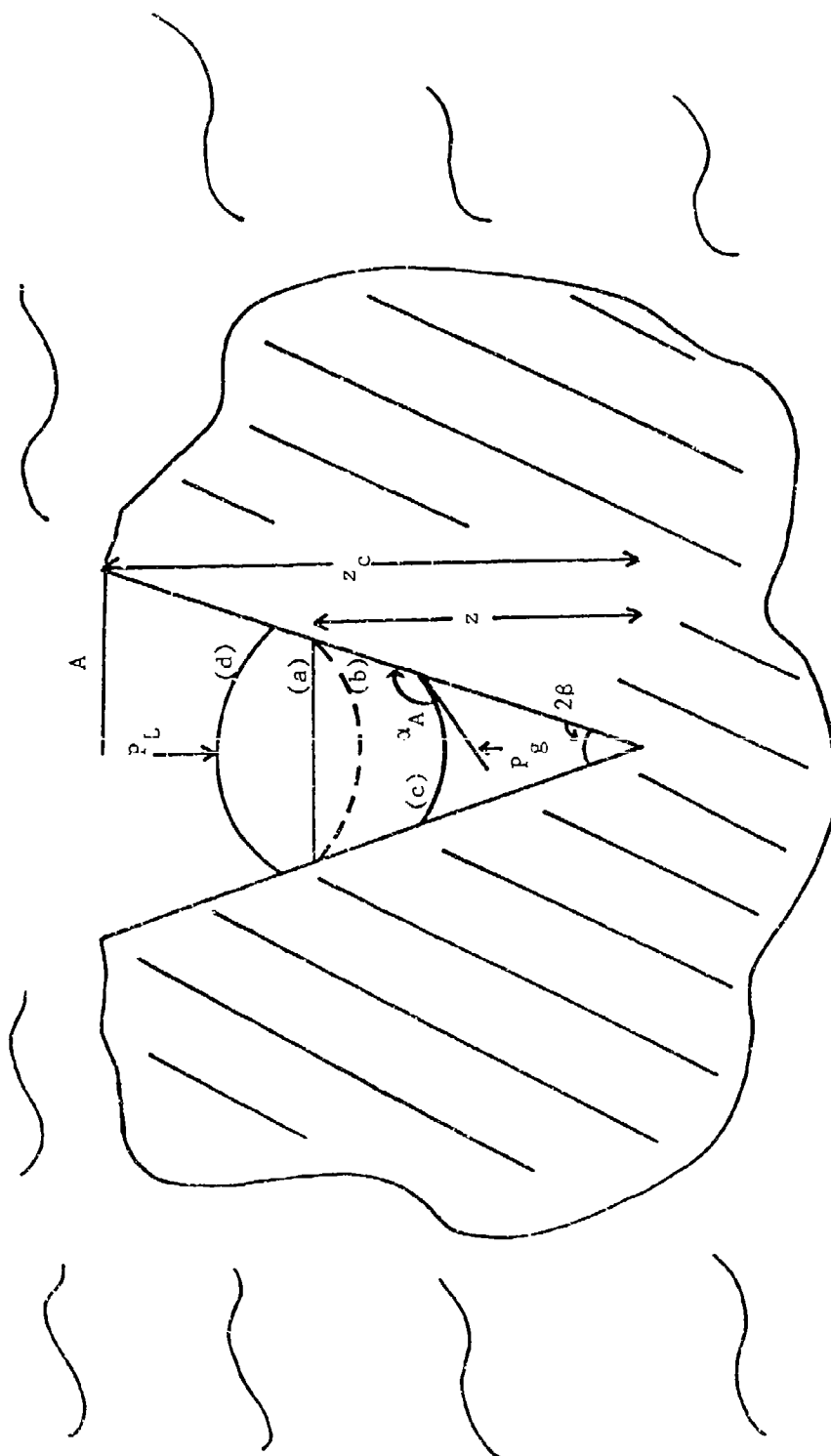


Figure 7. Diagram of a crevice model nucleus depicting the motion of the interface during the various phases of the nucleation process.

Assume P_A is such that $P_v > P_o - P_A$. During the negative half-cycle, the interface bows outward and a new equilibrium position is established. This process will be isothermal if the thermal diffusion length, L , is large compared to crevice dimensions. L is given by³⁹

$$L = \left(\frac{2k}{\rho c_p \omega} \right)^{1/2} \quad (14)$$

where k is the thermal conductivity of the gas, ρ is its density, c_p is the specific heat at constant pressure per unit mass, and $\omega = 2\pi f$ where f is the frequency of the acoustic field. For most gases at normal pressures and temperatures ($P_o \approx 1$ bar and $T \approx 200-500K$), k is on the order of $5 \times 10^{-6} \text{ kcal m}^{-1} \text{ s}^{-1} \text{ K}^{-1}$; the density of air is 1.1 kg m^{-3} ; c_p is $0.25 \text{ kcal kg}^{-1} \text{ K}^{-1}$. Therefore,

$$L \approx 2.4 \times 10^{-3} f^{-1/2} \text{ m} . \quad (15)$$

Notice that L is inversely proportional to the square root of the acoustic frequency, but even at megahertz frequencies, $L \approx 2.4 \mu\text{m}$. This is about an order of magnitude larger than the crevice sizes assumed here. Therefore, the isothermal assumption is a good one.

A bubble will be nucleated from this new position only if the radius of curvature of the interface is larger than the critical radius R_{cv} . The value of P_A necessary for this condition to be met is found as follows.

For isothermal processes,

$$P_1 V_1 = P_2 V_2 \quad (16)$$

where P_1 and V_1 are the internal gas pressure and nuclear volume in the initial degassed state whereas P_2 and V_2 are the interior gas pressure and nuclear volume at $P_L = P_o - P_A$. V_1 is given by

$$V_1 = V_{\text{cone}} - V_{\text{cap}} \quad (17)$$

(see figure 8). After some geometric and algebraic manipulation

$$V_1 = \frac{1}{3}\pi a_1^3 (\cot\beta - \eta_1) \quad (18)$$

where

$$\eta_1 = \left[\frac{1}{\delta_1} - \sqrt{\frac{1}{\delta_1^2} - 1} \right] \left[\frac{2}{\delta_1} + \sqrt{\frac{1}{\delta_1^2} - 1} \right] \quad (19)$$

and

$$\delta_1 = |\cos(\alpha_1 - \beta)|. \quad (20)$$

(Throughout this dissertation the subscripts associated with η and δ refer to the subscript associated with α .) The final volume, V_2 , is similarly given by

$$V_2 = \frac{1}{3}\pi a_2^3 (\cot\beta + \eta_2). \quad (21)$$

The interior pressures are given by

$$P_1 = P_g \quad (22)$$

and

$$P_2 = P_o - P_A - P_v + \frac{2\gamma}{R}. \quad (23)$$

Rearranging (16) gives

$$\frac{P_2}{P_1} = \frac{V_1}{V_2} \quad (24)$$

or

$$\frac{P_o - P_A - P_v + \frac{2\gamma}{R_2}}{P_g} = \frac{\frac{1}{3}\pi a_1^3 (\cot\beta - \eta_1)}{\frac{1}{3}\pi a_2^3 (\cot\beta + \eta_2)}. \quad (25)$$

Using the geometrical relationship that $a = \delta R$, (25) becomes (after some algebra)

$$R_2^3 + \frac{2\gamma}{P_o - P_A - P_v} R_2^2 - \left[\frac{P_g}{P_o - P_v - P_A} \right] \left[\frac{a_1}{\delta_2} \right]^3 \left[\frac{\cot\beta - \eta_1}{\cot\beta + \eta_2} \right] = 0. \quad (26)$$

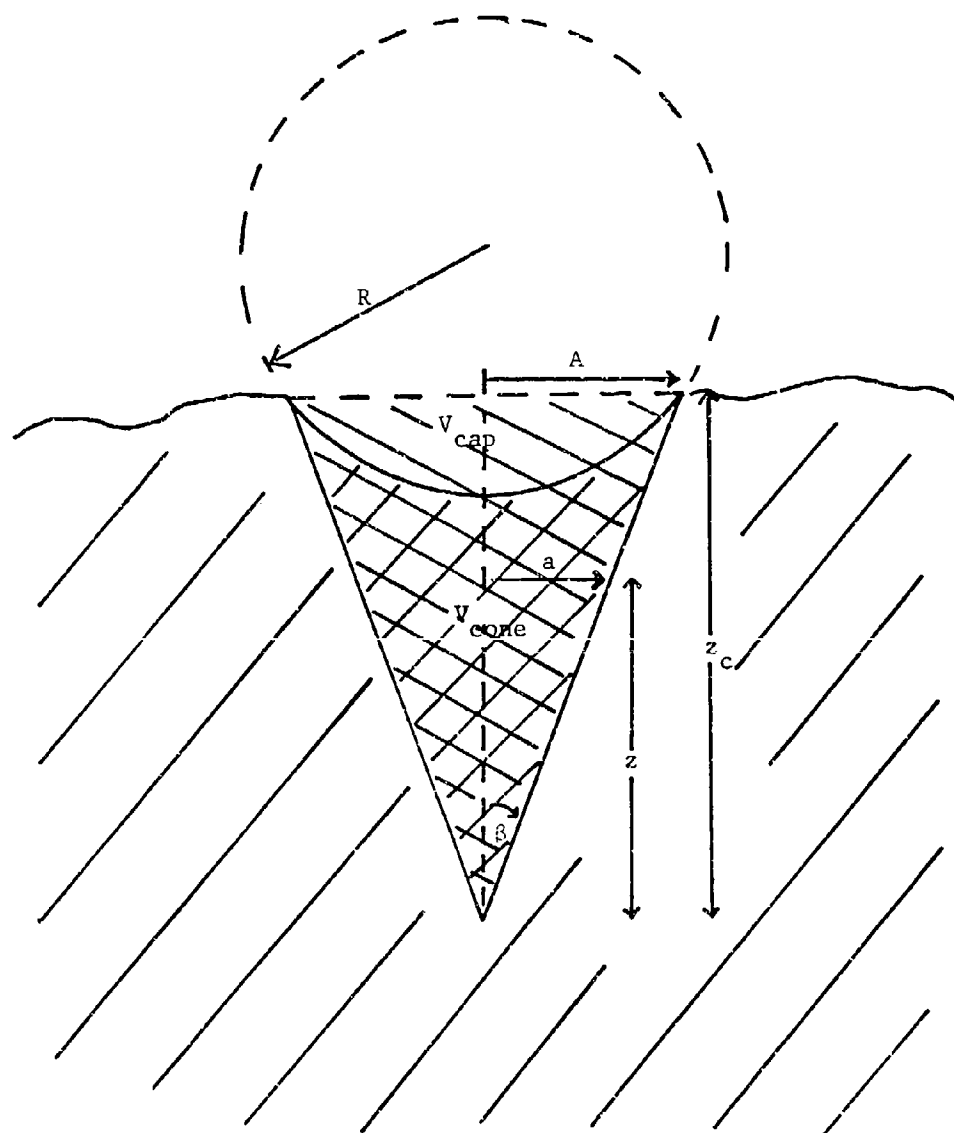


Figure 8. Illustration of crevice geometry.

At the initial state, $P_1 = P_g = t$. From equation (13) it is seen that

$$R_1 = \frac{2\gamma}{P_o - P_g - P_v} \quad (27)$$

or

$$a_1 = \frac{2\gamma\delta}{P_o - P_g - P_v} \quad (28)$$

Using this expression and letting

$$R_2 = R_{cv} = \frac{4\gamma}{3(P_v + P_A - P_o)} \quad (29)$$

gives

$$P_A = P_o - P_v + \frac{2}{3^{3/2}} P_g \left[\left(\frac{P_o - P_v}{P_g} - 1 \right)^3 \left(\frac{\delta_2}{\delta_1} \right)^3 \left(\frac{\cot\beta + \eta_2}{\cot\beta - \eta_1} \right) \right]^{1/2} \quad (30)$$

In general, in the degassed state, the contact angle is the advancing contact angle, $\alpha_1 = \alpha_A$. In the final state the contact angle equals the receding contact angle, $\alpha_2 = \alpha_R$. Equation (30) now becomes

$$P_A = P_o - P_v + \frac{2}{3^{3/2}} P_g \left[\left(\frac{P_o - P_v}{P_g} - 1 \right)^3 \left| \frac{\cos(\alpha_R - \beta)}{\cos(\alpha_A - \beta)} \right|^3 \left(\frac{\cot\beta + \eta_R}{\cot\beta - \eta_A} \right) \right]^{1/2} \quad (31)$$

This relationship gives the threshold for vaporous cavitation. Although a more detailed comparison will be made in the next chapter, a few brief comparisons to the old crevice model should be made here. Apfel's threshold is ³⁴

$$P_A = P_o - P_v - P_g + (P_o - P_v - P_g) \left| \frac{\cos(\alpha_R - \beta)}{\cos(\alpha_A - \beta)} \right| \quad (32)$$

This equation gives a linear dependence on gas content whereas (31) does not. The $|\cos(\alpha_R - \beta)/\cos(\alpha_A - \beta)|$ term appears in both but the dependence is different.

It was assumed throughout the derivation that the interface reaches the receding contact angle. For small values of P_A this may not be true. In order to find the value of P_A necessary for the interface to reach α_R , again assume isothermal conditions. The initial state is the degassed state mentioned above with

$$P_1 = P_g \quad (33)$$

and

$$V_1 = \frac{1}{3}\pi a_1^3 (\cot\beta - \eta_A). \quad (34)$$

The final state, 2, is such that the interface just reaches α_R so

$$P_2 = P_o - P_v - P_A + \frac{2\gamma}{R_2} \quad (35)$$

$$V_2 = \frac{1}{3}\pi a_1^3 (\cot\beta + \eta_R). \quad (36)$$

Recall that

$$a = \delta R \quad (37)$$

so

$$P_2 = P_o - P_v - P_A + \frac{2\gamma\delta R}{a_1}. \quad (38)$$

Using (16), (28), and (37) it can be shown that

$$P_o - P_v - P_A + \frac{\delta R}{\epsilon_A} (P_o - P_v - P_g) = P_g \left[\frac{\cot\beta - \eta_A}{\cot\beta + \eta_R} \right] \quad (39)$$

or

$$P_A^* = P_o - P_v - P_g \left[\frac{\cot\beta - \eta_A}{\cot\beta + \eta_R} \right] + (P_o - P_v - P_g) \left[\frac{\cos(\alpha_R - \beta)}{\cos(\alpha_A - \beta)} \right]. \quad (40)$$

The asterisk refers to the fact that this is the critical value of P_A below which nucleation will not occur. (In this dissertation an asterisk will always denote some type of "critical" pressure.) Why is

this a critical value? Assume the outwardly bowed interface has a radius of curvature greater than R_{cv} , yet it has not reached the receding contact angle. The nucleus is unstable and so the radius of curvature will not spontaneously decrease. However, this would be required in order for the contact angle to decrease to α_R . Since the interface will not move before it reaches the receding contact angle, there is no nucleation. It should be noted that equation (40) is almost identical to equation (32), Apfel's threshold equation. The only difference is that in deriving equation (32) it was assumed that gas diffusion can keep up with the motion of the interface. This assumption was not made in deriving equation (40), hence the additional factor associated with P_g . If gas diffusion can keep up with the motion of the interface then that factor equals one.

The implications of these thresholds will be discussed in detail in the next chapter. We turn now to the threshold for the nucleation of a bubble by gaseous diffusion.

2-3.2 Diffusion Cavitation Nucleation

Once again assume a deep crevice, partially filled with gas, exists in a hydrophobic solid surrounded by a gas-saturated liquid that exerts a static, ambient, pressure P_0 on the interface. In equilibrium, the pressure balance equation (12) holds; the interface is essentially flat and a height z_0 above the apex. Assume the ambient pressure is increased from P_0 to P_m . This change in pressure appears at the interface as an increase in the liquid pressure causing it to bow inward

(see figure 9). The interface will advance toward the apex if it reaches the advancing contact angle. The pressure at which this occurs is found by assuming an isothermal compression from $V_i = V_{\text{cone}}$ to $V_f = V_{\text{cone}} - V_{\text{cap}}$. That is, from

$$V_i = \frac{1}{3}\pi a^3 \cot\beta \quad (41)$$

to

$$V_f = \frac{1}{3}\pi a^3 (\cot\beta - \eta_A) . \quad (42)$$

The internal pressure also changes from $P_i = P_g = P_o$ (neglecting P_v) to

$$P_f = P_m - \frac{2\gamma}{R} = P_m - \frac{2\gamma\delta_A}{a} . \quad (43)$$

Using $P_i V_i = P_f V_f$, we have

$$P_o = \left(P_m - \frac{2\gamma\delta_A}{a} \right) (1 - \eta_A \tan\beta) . \quad (44)$$

Let $P_{\text{crush}} = P_m - P_o$ (see reference 26). Substitution into equation (44) gives

$$P_{\text{crush}}^* = P_o \left[\frac{\eta_A \tan\beta}{1 - \eta_A \tan\beta} \right] + \frac{2\gamma\delta_A}{a} \quad (45)$$

where the asterisk indicates that this is the critical value of P_{crush} . Let the crevice mouth have a radius A and define the ratio a/A as h . This non-dimensional parameter is a measure of the degree of fullness of the crevice. From the conical geometry it is seen that

$$\frac{a}{A} = \frac{z}{z_c} = h \quad (46)$$

where z_c is the depth of the crevice. Using this relationship the expression for the critical crushing pressure becomes

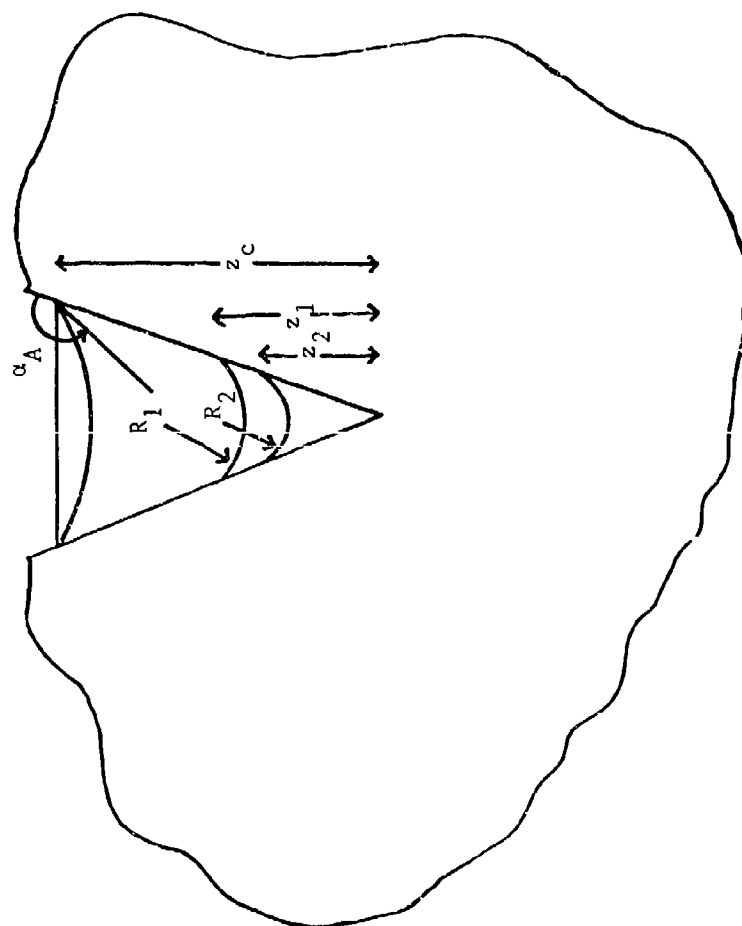


Figure 9. Illustration of interfacial motion during the compression phase of a compression/decompression process (diffusion cavitation).

$$P_{\text{crush}}^* = P_o \left[\frac{\eta_A \tan \beta}{1 - \eta_A \tan \beta} \right] + \frac{2\gamma \delta_A}{hA} . \quad (47)$$

For crushing pressures less than this value, the interface does not reach the advancing contact angle and therefore cannot move.

If the crushing pressures exceed P_{crush}^* , the interface advances until

$$P_m = P_g' + \frac{2\gamma}{R_1} . \quad (48)$$

The prime indicates that the gas pressure is no longer equal to t , but is greater. Since the liquid is assumed incompressible, the change in liquid pressure does not cause an immediate change in t , as it does in P_g . The change in gas tension occurs at a rate controlled by the diffusion of gas from the atmosphere into the liquid. Thus, for a time, the nucleus is supersaturated. Gas diffuses out of the nucleus until, once again, $P_g = t$. At this point, the interfacial radius of curvature is less than R_1 because $P_g < P_g'$. Therefore, since the interface is already at α_A , this reduction in radius implies that the diffusion causes the nucleus to contract; that is, h decreases. At this equilibrium position

$$P_m = P_g + \frac{2\gamma}{R_2} \quad (49)$$

where $P_g < P_g'$ and $R_2 < R_1$.

If, at this point, the ambient pressure were reduced back to P_o , the nucleus would expand, but not to its original volume since there are fewer gas molecules within the nucleus. This net reduction in the

volume of the nucleus would result in a higher cavitation threshold than that of an identical, non-pressurized nucleus. Such an increase in threshold is well documented.^{16,18} If the liquid pressure is maintained at P_m long enough, however, the dissolved gas pressure will eventually reach P_m ; that is, $t_m = P_m$. This results in the diffusion of gas back into the nucleus until $P_g = P_m$, at which point the interface is essentially flat and a height z_2 above the apex.

Suppose now the atmospheric, and therefore the liquid, pressure were reduced to a final pressure P_f . The internal gas pressure of the nucleus will be greater than the external ambient pressure; the interface bows outward. In order for the interface to reach the receding contact angle the volume must change from

$$V_i = \frac{1}{3}\pi a^3 \cot\beta \quad (50)$$

to

$$V_f = \frac{1}{3}\pi a^3 (\cot\beta + \eta_R) \quad (51)$$

while the gas pressure inside the nucleus changes from P_m to

$$P_f + \frac{2\gamma}{R} = P_f + \frac{2\gamma\delta_R}{h_2 A} \quad (52)$$

Assuming isothermal conditions, we have

$$P_m = \left(P_f + \frac{2\gamma\delta_R}{h_2 A} \right) (1 + \eta_R \tan\beta) \quad (53)$$

The extent to which the nucleus is supersaturated can be characterized by defining the supersaturation pressure $P_{ss} = P_m - P_f$. Using this expression and noting that

$$P_f = P_o + P_{crush} - P_{ss} \quad (54)$$

equation (53) becomes

$$P_{ss}^* = (P_o + P_{crush}) \left[\frac{\eta_R \tan \beta}{1 + \eta_R \tan \beta} \right] + \frac{2\gamma \epsilon_R}{h A} . \quad (55)$$

Notice the similarity between this equation and equation (47). The difference in sign in the denominator arises from the fact that in one instance the calotte adds to the volume of the nucleus, while in the other it subtracts from it.

For supersaturation pressures greater than P_{ss}^* , the interface reaches the receding contact angle and moves outward. If the change in volume is such that the radius of curvature of the interface is larger than R_{cg} , equation (6), the nucleus will grow by gas diffusion. In general, the final volume (51) is given by

$$V_f = \frac{1}{3} \pi a_3^3 (\cot \beta + \eta_R) \quad (56)$$

where $a_3 > a_2$. In this case (53) becomes

$$P_m = \left[P_f + \frac{2\gamma}{R_{cg}} \right] \left(\frac{a_3}{a_2} \right)^3 (1 + \eta_R \tan \beta) . \quad (57)$$

Recall that

$$R_{cg} = \frac{2\gamma}{t - P_L} . \quad (58)$$

In this case, $t = P_m$ and $P_L = P_f$. Therefore,

$$R_{cg} = \frac{2\gamma}{P_{ss}} . \quad (59)$$

By definition, $P_m = P_f + P_{ss}$. Therefore, equation (57) reduces to

$$\left(\frac{a_3}{a_2} \right)^3 (1 + \eta_R \tan \beta) = 1 . \quad (60)$$

Also note that $a_2 = \delta_A R_2$ where R_2 is defined in (49). Equation (49) can be rewritten as

$$\frac{2\gamma}{R_2} = P_m - P_g = P_{\text{crush}}. \quad (61)$$

Substituting (61) into (60) and recalling that $a_3 = \delta R_{cg}$, one finds that

$$P_{ss} = P_{\text{crush}} \left(\frac{\delta_R}{\delta_A} \right) (1 + \eta_R \tan \beta)^{\frac{1}{3}} \quad (62)$$

or

$$P_{ss} = P_{\text{crush}} \left| \frac{\cos(\alpha_R - \beta)}{\cos(\alpha_A - \beta)} \right| (1 + \eta_R \tan \beta)^{\frac{1}{3}}. \quad (63)$$

This is the threshold for the growth of a nucleus by gas diffusion provided that $P_{ss} > P_{ss}^*$ and $P_{\text{crush}} > P_{\text{crush}}^*$.

Before getting into the analysis of the model equations presented here, it is perhaps worthwhile to dwell a bit longer on the concept of a critical crushing pressure. P_{crush}^* is given by equation (47):

$$P_{\text{crush}}^* = P_o \left[\frac{\eta_A \tan \beta}{1 - \eta_A \tan \beta} \right] + \frac{2\gamma \delta_A}{hA}. \quad (64)$$

Solving this for the radius of the crevice mouth gives

$$A = \frac{2\gamma \delta_A}{h} \left[P_{\text{crush}}^* - P_o \left(\frac{\eta_A \tan \beta}{1 - \eta_A \tan \beta} \right) \right]^{-1}. \quad (65)$$

Writing P_{crush}^* as $P_m^* - P_o$, (65) becomes

$$A = \frac{2\gamma \delta_A}{h} \left[P_m^* - P_o \left(\frac{1}{1 - \eta_A \tan \beta} \right) \right]^{-1}. \quad (66)$$

From equation (44) one sees that the second term inside the brackets is simply equal to the final gas pressure, P_g' , inside the nucleus. Using this (66) becomes

$$A = \frac{2\gamma}{h} \frac{|\cos(\alpha_A - \beta)|}{(P_m^* - P_g')}. \quad (67)$$

Apfel²² defines a critical crevice radius for acoustic cavitation as

$$A^* = \frac{2\gamma |\cos(\alpha_A - \beta)|}{(P_L - P_g)} \quad (68)$$

(neglecting vapor pressure). Apfel's P_L and P_g are analogous to P_m^* and P_g' in equation (67). Therefore, the concept of P_{crush}^* in diffusion cavitation is analogous to Apfel's concept of A^* in acoustic cavitation, the only difference being that Apfel considers only full crevices ($h = 1$).

Chapter 3

Analysis of the Critical Radius Approach to the Crevice Model

3-1 Introduction

In this chapter the critical radius approach to the crevice model will be analyzed on the basis of its ability to predict cavitation thresholds. The discussion will include both acoustic and diffusion cavitation and only the crevice model will be considered. In a later chapter other stabilization and nucleation models will be analyzed.

3-2 Application of the Crevice Model to Acoustic Cavitation

The acoustic cavitation threshold of water will be predicted as a function of dissolved gas pressure, surface tension, and temperature. Unless otherwise stated, all theoretical predictions will be based on the critical radius criterion.

3-2.1 The Effect of Dissolved Gas Pressure

Recall equations (31) and (40) from the previous chapter:

$$P_A = P_o - P_v + \frac{2}{3^{3/2}} P_g \left[\left(\frac{P_o - P_v}{P_g} - 1 \right)^3 \left| \frac{\cos(\alpha_R - \beta)}{\cos(\alpha_A - \beta)} \right|^3 \left(\frac{\cot\beta + \eta_R}{\cot\beta - \eta_A} \right) \right]^{1/2} \quad (31)$$

and

$$P_A^* = P_o - P_v - P_g \left(\frac{\cot\beta - \eta_A}{\cot\beta + \eta_R} \right) + (P_o - P_v - P_g) \left| \frac{\cos(\alpha_R - \beta)}{\cos(\alpha_A - \beta)} \right|. \quad (40)$$

These equations are the expressions for the acoustic pressures necessary for the interface to reach the critical radius (R_{cv}) and the receding contact angle, respectively. Equation (40) is essentially the same as

the threshold predicted by the previous formulation of the crevice model.

The dependence of these thresholds on the dissolved gas pressure is explicitly stated. (We shall see later that the dependences on surface tension and temperature are not so explicit.) Recall that P_g is equivalent to the partial pressure that the gas inside the nucleus exerts on the interface in both the saturated and undersaturated (degassed) states. In the absence of gas diffusion, the partial pressure of the gas in an expanding nucleus is less than P_g .

Figures 10a and 10b show the cavitation threshold as a function of dissolved gas content for two representative values of surface tension. These graphs illustrate several important points. First, the two nucleation criteria are equivalent over a short range of gas pressures. This equivalence is difficult to show analytically; however, numerically it is easily demonstrated. Hence for threshold measurements made in these regions, the different criteria give equivalent predictions. The theories diverge on either side of this equivalent region. At no value of gas pressure is the threshold predicted by the critical radius criterion (P_A) less than that predicted by the receding contact angle criterion (P_A^*). In other words, while P_A^* is a necessary condition for nucleation, P_A is both a necessary and sufficient condition for nucleation.

At low gas pressures, the receding contact angle criterion gives a limiting threshold value of between about 6 and 12 bars for the ranges of surface tensions discussed here. The exact values are not important.

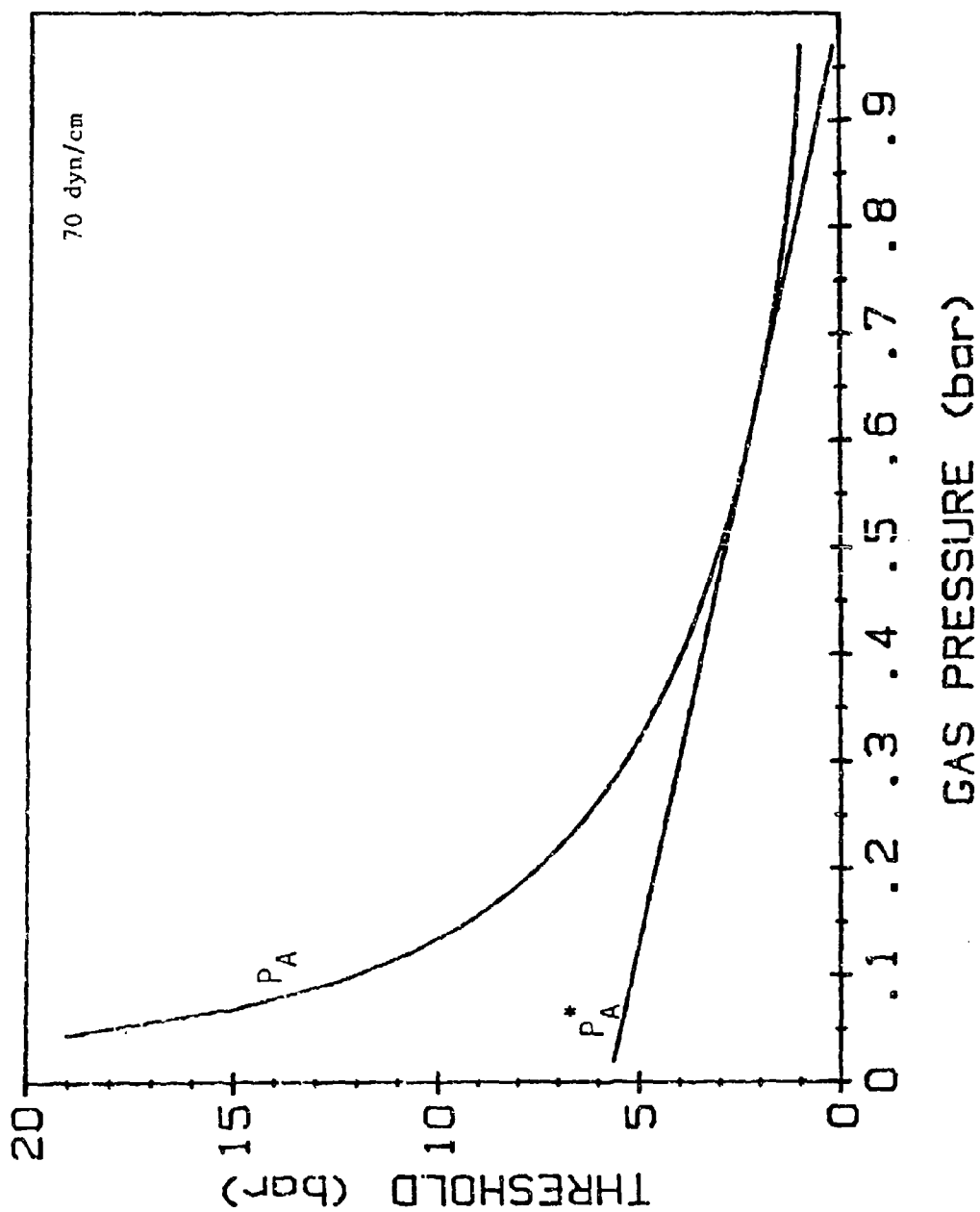


Figure 10a. Theoretical prediction of the cavitation threshold as a function of dissolved gas pressure for a surface tension of 70 dyn/cm.

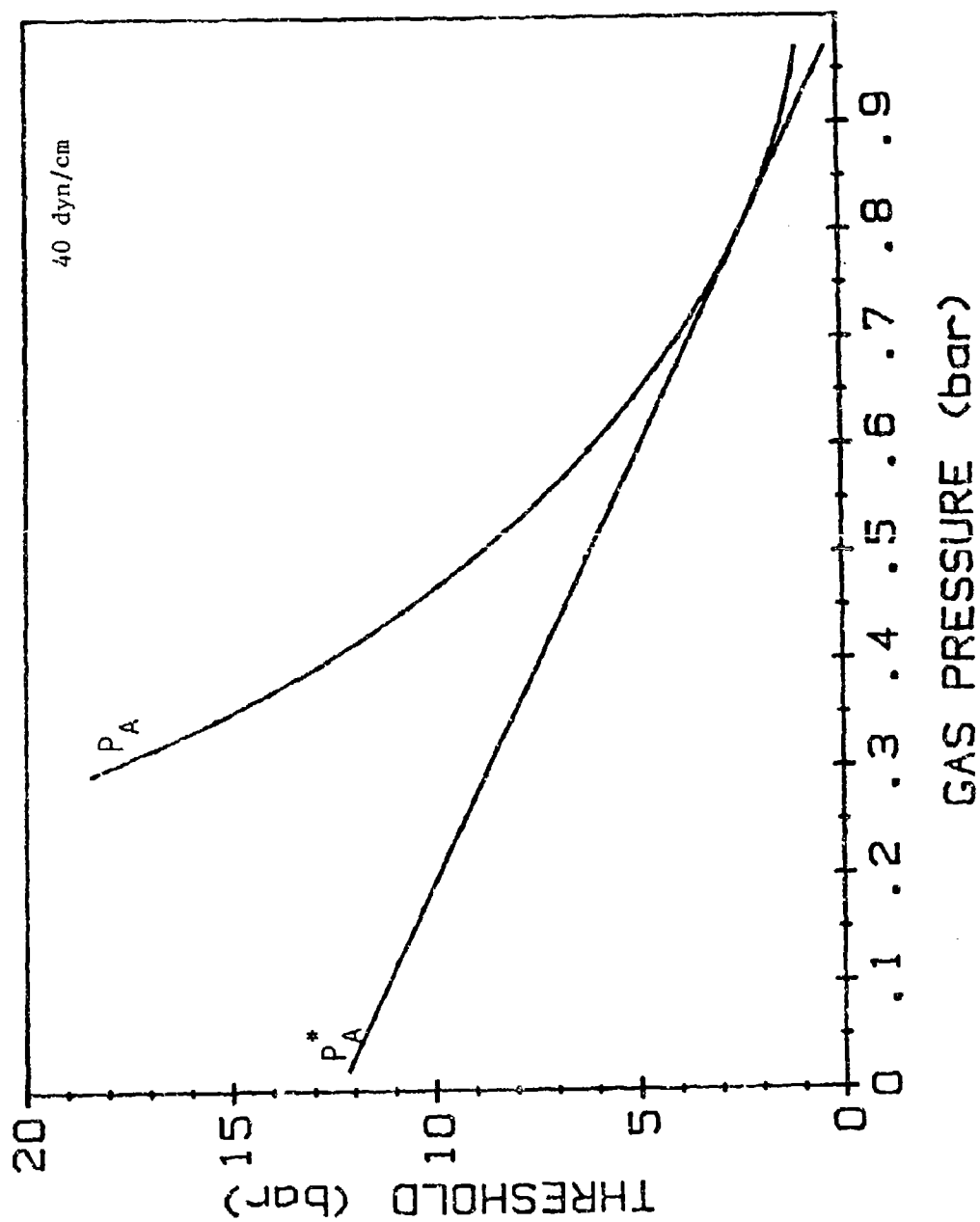


Figure 10b. Theoretical prediction of the cavitation threshold as a function of dissolved gas pressure for a surface tension of 40 dyn/cm.

What is important is that the values are relatively small compared to the threshold for homogeneous nucleation as discussed in the first chapter. This relatively low prediction is not a realistic one. It has been assumed that the nuclei are gas-filled; the fact that prepressurization and variation of gas pressure have experimentally been shown to have an effect on thresholds¹⁶ verifies this assumption of gas-filled nuclei. It follows, therefore, that if all of the gas is removed from the water, that is if the gas pressure is decreased to zero, the nuclei would in effect be removed. Hence, the threshold for completely degassed systems should approach homogeneous nucleation thresholds. This expected behavior is predicted by the critical radius criterion.

Figures 11a and 11b are two graphs of the cavitation threshold versus gas pressure. Plotted are the theoretically predicted thresholds as well as thresholds measured by Strasberg¹⁶, Connolly and Fox¹⁷, and Galloway¹⁸. No attempt has been made to normalize any of the data, although the calibrations of the various experimental systems were based on different standards. Three comparisons are evident. If the "lone" data point at a gas pressure of about 0.1 bar were eliminated, there would appear to be a linear dependence on gas pressure. However, the "lone" data point is not actually "lone". Figure 11b is an expanded version of figure 11a which includes Galloway's data for gas pressures below 0.1 bar. (These are the only data available for these extreme values of gas pressure.) Emphasis should not be placed on the absolute values of his data; thresholds of those magnitudes are uncommon. The trend of the data, however, is important and in good agreement with the

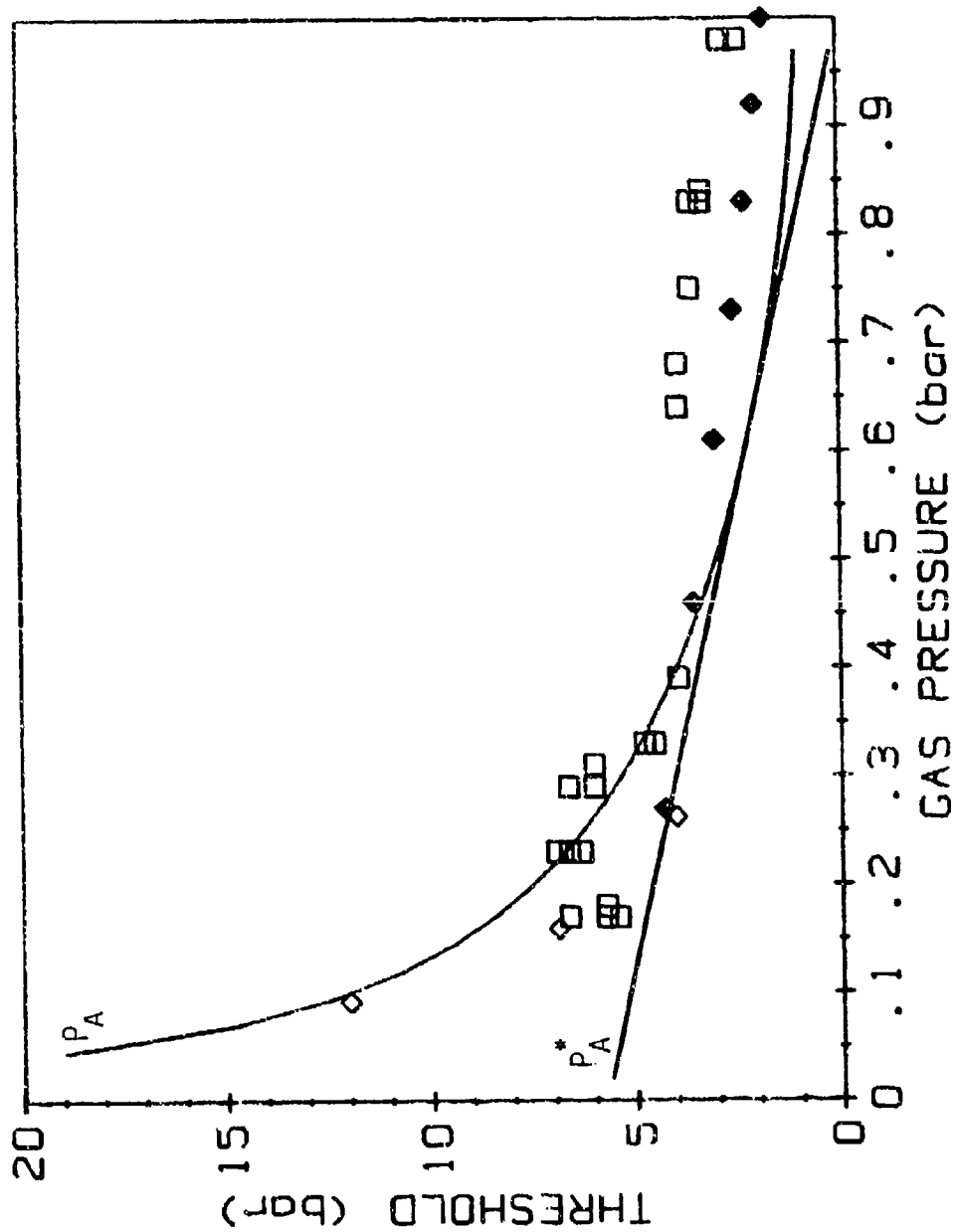


Figure 11a. Graph of threshold versus gas pressure. The data are: Strasberg's (\square), Galloway's (\diamond), and Connolly and Fox's (\diamond).

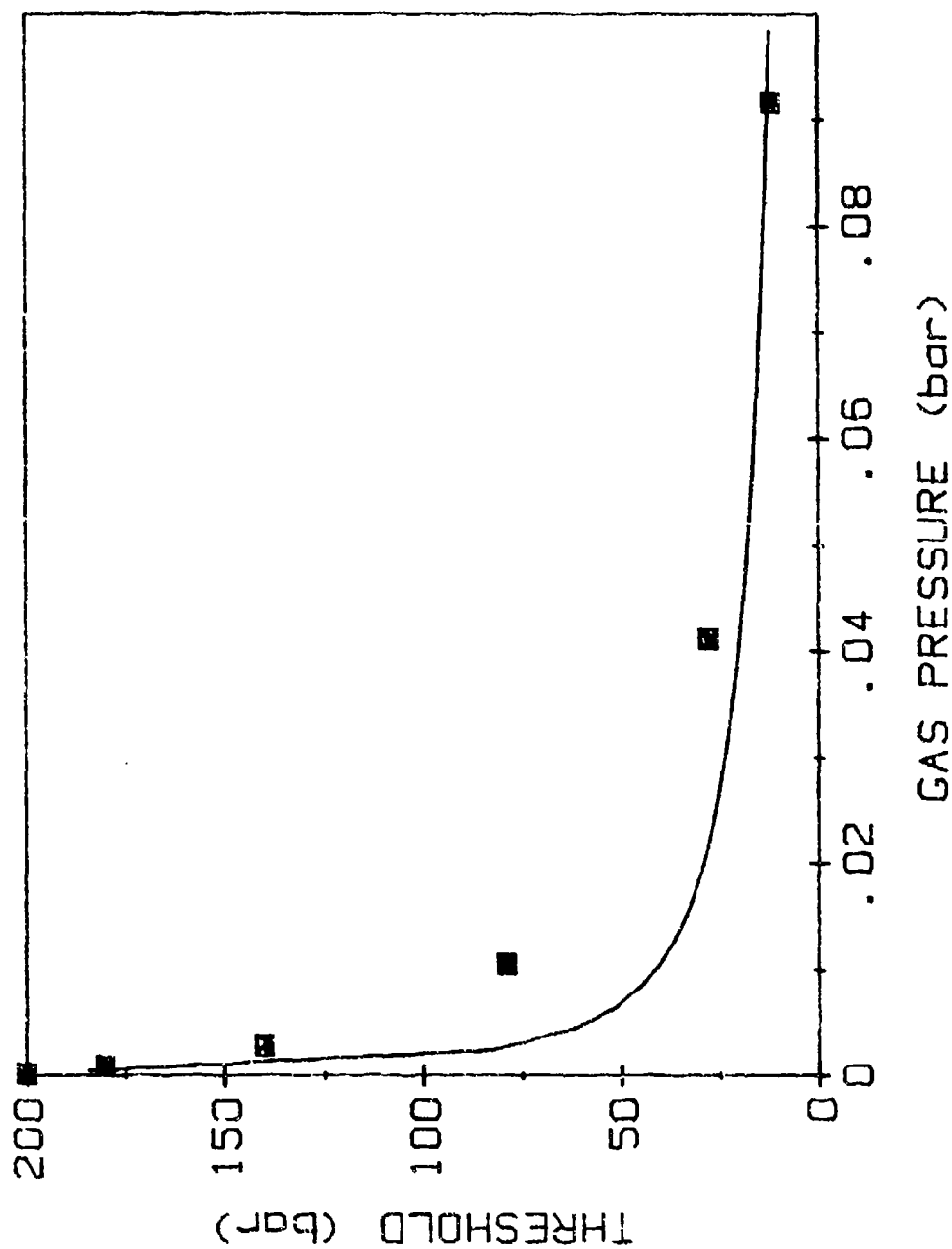


Figure 11b. Graph of threshold versus gas pressure for low gas pressures. The data are Galloway's and the solid line is the prediction of the critical radius approach to the crevice model.

critical radius prediction. It should be pointed out that the limiting value of the threshold as predicted by the receding contact angle criterion differs from the experimental and theoretical values given in figure 11b by well over an order of magnitude.

As shown in figure 10, the receding contact angle criterion predicts a threshold of zero bars for near-saturated solutions. On the other hand, the critical radius criterion predicts a threshold near 1 bar (actually $P_O - P_V$, which is approximately 1 bar for low temperatures). The difference is inherent in the definition of R_{cv} (given by equation 11 of the previous chapter) in that the expression for R_{cv} is valid only for total external pressures ($P_O - P_A$) less than P_V . There is no such restriction on P_A^* . This difference, although forced, should be experimentally verifiable.

Referring to figure 11a, it is seen that the experimental thresholds tend to be about 2 bars for saturated solutions. Although this is in closer agreement with P_A than P_A^* , the discrepancy is troublesome. This discrepancy may result from the fact that the theoretical model does not strictly reproduce the experimental procedure. That is, the lines on the graphs represent the acoustic pressure amplitude necessary for the nucleus to become mechanically unstable. The experimental thresholds are measured values of the acoustic pressure amplitude within the liquid at the time a bubble was detected. It should not be assumed that these two pressure amplitudes are always the same. The process by which a nucleated bubble (or nucleate) becomes a detected bubble is indeed complex, as alluded to at

the close of the first chapter. One factor which can complicate the evolution of a nucleate is gas diffusion into the expanding bubble. This factor is ignored in the theoretical threshold predictions. However, the effects of gas diffusion should diminish as the gas content of the system decreases. This conclusion is consistent with the results shown in figure 11a; there is better agreement between theory and experiment at gas pressures below about 0.5 bar.

A somewhat quantitative explanation of the discrepancy can be made with the use of Apfel's work on acoustic cavitation prediction.³⁵ Apfel defined thresholds for various types of cavitation and uses these definitions to predict which of the types of cavitation will occur under a given set of experimental conditions. The thresholds reproduced in figure 11 were described by the experimenters as corresponding to "transient" cavitation events. If an order of magnitude estimate of the initial radius of a nucleate is made, Apfel's criteria for transient cavitation can be applied to find the pressure amplitude necessary for a nucleate to evolve into a detected bubble. The term "detected bubble" refers to a bubble from which a vaporous cavity can form in the presence of a sound field of sufficient amplitude.

Up to this point little has been said concerning the physical size of the crevice. Apfel²² estimated the radius of a crevice mouth to be about 0.5 μm . Assume that the crevice has a depth equal to its mouth diameter. This results in a crevice volume of about $3 \times 10^{-19} \text{ m}^3$. Let us further assume that the nucleation process deactivates the crevice. By

this it is meant that when the critical radius is reached, the expanding vapor cavity will eventually detach itself from the solid, removing all of the gas from the crevice in the process. Thus, shortly after nucleation, a mostly-vapor-filled cavity exists which contains an amount of gas such that under average conditions (zero acoustic pressure) would have a volume of $3 \times 10^{-19} \text{ m}^3$. Therefore in order to predict the future of this nucleate, we shall examine the evolution of a spherical bubble having that volume, or equivalently, a bubble having an initial equilibrium radius of about $0.4 \text{ } \mu\text{m}$.

Apfel's analysis indicates that a bubble small compared to its resonance radius will become transient when the acoustic pressure amplitude exceeds the Blake threshold. The Blake threshold is the free bubble analogy to the critical radius approach to the crevice model. It is derived by combining the value of R_{cv} with the pressure balance equation for a free bubble. The Blake threshold is

$$P_B = P_0 \left[1 + \frac{4}{9} X_B \left(\frac{3X_B}{4(1+X_B)} \right)^{\frac{1}{2}} \right] \quad (69)$$

where

$$X_B = \frac{2\gamma}{P_0 R_0} \quad (70)$$

Here, R_0 is the equilibrium size of the bubble. Using $P_0=1 \text{ bar}$, $\gamma=70 \text{ dyn/cm}$, and $R_0=0.4 \text{ } \mu\text{m}$, the calculated value of P_B is 2.2 bar . Figure 11a has been reproduced in figure 12 with the exception that P_B is shown instead of P_A^* . The lines intersect at a gas pressure of about 0.6 bar . Below this value P_A is larger and the fit with the data is good in this region. However, above 0.6 bar the prediction of P_A diverges from experiment and it is seen that P_B is a much better predictor. It should

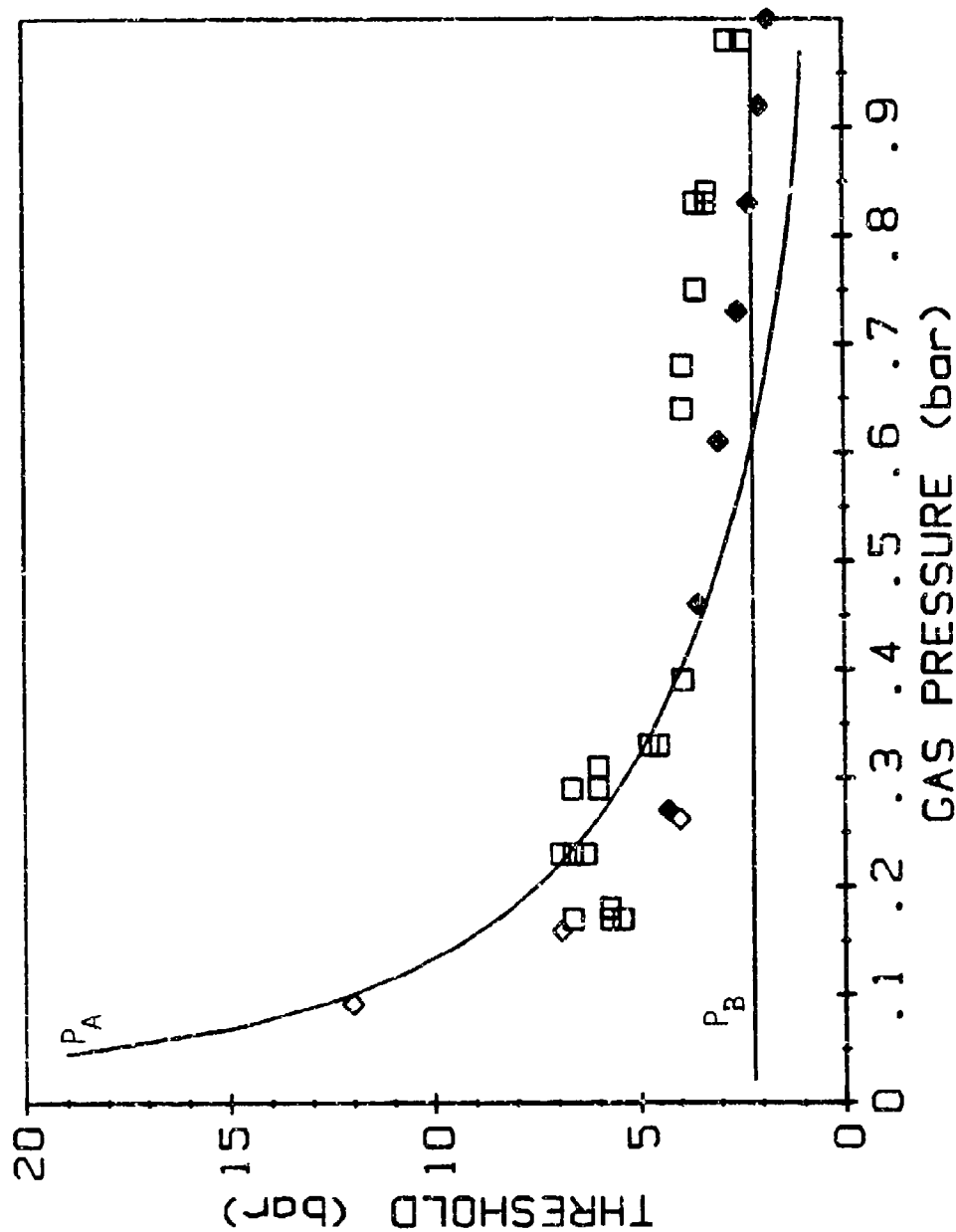


Figure 12. Graph of threshold versus gas pressure. This figure is similar to figure 11a except that the Blake threshold is plotted rather than P_A .

be pointed out that the straight solid line assumes a constant value of R_0 .

This analysis of thresholds near saturation does not prove that the cavitation nucleus is in fact a gas-filled crevice. It is, however, not inconsistent with the hypothesis. It is seen that a gas-filled crevice could give rise to a nucleate which would later grow as a free bubble to a detectable size because the Blake threshold exceeds the crevice model threshold in the near saturation region. For liquids far below saturation, the crevice model is a good predictor of cavitation thresholds. In this region the critical radius criterion appears to be a necessary and sufficient condition not only for bubble nucleation but also for bubble detection.

3-2.2 The Effect of Surface Tension

The functional dependence of the critical radius threshold on the liquid-gas surface tension is not as obvious as with the case of gas pressure. To understand this dependence, we follow the lead of Crum³⁴, who used an empirical relationship discovered by Bargeman and Van Voorst Vader⁴⁰, viz.,

$$\cos \alpha_E = \frac{c}{\gamma} - 1 \quad (71)$$

where α_E is the equilibrium contact angle and c is a constant. For many nonpolar solids c has a value of about 50 dyn/cm. This relationship is valid for surface tensions greater than about 10 dyn/cm. In the analysis given by Crum as well as the one to follow, it is assumed that $\alpha_E = \alpha_A$ and that $\alpha_R = \alpha_A - \alpha_H$, where α_H is the hysteresis contact angle. (Hysteresis is

what gives rise to the asymmetrical shape of droplets sliding down windows.) Using these relationships, the crevice model becomes a model with two adjustable parameters: α_H and β . In the analysis of this model, the sum of these two parameters ($\phi = \alpha_H + \beta$) was held constant. The value of the sum is an arbitrary choice, 35° giving good results. Figure 13 is a graph of threshold versus surface tension. Two sets of data are shown corresponding to two different values of gas pressure. The data are Crum's.³⁴ It is seen that the agreement between theory and experiment is quite good. It should be pointed out that the receding contact angle criterion offers a good fit as well. Thus, while these predictions offer no direct comparison between the two criteria, they do show that the crevice model (in either form) explains the dependence on surface tension quite well.

3-2.3 The Effect of Temperature

Temperature variations affect the cavitation threshold through three measureable parameters: gas content, surface tension, and vapor pressure. The largest variation is associated with the temperature dependence of the dissolved gas content; however, all of the dependencies are taken into account in the following analysis. We examine the temperature dependence of gas pressure first.

Suppose a volume of water is in equilibrium with a gas atmosphere of pressure P_g^0 , the entire system being at temperature T_0 . Then according to Henry's Law, the mole fraction of the gas dissolved in the liquid, X , is given by $X^0 = P_g^0 / K^0$. K is called Henry's Law constant and

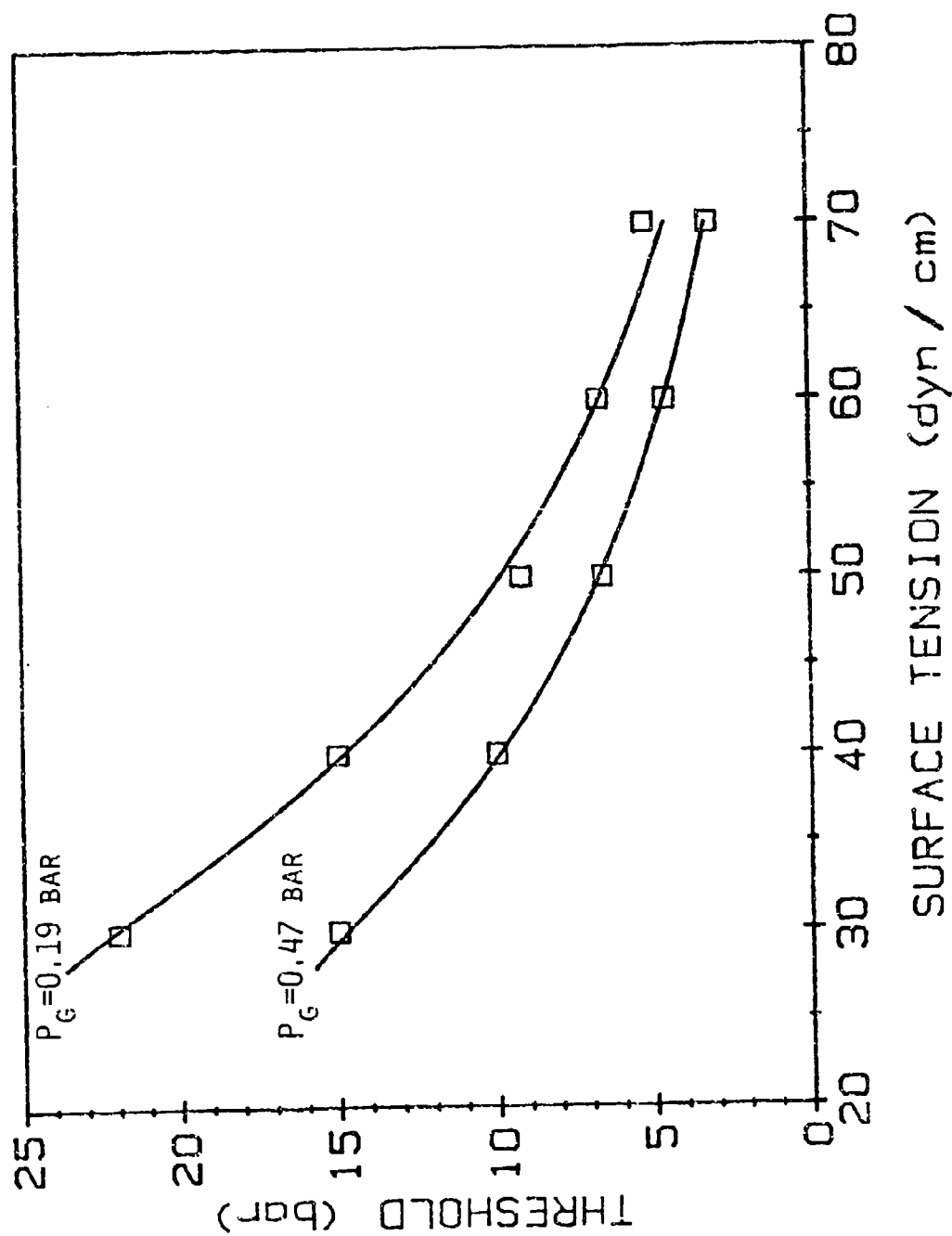


Figure 13. Graph of threshold versus surface tension. The data are Crum's and the solid lines are calculated from equation (31) using $\beta=12.85^\circ$ and $\alpha_H=22.15^\circ$ for $P_g=0.47$ bar and $\beta=10.8^\circ$ and $\alpha_H=24.2^\circ$ for $P_g=0.19$ bar.

is a function of temperature. If the temperature is changed to T , then gas goes into or out of solution until again $X \neq P_g/K$. For large volumes of water, the amount of gas which diffuses into the nucleus is negligible. Thus, the mole fraction can be considered constant and the equilibrium gas pressure at a temperature T becomes

$$P_g(T) = P_g^0 \frac{K(T)}{K^0} \quad (72)$$

where the temperature dependence is indicated.

In order to evaluate this dependence, data taken from the International Critical Tables⁴¹ for the variation of K with temperature, were fit, using a least squares method, to a third degree polynomial, viz.,

$$K = (3.24 \times 10^7) + (9.59 \times 10^5) T - (2.17 \times 10^3) T^2 - 2.59 T^3. \quad (73)$$

The units of K are bar per mole of gas per mole of water. T is measured in degrees C. The coefficient of correlation of this fit is 0.999. Figure 14a is a graph of K versus temperature. In the temperature range of interest, the fit is indeed quite good. The initial value of K , K^0 , is calculated from a knowledge of the initial gas pressure and the temperature at which the sample was degassed.

Although analytical expressions for the temperature dependence of surface tension exist, in this analysis we chose to employ a least squares fit of values for the surface tension of water taken from the CRC Handbook of Chemistry and Physics (56th edition).⁴² A second degree polynomial least squares fit was used, viz.,

$$\gamma(T) = 75.65 - 0.142 T - (2.63 \times 10^{-4}) T^2. \quad (74)$$

Surface tension is in dyn/cm and temperature in degrees C. The

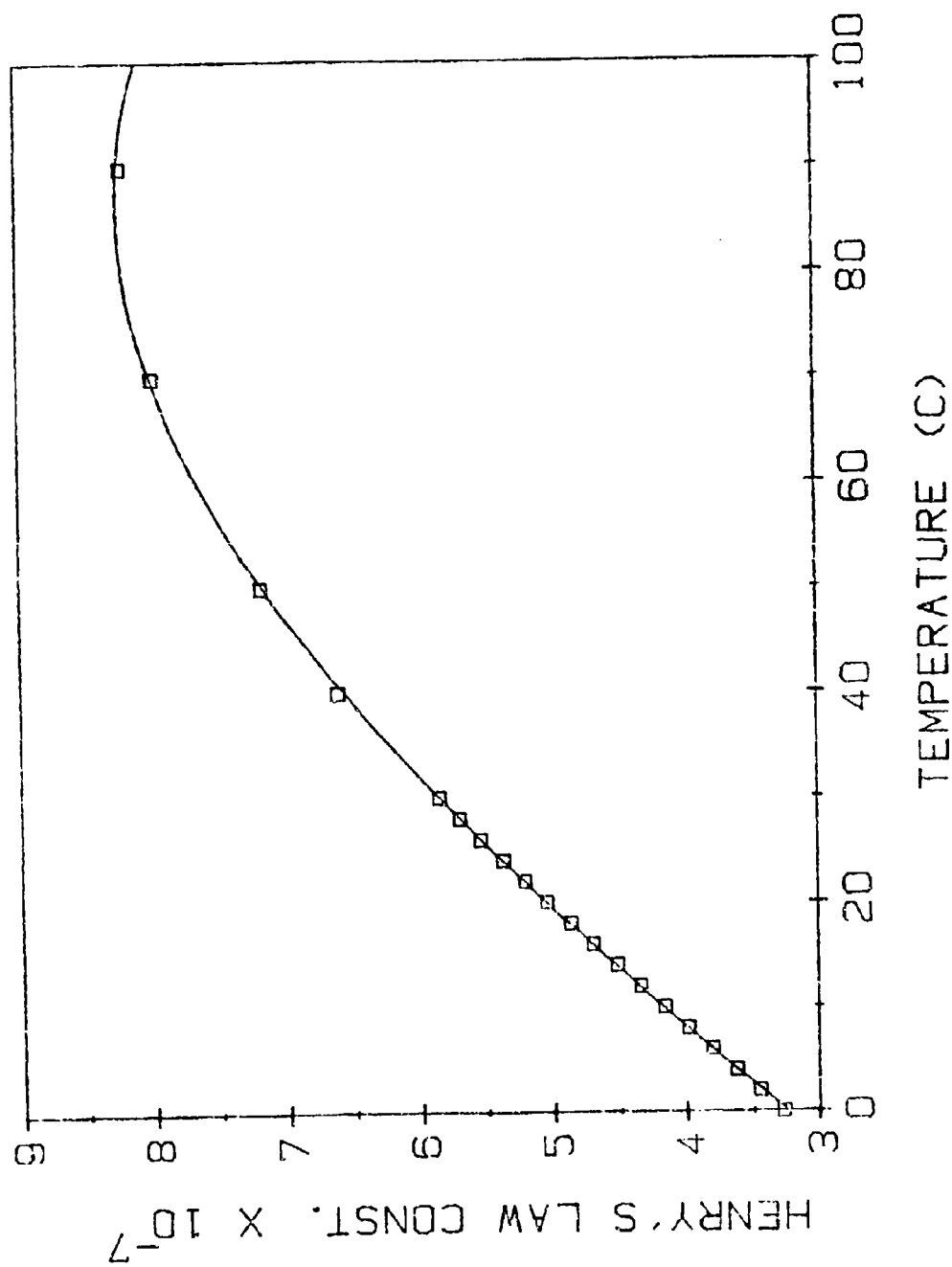


Figure 14a. This figure illustrates the polynomial used to determine Henry's law constant as a function of temperature. The open squares are data from reference 41.

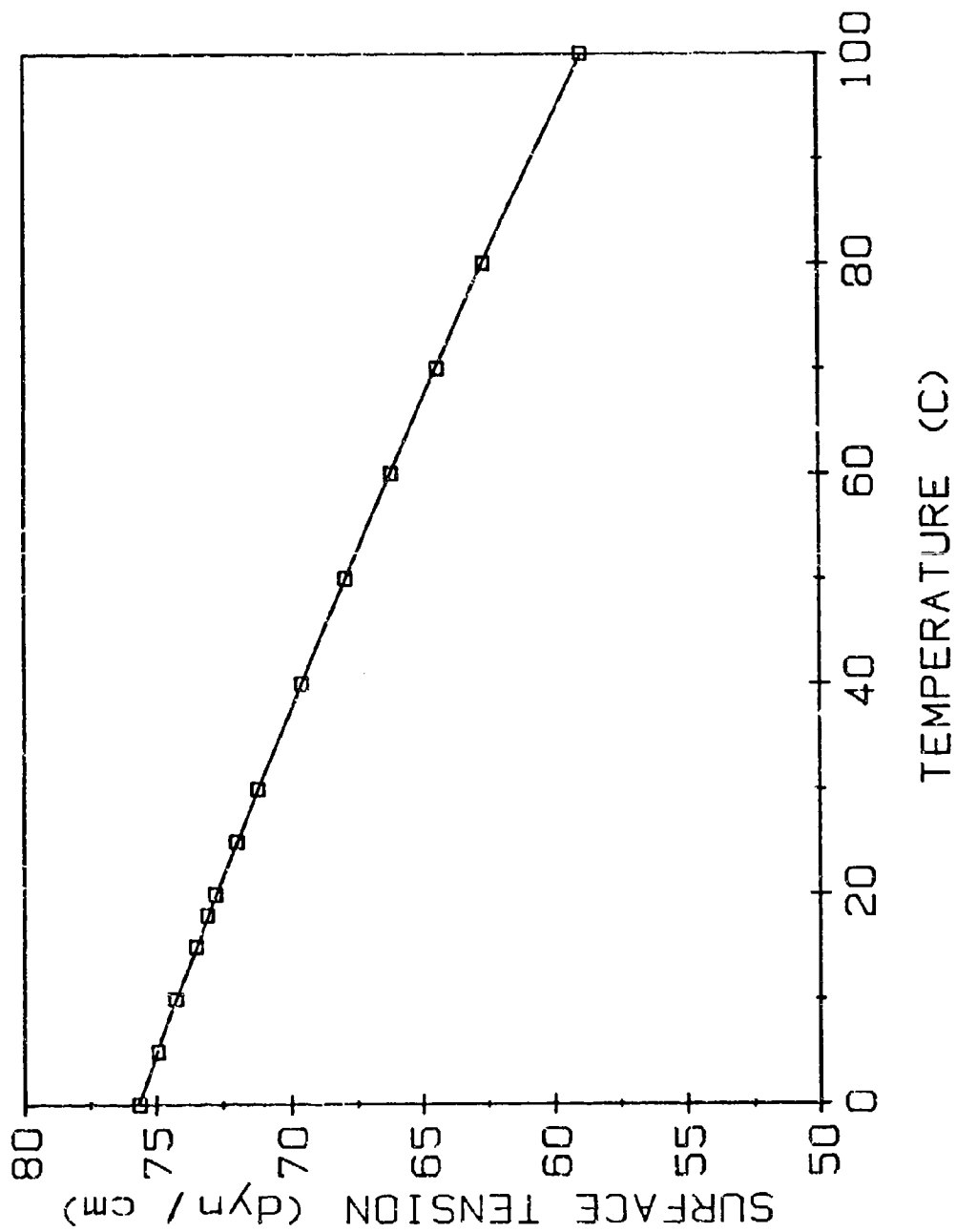


Figure 14b. This figure illustrates the fit of the polynomial equation used to determine the variation of the surface tension of water with temperature. The open squares are data taken from reference 42.

coefficient of correlation is 0.999. Figure 14b displays the data and least squares fit for the surface tension dependence on temperature.

The final temperature variation to be considered is that due to vapor pressure. For this parameter, an analytical expression was used. The expression is that of Osborne and Meyers⁴³.

$$\log P_v = A + \frac{B}{T_A} + \frac{CX}{T_A} \left(10^{DX^2} - 1 \right) + E \left(10^{FX^{\frac{5}{4}}} \right) \quad (75)$$

where

| | |
|--------------------------------------|------------------------------|
| T = temperature in degrees Celcius | $C = 1.3869 \times 10^{-4}$ |
| T_A = absolute temperature | $D = 1.1965 \times 10^{-11}$ |
| $X = T_A^2 - K$ | $K = 2.937 \times 10^5$ |
| $Y = 374.11 - T$ | $E = -0.0044$ |
| $A = 5.4267$ | $F = -5.715 \times 10^{-3}$ |
| $B = -2005.1$ | |

According to Eisenberg and Kauzmann⁴³, this expression is accurate to within five parts in 10^4 .

The cavitation threshold is plotted as a function of temperature for a range of dissolved gas pressures in figure 15. The open squares represent Galloway's data and the solid squares represent Crum's data. The solid lines represent the threshold as predicted by the critical radius criterion for $\beta = 12.85^\circ$ and $\beta + \alpha_H = 35^\circ$. The data have been normalized to fit the theory at room temperature (23°C). The variation with temperature is predicted well by the crevice model employing the critical radius criterion. Although there are no data to test the theory above 50°C , the threshold must approach the vapor pressure at the boiling point. This behavior is suggested by the "tail" at high

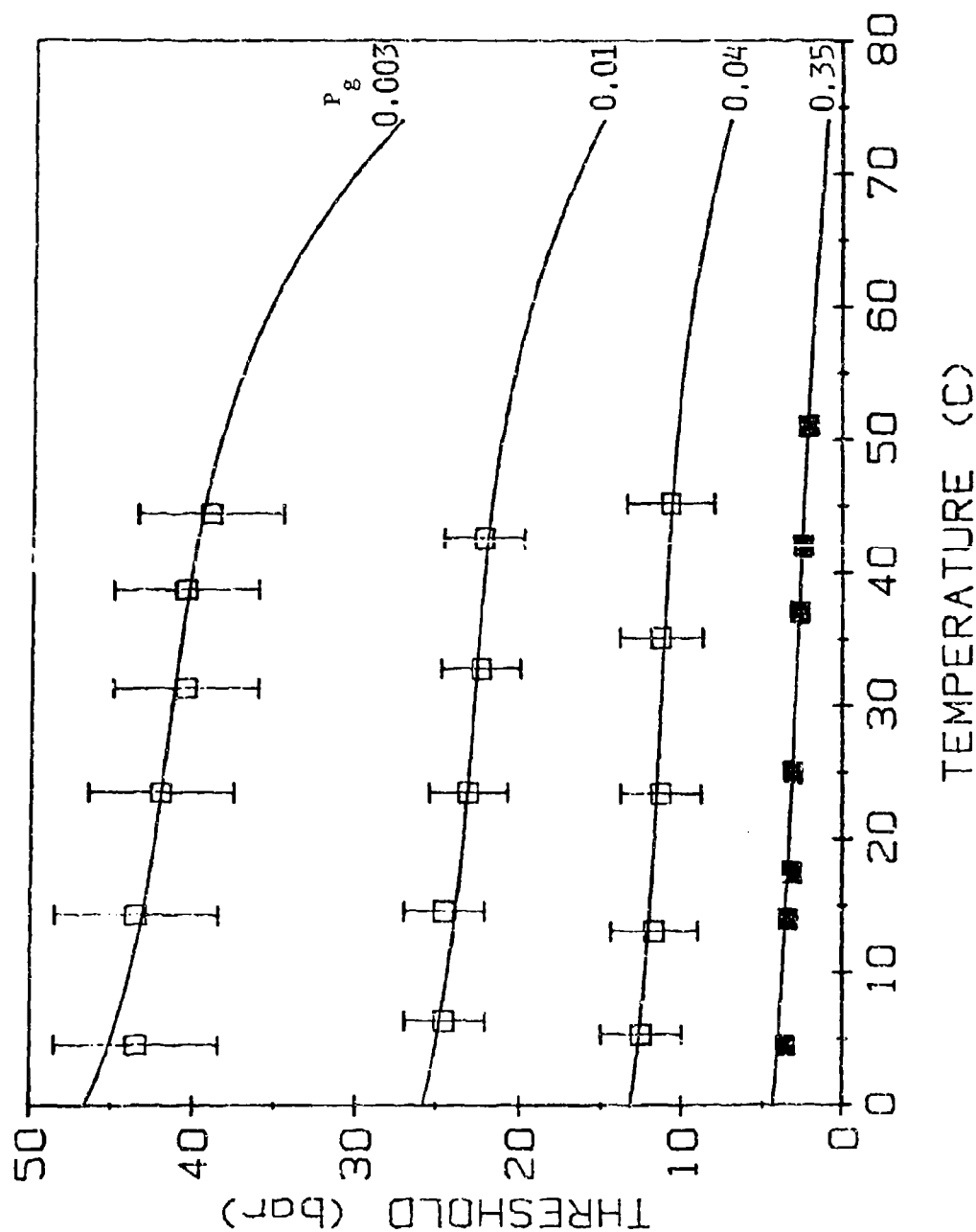


Figure 15. Graph of threshold versus temperature. The data are Galoway's (\square) and Crum's (\blacksquare) and have been normalized to fit the theory at room temperature. The solid lines are calculated with equation (31) using $\beta=12.85^\circ$ and $\alpha=22.15^\circ$.

temperatures.

3-2.4 Comments on Sensitivity

It was shown that the critical radius approach to the crevice model provides a good explanation of acoustic cavitation thresholds. However, all of these predictions have been made a posteriori. That is, values of β and ϕ were chosen to provide the best fit to the data. For the majority of the analysis, β was chosen to be 12.85° and $\phi = 35^\circ$. The exception was the prediction of threshold versus surface tension (figure 13) for $P_g = 0.19$ bar. For this line $\beta = 10.8^\circ$, yet ϕ remained equal to 35° . The model is very sensitive to changes in β . Figure 16a shows theoretical predictions of threshold versus surface tension. In each line, the parameter ϕ is constant and equal to 35° . For the middle line, $\alpha_H = 22.15^\circ$ and $\beta = 12.85^\circ$. These are the same parameters for the $P_g = 0.47$ bar prediction in figure 13. The upper curve is for $\alpha_H = 21.15^\circ$, $\beta = 13.85^\circ$; the lower curve is for $\alpha_H = 23.15^\circ$, $\beta = 11.85^\circ$. Figure 16b is similar to figure 16a, however, in this figure $\alpha_H = 22.15^\circ$ for all the curves and $\beta = 12.85 \pm 1^\circ$ for the middle, upper and lower curves respectively. In figure 16c, $\beta = 12.85^\circ$ and $\alpha_H = 22.15 \pm 1^\circ$ for the middle, upper and lower curves, respectively.

It is seen that varying α_H has little effect. However, variation of β produces a large change in predicted thresholds. This is unfortunate. It means that extremely accurate a priori predictions of cavitation thresholds are not possible. However, the purpose of this research is not to predict cavitation thresholds, per se, but to

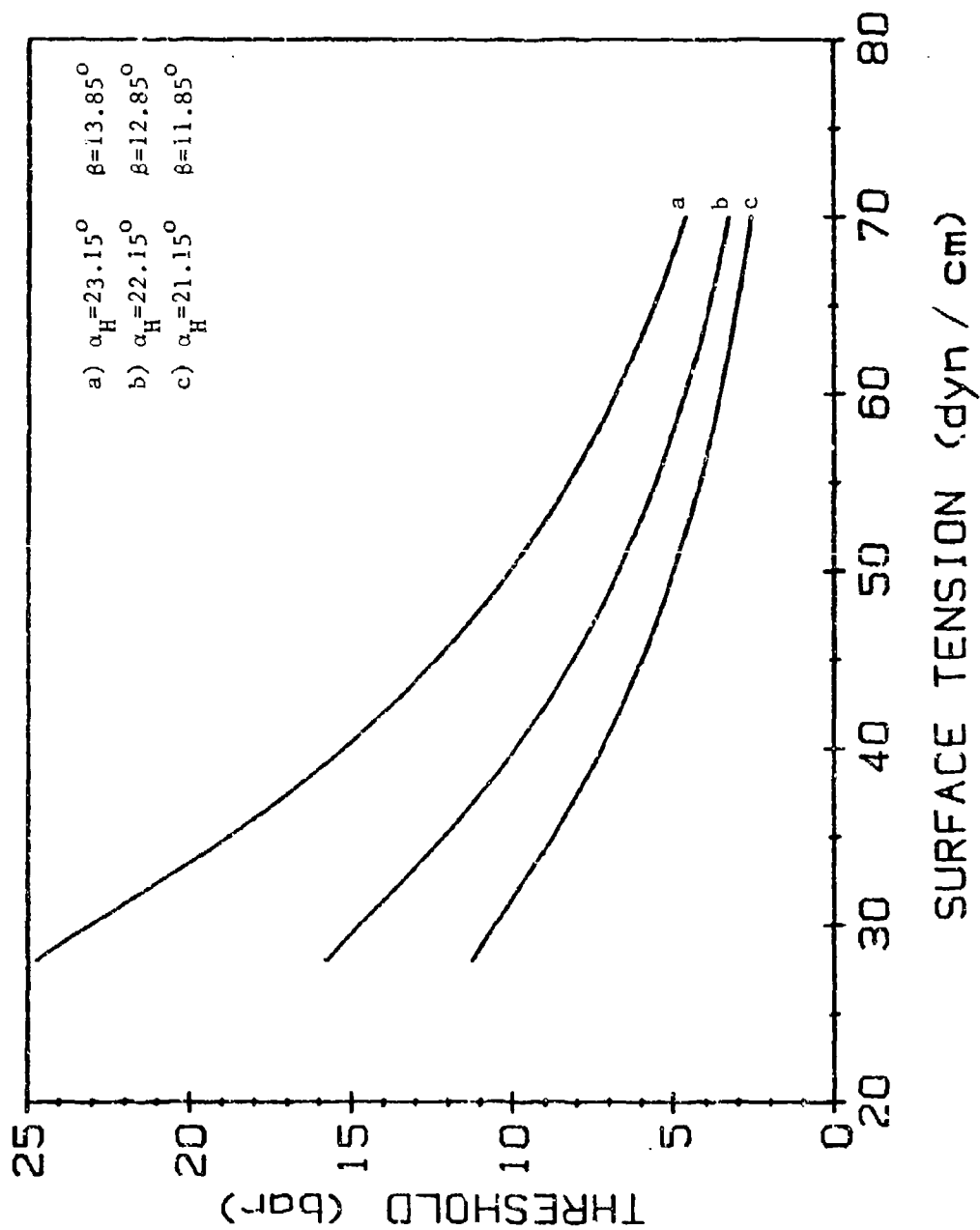


Figure 16a. Graph of threshold versus surface tension illustrating the sensitivity of equation (31) to various parameters.

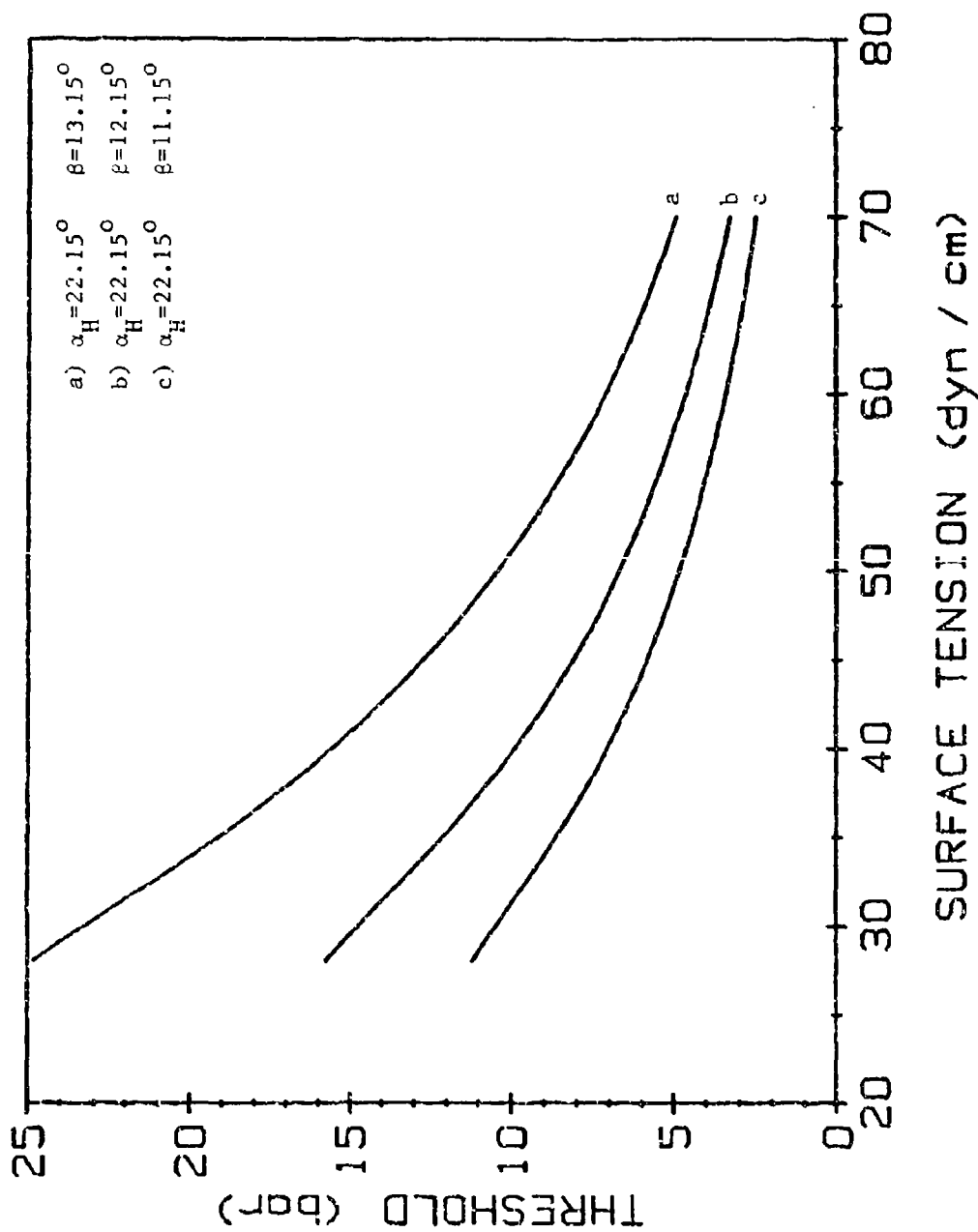


Figure 16b. Graph of threshold versus surface tension illustrating the sensitivity of equation (31) to changes in various parameters.

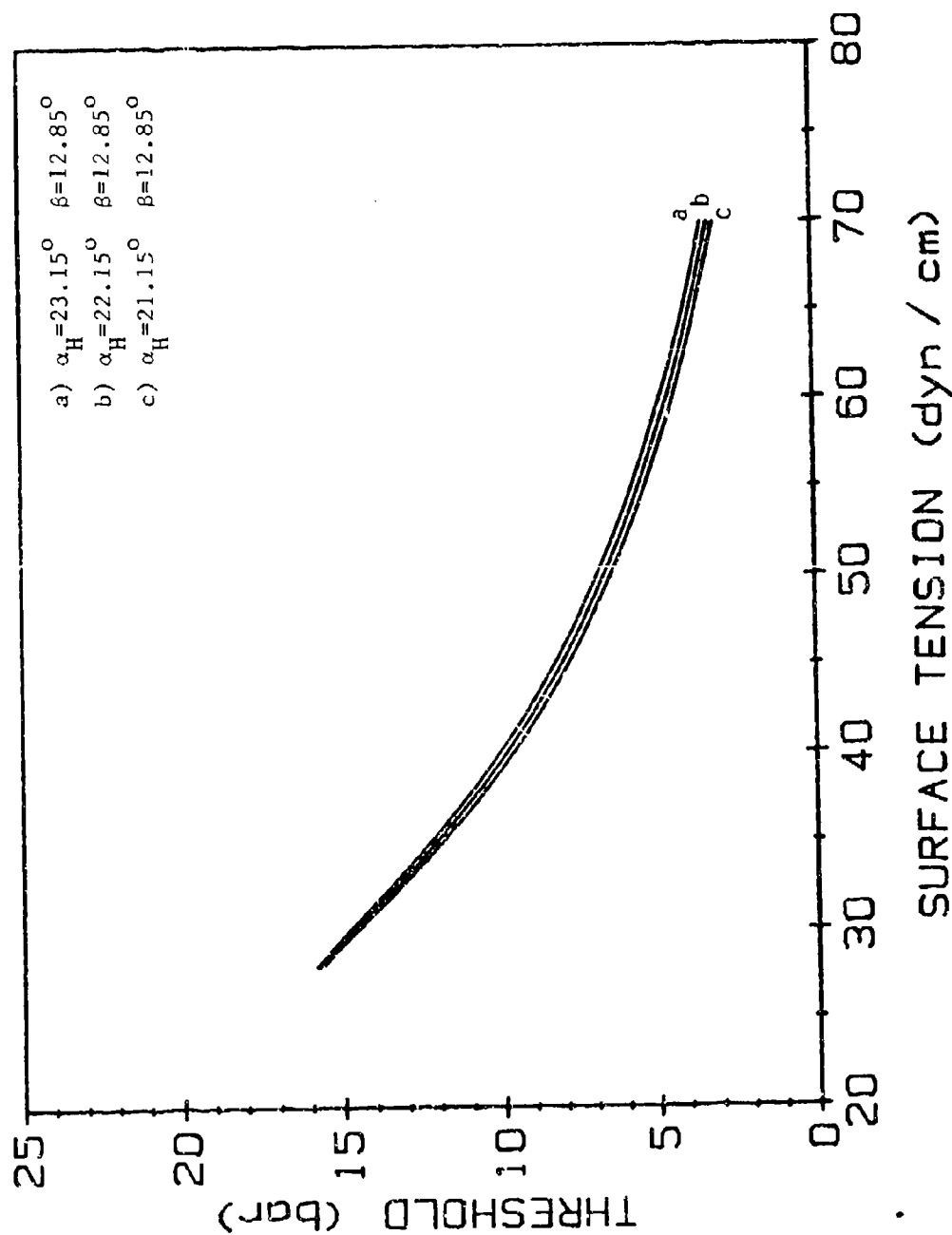


Figure 16c. Graph of threshold versus surface tension illustrating the sensitivity of equation (31) to changes in various parameters.

identify possible candidates for the cavitation nucleus. The degree to which the a posteriori predictions agree with measured values indicate that the crevice model is, indeed, a plausible nucleation model for acoustic cavitation. In addition, even in the worst case, using typical values of the parameters, a priori predictions of the cavitation threshold can be made that disagree with measured thresholds by no more than a factor of two.

3-3 Application of the Crevice Model to Diffusion Cavitation

The analysis presented in this section is unique; it is the first attempt, that we know of, at applying the crevice model to diffusion cavitation. Reference will be made to the diffusion cavitation data published by Yount²⁶, an example of which was reproduced as figure 4. Yount has explained his data in terms of the varying-permeability organ skin model. The variation of the permeability is necessary to account for the change in slope of the isopleths for the various numbers of bubbles. This change in slope is something which Yount claims is inexplicable in terms of the crevice model. The version of the crevice model to which Yount is referring to is the previous formulation. An explanation of this phenomenon can be provided employing the revised crevice model.

As pointed out in the previous chapter, the concept of P_{crush}^* is analogous to that of a critical size of a crevice. Yount also uses P_{crush}^* to mean the crushing pressure at which the organic skin becomes impermeable. Drawing an analogy between the two definitions of P_{crush}^* ,

we can say that the crevice model analogy of a permeable/impermeable transition is the interface reaching the advancing contact angle. Equation (63) was derived for crushing pressures greater than P_{crush}^* ; i.e., it is analogous to a process in Yount's impermeable region. For crushing pressures less than P_{crush}^* , equation (63) becomes

$$P_{ss} = P_{crush} \left| \frac{\cos(\alpha_R - \beta)}{\cos(\alpha - \beta)} \right| (1 + \eta_R \tan \beta)^{\frac{1}{3}}. \quad (76)$$

The only difference between equations (63) and (76) is that in equation (76), the interface is at an angle α and not the advancing contact angle α_A . Moreover, $90^\circ \leq \alpha - \beta \leq \alpha_A - \beta$, which means that $|\cos(\alpha - \beta)| \leq |\cos(\alpha_A - \beta)|$. Hence, $d(P_{ss})/d(P_{crush})$ is greater when the crushing pressure is less than P_{crush}^* . This result is consistent with Yount's findings.

In the experiments described by Yount, bubbles were formed in gelatin samples which had an average surface tension of about 53 dyn/cm. Using equation (71), one finds that the advancing contact angle for this surface tension is around 93° . It can be seen from geometrical considerations that for stability $\alpha_A > \frac{\pi}{2} + \beta > \alpha_R$. Therefore, if $\alpha_A = 93^\circ$, the crevice half-angle must be between zero and three degrees. Crevices with half-angles greater than 3° are unstable and become deactivated (thoroughly wetted). For the calculations to follow, β was assumed to be 1° ; the crevice has become a narrow crack. For such a narrow crevice with an advancing contact angle close to 90° , one would expect that the hysteresis angle would be small; assume it to be 3° . A typical value of P_{crush}^* is about 8 bars.²⁶ Solving equation (47) for

the product hA and using these values for the various parameters, one finds that hA is about 6 nm. One possible interpretation of this result is that the nucleus is located at the bottom of a deep, narrow crevice. For $P_{\text{crush}} < P_{\text{crush}}^*$, one finds from equation (76) that $d(P_{\text{ss}})/d(P_{\text{crush}})$ is between 0.5 and 1; for $P_{\text{crush}} \geq P_{\text{crush}}^*$, $d(P_{\text{ss}})/d(P_{\text{crush}}^*)$ is about 0.5. These values are reasonably consistent with measured values.²⁶ The main difference is that the data show a range of slopes for $P_{\text{crush}} > P_{\text{crush}}^*$ from about 0.2 to 1. The crevice model result is within this range. This discussion is illustrated in figure 17. The predictions shown in this figure are reminiscent of those in figure 4.

The results of these calculations are very sensitive to the chosen parameters and more work needs to be done on these concepts. The size of the nucleus involved with these processes is very small and it is possible that some phenomenon not taken into account in this model may well become important at these small sizes. However, two points have been made. First, the crevice model can explain the change in slope of the isopleths. Second, the calculated values of the slopes are reasonable. Perhaps one final comment is appropriate. Yount and others have carried out an extensive microscopic investigation of bubble formation nuclei,⁴⁴ about which more will be discussed later. The investigators make the statement "In no case have we observed a gas phase embedded in a crevice, as would be required by the crevice model..." This absence is exactly what one would expect according to

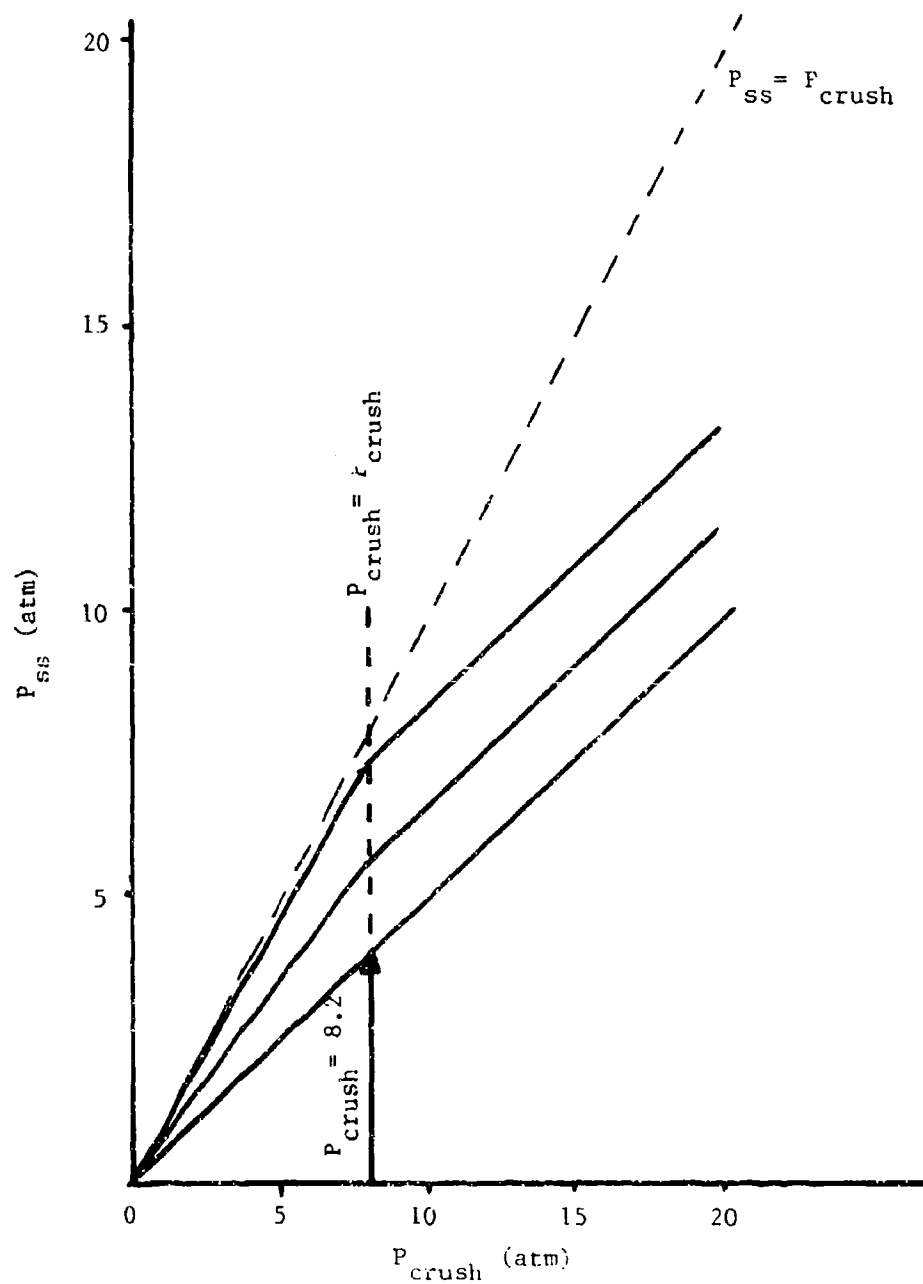


Figure 17. Plot of P_{ss} versus P_{crush} illustrating the change in slope at $P_{crush} = P_{crush}^*$ as predicted by the crevice model.

the argument given above, which showed that the gas phase should be very small and located at the bottom of a deep narrow crevice.

As has just been shown, the critical radius approach to the crevice model offers an explanation of results of both acoustic and diffusion cavitation experiments. There are, however, other nucleation models and they are taken up next.

Chapter 4

Other Candidates for the Cavitation Nucleus

4-1 Introduction

The previous chapters have been devoted to the critical radius approach to the crevice model. It was shown that, based upon its a posteriori predictive powers, it is a plausible nucleation model. There are, however, alternative models and this chapter is devoted to them. It was stated in the introduction that only two other nucleation models are considered feasible. One is the ionic skin model of Akulichev²⁰ and the other is the organic skin model most recently advanced by Yount.²⁸ In this chapter, these models will be analyzed to determine whether or not they really are plausible models.

4-2 Ionic Skin Model

The ionic skin model proposed by Akulichev was reviewed in the first chapter. That review is adequate for this analysis and the reader should refer back to it if necessary. The strongest evidence that Akulichev presents in support of his model is the increase in threshold with decreasing ion concentration. This behavior must exist if his model is feasible. It is to this behavior that we direct our attention.

Two points become evident upon investigating Akulichev's work. First, the lower limit of the concentrations used in his experiments was

about 1 mmol/l. In fact, he published only two data points below this concentration, one at about 0.6 mmol/l and the other about 0.3 mmol/l. Second, his conclusions about thresholds for concentrations below 1 mmol/l are based upon extrapolations of trends present at higher concentrations, not upon experimental measurements. (Refer to figure 1.) In an effort to extend this lower limit and experimentally determine the influence of the dissolved ion concentration on the cavitation threshold, we performed a series of measurements of the effect of ions on the cavitation threshold. The details of this experiment are presented in the appendix; only those details necessary for the present discussion will be mentioned here.

Figures 18a and 18b represent typical results of the experiment. It should be pointed out that zero on the abscissa corresponds to a concentration of 1 mmol/l. The data in the figures have been normalized to the threshold value at the lowest concentration. The experimental scatter is such that no strong conclusions can be drawn about the possible fine structure present in the data. However, one conclusion can be made. The threshold does not increase monotonically with decreasing concentration. On the contrary, in every set of measurements made, the trend is for the threshold to decrease. It is true that no direct comparison of these data and Akulichev's is possible because the experiments were performed at different dissolved gas concentrations. However, it is not at all clear why this difference in gas content should alter the results so as to produce the opposite behavior. It may, therefore, be concluded that the nuclei of the cavitation detected

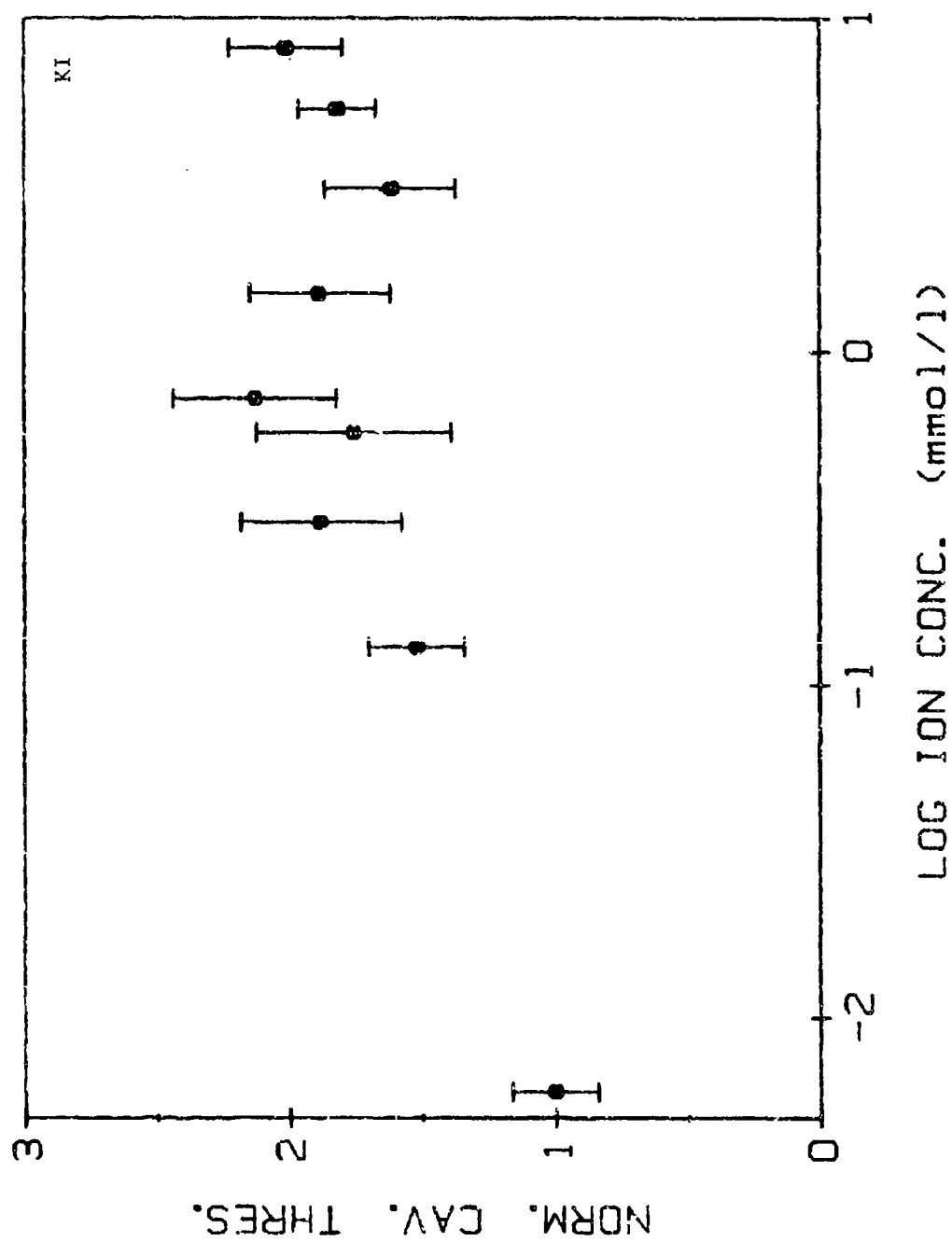


Figure 18a. Graph of normalized cavitation threshold versus the log of the dissolved ion concentration for KI.

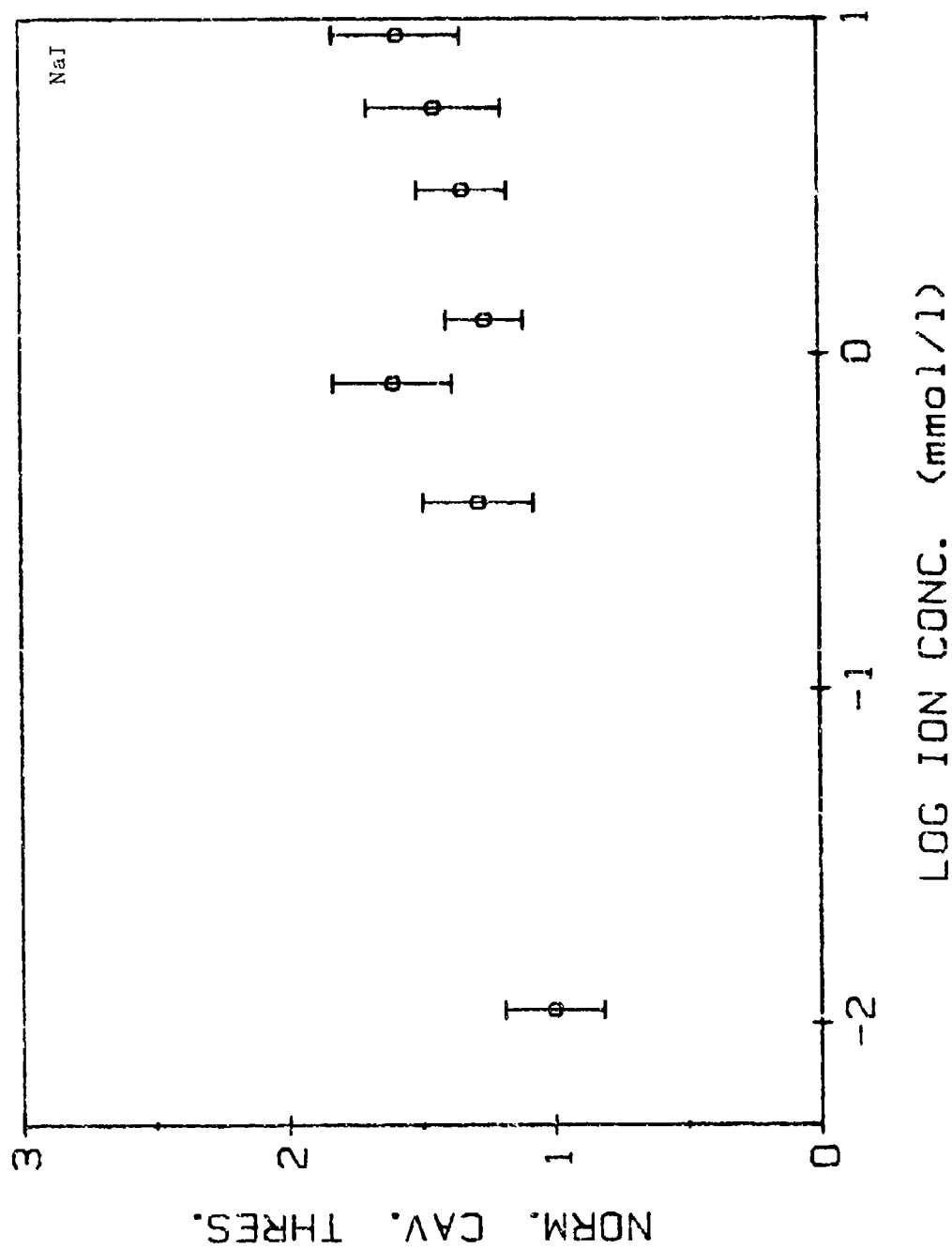


Figure 18b. Graph of the normalized cavitation threshold versus the log of the dissolved ion concentration for NaI.

in our experiments were not ionically stabilized.

Although not statistically significant, there is a recurring trend in all of the data for the threshold to reach a maximum value at a concentration of about 1 mmol/l. This behavior is reminiscent of the trend in Akulichev's data. It is an interesting observation and it makes theoretical analysis more difficult. This trend leads to a second conclusion that can be drawn from the ion data. The dissolved ion concentration does, in fact, influence the cavitation threshold. This influence is, perhaps, not a simple one and it appears that it is not attributable to a purely ionic skin. The trend in the data may indicate a transition region, above which one type of nucleus is predominant and below which a second, different, type of nucleus is the predominant cause of the cavitation. For example, the cavitation detected at concentrations above 1 mmol/l may, in fact, be due to Akulichev's nuclei. Decreasing the concentration would increase the threshold of these nuclei. However, the decrease in concentration may decrease the threshold of some other type of nucleus so that it is able to produce a bubble at a lower threshold than an Akulichev nucleus. This statement is speculative but plausible.

4-3 Varying-Permeability Model

In section 3-3, the crevice model was applied to diffusion cavitation, a process which had been explained, almost exclusively in terms of the organic skin model²⁸. In this section, the organic skin model will be applied to acoustic cavitation, a process which has been

explained well in terms of the crevice model. The dependence on dissolved gas pressure will be discussed first.

In order to determine the variation in the acoustic cavitation threshold with dissolved gas pressure based upon an organic skin nucleus, it must first be determined how such a nucleus is affected by the degassing process. The degassing of a liquid is generally accomplished in the following manner. The atmosphere surrounding the liquid is evacuated to a certain pressure, say P_d ("d" for degassing pressure). This is equivalent to the decompression phase of Yount's experiments. The liquid comes to equilibrium with the atmosphere so that the dissolved gas pressure P_g equals P_d . At this point the ambient pressure is returned to atmospheric pressure, which is equivalent to the compression phase of Yount's experiments. The measurements are then made before the liquid has enough time to come back into equilibrium with the atmosphere. The process just described is a Yount experiment in reverse; the decompression phase occurs first, then the equilibration phase, and finally the compression phase. Therefore, in order to determine the effect of gas pressure, the effect that the degassing process has on the radius of the nucleus must be determined. Since the changes in pressure are always less than one atmosphere, the skin can always be considered permeable.

Assume that a varying-permeability (V-P) nucleus with an initial radius R_0 is degassed to a pressure P_d . This decompression is governed by equation (19c) of reference 26, viz.,

$$2(\gamma_c - \gamma) \left[\frac{1}{R_d} - \frac{1}{R_0} \right] = P_d - P_0. \quad (77)$$

(The notation has been altered.) γ_c is called the skin compression. The decompression results in the liquid being supersaturated, so the nucleus will grow by diffusion if the final radius R_d exceeds R_{cg} . Using this criterion along with the preceding equation, one finds that the largest radius which a nucleus can have and survive degassing (i.e. will not grow by diffusion) is

$$R_o = \frac{2\gamma}{P_{ss}} \left[\frac{\gamma_c - \gamma}{\gamma_c} \right]. \quad (78)$$

According to the V-P model, the following relationship exists among γ_c , γ and R_o :

$$\gamma_c = \gamma + \frac{bR_o}{2}. \quad (79)$$

(The variable b is the same as beta in reference 26.) b is a variable which depends upon thermodynamic considerations but is constant for a given sample. For the experiments discussed by Yount it has a value of about $1.43 \times 10^5 \text{ N/m}^2$. Substituting equation (79) into (78) gives

$$R_o = 2\gamma \left[\frac{1}{P_{ss}} - \frac{1}{b} \right]. \quad (80)$$

Following the decompression, the liquid eventually comes to equilibrium with the reduced atmosphere. It is not clear exactly what the response of the nucleus will be to this equilibration. However, two possible extreme cases can be discussed. The first case is one in which the equilibrium radius, R_e , is the same as the degassed radius, R_d . In order for this to be the actual case, enough additional surfactant molecules must be adsorbed onto the skin to stabilize the skin at this radius. The second extreme case is one in which the nucleus shrinks back to its initial radius, R_o . In this case it is

assumed that no additional surfactant molecules attach themselves to the skin. Moreover, one would not expect any molecules to leave the skin during the decompression. Hence, since the skin consists of the same number of molecules the nucleus should be stabilized at the same radius, namely, R_0 .

In either case, during the subsequent compression back to P_0 , the nucleus should obey the relationship²⁶

$$2(\gamma_c - \gamma) \left[\frac{1}{R_f} - \frac{1}{R_e} \right] = P_0 - P_g \quad (81)$$

where R_f is the final radius after compression, R_e is the equilibrium radius (either R_0 or R_d), and P_g is the dissolved gas pressure in the liquid and equal to P_d . Comparing equations (77) and (81), it is easily seen that if the first case is true ($R_e = R_d$) then $R_f = R_0$. If the second case is true then it can be shown from equations (79) and (81) that

$$R_f = R_0 \left[1 + \frac{P_0 - P_g}{b} \right]^{-1} \quad (82)$$

The compressed nucleus will be supersaturated so gas will diffuse out of it; however, this diffusion does not result in a change in radius (see equation 16 of reference 26). Now that the response of a V-P nucleus to the degassing process is known, it must be determined how such a nucleus will react to an applied acoustic field. Previously, it was stated that a V-P nucleus will grow during degassing if its radius exceeds R_{cg} . This criterion is consistent with the derivation of the V-P model (see equation 17a of reference 26). Therefore, one would expect that such a nucleus will grow in an acoustic field when the radius exceeds R_{cv} (if

$P_A < P_0 - P_v$). This criterion is given by the Blake threshold (see equation (69) of Chapter 3). Figure 19a shows the Blake threshold as a function of dissolved gas pressure for the two extreme cases discussed above. It can be seen that the threshold is relatively insensitive to variations in gas pressure and that the difference between the two cases is negligible. However, there is a hint that the proper trend is present.

There is one large caveat in this discussion; it is the choice of the value of b . For the results shown in figure 19a, the value of b was that computed in reference 26. That is, it was based on measurements made on gelatin samples having a surface tension of about 51 dyn/cm. However, the data presented in figure 19a were taken in water having a surface tension of about 70 dyn/cm. The dependence of b on surface tension is given in equation (39b) of reference 26,

$$b = 2.80 \times 10^4 \gamma \text{ dyn/cm.} \quad (83)$$

For $\gamma = 70$ dyn/cm, $b = 1.96$ bar. Figure 19b is a graph of threshold versus gas pressure for $b = 1.96$ bar. Comparing figures 19a and 19b, it is seen that this modification makes the prediction worse instead of better.

Upon examination of equation (82) it is seen that if b is increased, R_f increases as well; a larger R_f results in a lower threshold. Therefore, increasing b from 1.43 to 1.96 bar results in the threshold decreasing. In order for the V-P model to predict the acoustic cavitation threshold as a function of dissolved gas pressure, b

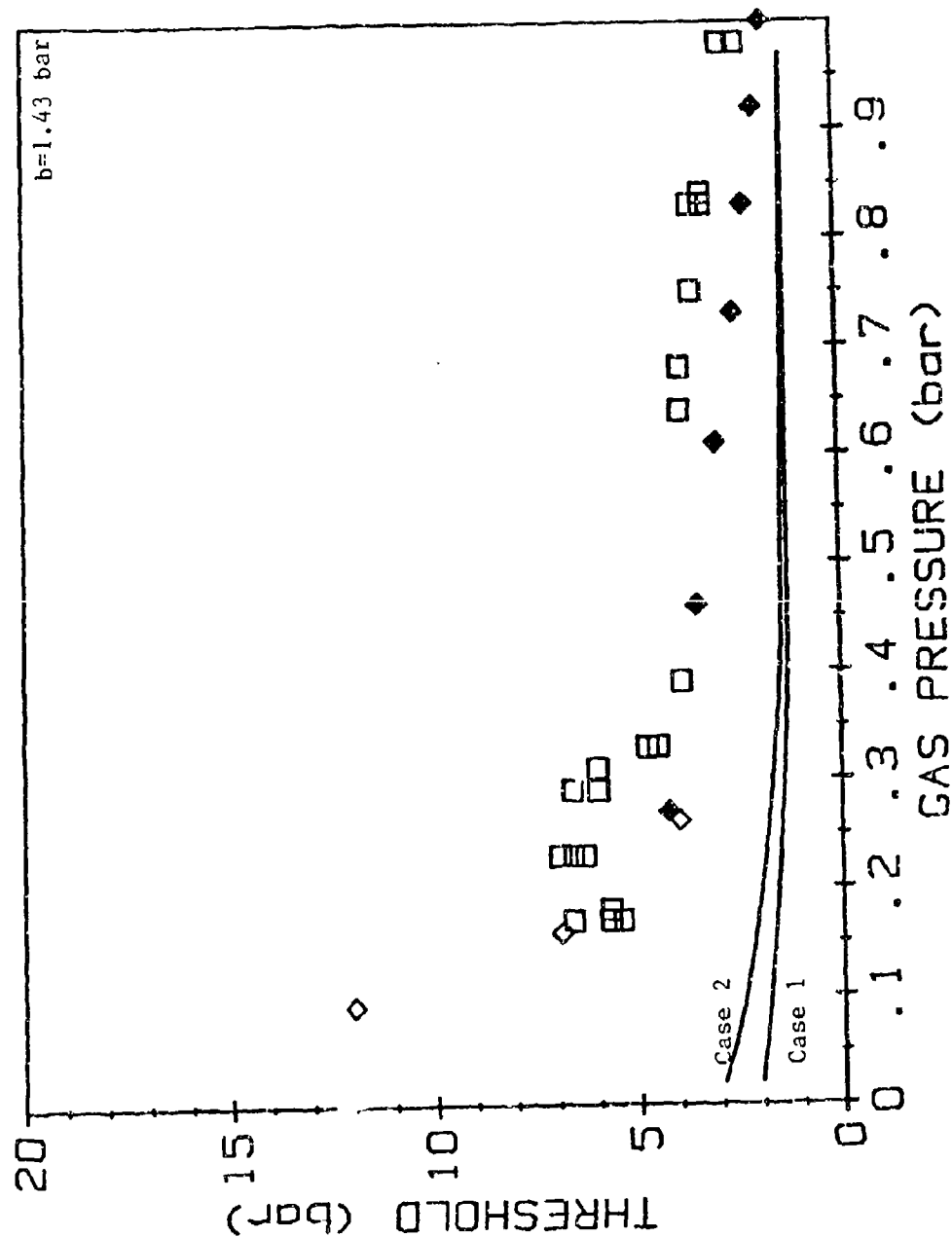


Figure 19a. Graph of the cavitation threshold versus dissolved gas pressure for a V-P nucleus with $b=1.43$ bar. (Refer to figure 11a.)

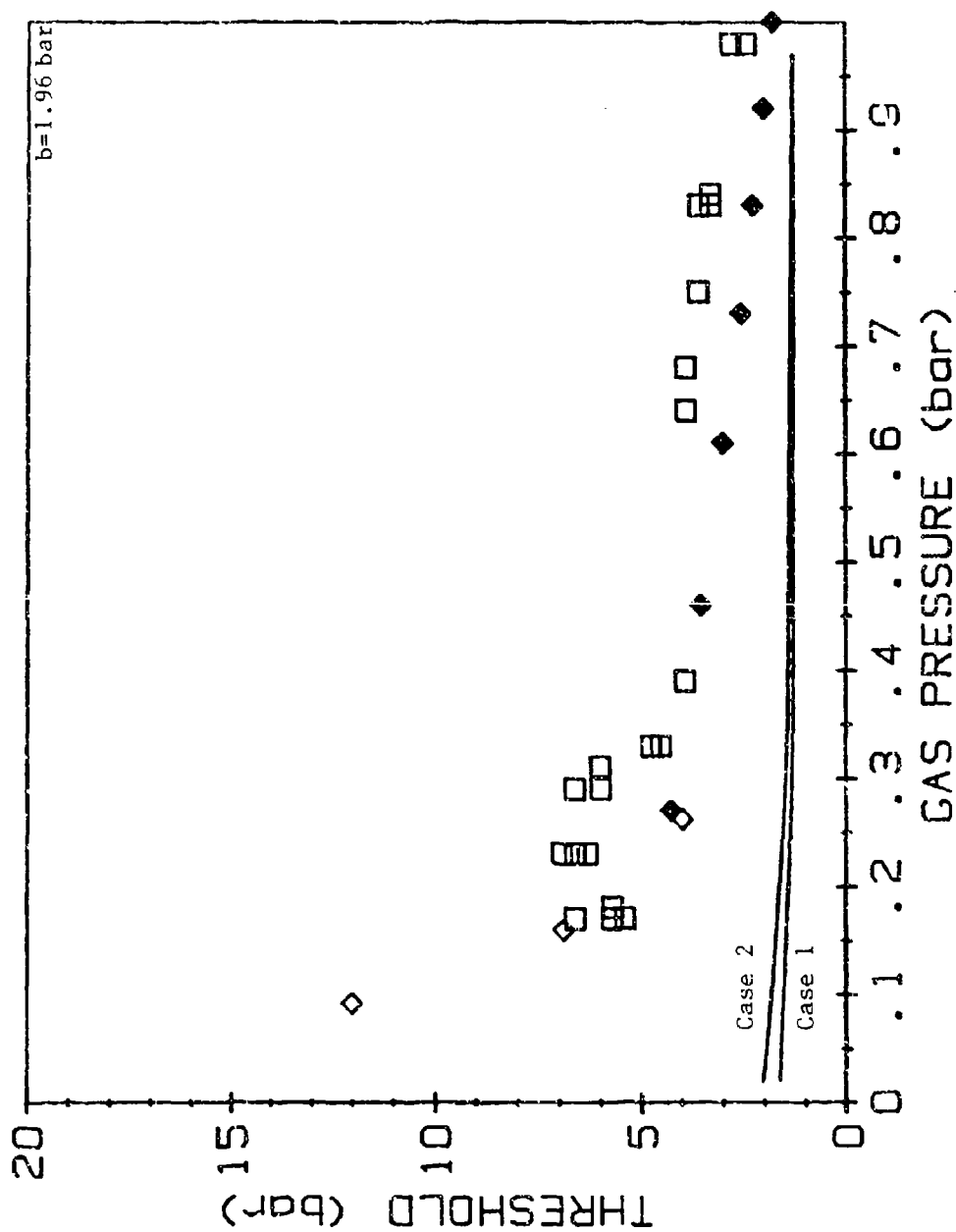


Figure 19b. Graph of the cavitation threshold versus dissolved gas pressure for a V-P nucleus with $b=1.96$ bar. (Refer to figure 11a.)

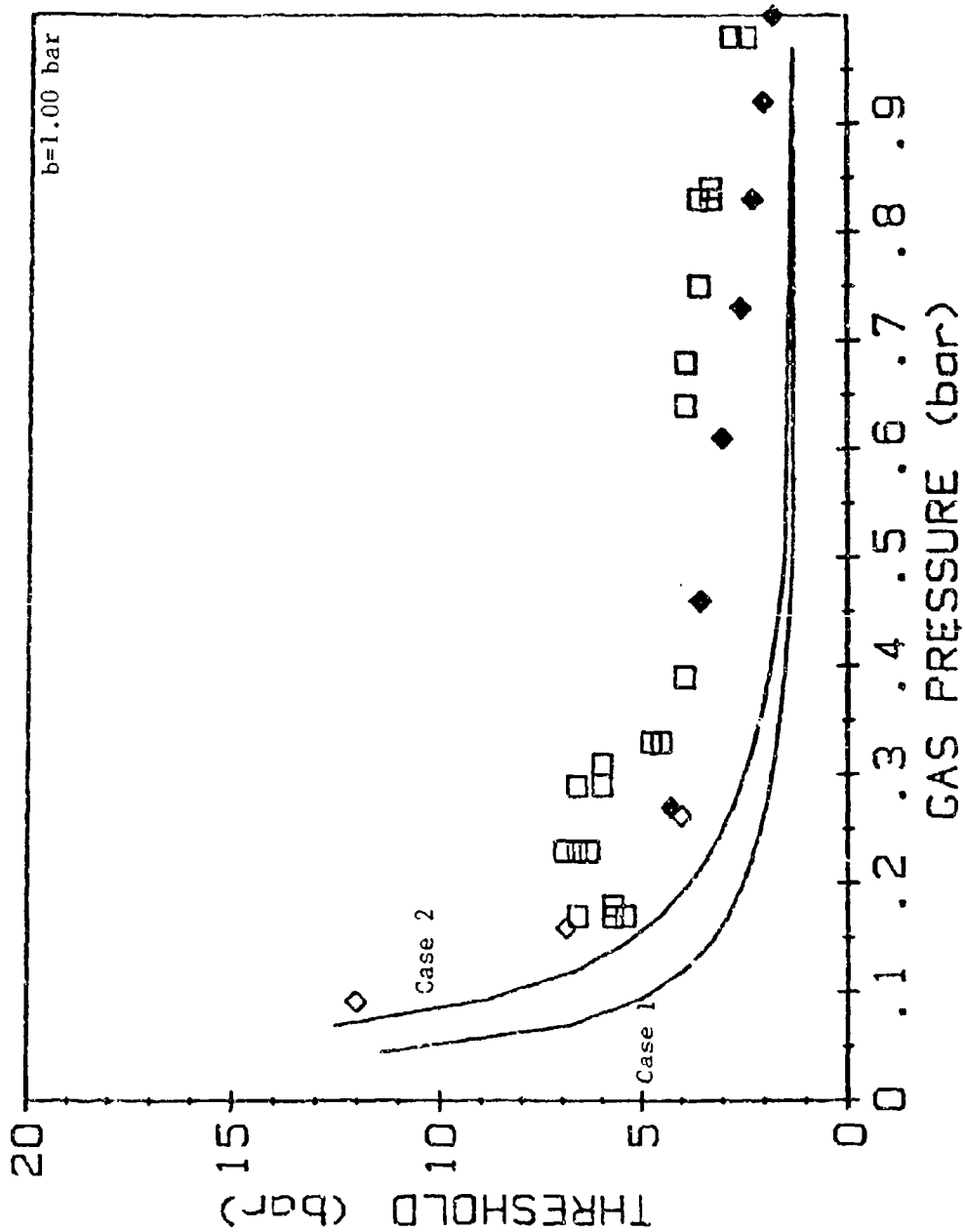


Figure i9c. Graph of the cavitation threshold versus dissolved gas pressure for a V-P nucleus with $b=1.00$ bar. (Refer to figure 11a.)

must be less than 1.43 bar, not greater. The lower limit on b is 1 bar. If b were less than 1 bar, equation (80) would predict negative radii for some values of P_{ss} . Figure 19c represents the threshold dependence on gas pressure for $b = 1$ bar. The agreement is much better, however, the means by which the agreement was improved is not consistent with the V-P model.

From this discussion, either of two conclusions may be drawn. The first, and most severe, conclusion that may be drawn is that the V-P model is not adequate. A second, and perhaps more realistic, conclusion is that the experimental confirmation of the V-P model has been inadequate. The only measurements to which the V-P model has been applied have involved diffusion cavitation occurring in gelatin. The numerical factor (2.80) present in equation (83) is based upon a set of measurements made on a single sample of gelatin. It is possible that this factor varies with the experimental conditions and is not a "universal" constant. This possibility could account for the discrepancy present in figure 19.

Aside from the limited experimental confirmation of the V-P model, its complexity leaves it cumbersome to apply. For instance, consider the effect that a variation in surface tension might have on the nucleus. Since the model depends upon the chemical potential of the surfactants, it is not at all clear that if different types of surfactants are used to alter the surface tension, the threshold would not be affected in different ways. Even the model's chief advocate is not certain how the addition of surfactants affect the nucleus. In

reference 28, the statement is made "Another standard method [of increasing the threshold for bubble formation] is to add detergents or other substances which presumably operate by changing [b]". The effect of temperature variation on a V-P nucleus is an equally complex matter. In fact, not even a qualitative description of the temperature dependence is offered in reference 28, only the statement "A dependence on temperature is also predicted".

The discussion in this section may be summarized as follows. Although the varying-permeability model is elegant and explains diffusion cavitation in gelatin, its application to acoustic cavitation is cumbersome at best. Since these nuclei have been observed using microscopic techniques⁴², their existence is difficult to deny. However, the model needs to be extended to explain acoustic cavitation processes.

Chapter 5

Summary, Conclusions and Topics for Further Study

5-1 Summary of the Dissertation

As stated at the outset, the purpose of the research discussed in this dissertation was to advance the state of knowledge of the cavitation nucleus. The advances made toward this goal may be summarized as follows:

1) The crevice model was revised in terms of a more physically realistic nucleation criterion. This new criterion was shown to be both a necessary and sufficient condition for cavitation nucleation.

2) The predictions of the acoustic cavitation threshold based on this revised model (called the critical radius approach to the crevice model) were found to be in good agreement with experimental results.

3) The revised crevice model was applied to diffusion cavitation (the first such application) and it was shown to predict results previously explained only in terms of the varying-permeability model.

4) It was shown that in liquids with low surface tensions, nanometer-sized nuclei are capable of producing cavitation.

5) The first extensive measurements of the acoustic cavitation threshold as a function of dissolved ion concentration were made for concentrations less than 1 mmol/l.

6) These measurements indicate that the cavitation observed could

not have been produced entirely by a purely ionic skin as proposed by Akulichev.

7) The varying permeability model was applied to acoustic cavitation (another unique application). It was found that although the model could explain the increase in threshold with decreasing gas content, certain inconsistencies arose which indicated that the model should be developed further to facilitate its application to acoustic cavitation.

5-2 Conclusions

In this dissertation, three different cavitation nucleation mechanisms were considered. Based upon the findings of this work, we conclude that the critical radius approach to the crevice model is the most satisfactory of these models. Using this model, the threshold for acoustic cavitation can be accurately predicted as a function of various parameters. In addition, some aspects of diffusion cavitation are seen to be natural consequences of the crevice model. We should stress, however, that this conclusion is based on measurements made in water. It should not be assumed that these findings can be extrapolated to other fluids without some detailed analysis.

Cavitation is a vastly complicated phenomenon and to conclude that a single type of nucleus accounts for all cavitation processes is almost certainly in error. We do feel that the critical radius approach to the crevice model is the most satisfactory theory at present. Indeed, the crevice model may account for the largest part of the entity referred to

as "the" cavitation nucleus. However, the fact remains that there is no theoretical reason, nor any conclusive experimental results, that discounts the existence of the other two proposed nuclei. (In fact, organic skin nuclei have been observed by Yount.⁴²) These models should be developed further. As was stated earlier, we have advanced the state of knowledge concerning the nucleation of cavitation in water. The next step to be taken should be toward uniting these models into "a" cavitation nucleation model.

5-3 Topics for Further Study

As the research presented in this dissertation progressed, it became clear that some aspects of this research deserved further study. In the previous section some of these topics were mentioned. In this section we will mention some others.

1) More measurements need to be taken in different fluids. In particular, biological fluids are presently in need of extensive investigation because of the possible hazards associated with the use of ultrasound in medicine.

2) The results of the measurements of threshold as a function of ion concentration are not easily explained in terms of our present knowledge. The explanation of these results has the potential of advancing our knowledge of nucleation processes significantly.

3) The modification of the experimental apparatus used to make the ion measurements (to be discussed in the appendix) should make it possible to verify the existence of the surfactant or ionic skin nuclei.

With these modifications it should be possible to remove the vast majority of the existing cavitation nuclei. Bubbles could then be introduced into the liquid (perhaps through electrolysis) in the presence of surfactants or ions. Since some of these bubbles should stabilize, the result should be a (significantly) lower cavitation threshold.

4) A further modification of the apparatus would make it possible to perform threshold measurements with ambient liquid pressures close to the vapor pressure. To the author's knowledge, this type of measurement has never been performed. The results of such measurements are easily predictable in terms of the revised crevice model, and therefore this measurement should be a good test of the model.

5) Another topic for further study is the measurement of the cavitation threshold as a function of dissolved gas pressure for ambient pressures greater than atmospheric. Such an experiment may prove useful in understanding more fully the reason for the discrepancy between the predicted threshold based on equation (31) and the measured threshold for gas pressures near saturation (refer to figure 11a).

6) The last topic we mention is of a different sort. Assume that molecular skin nuclei are confirmed to exist. Certain types of molecules should be better stabilizers than others. Nuclei composed of good stabilizers may be relatively rugged and able to exist in harsh liquid conditions. These nuclei would be long lived "seeds" which could be activated at a certain time for a certain purpose. The development of such technology may prove to be quite useful.

REFERENCES

- 1) C. Tomlinson, "On the so-called "inactive" condition of solids", Phil. Mag. 34, 136-143, 220-230 (1867).
- 2) M. Gernez, "On the disengagement of gases from their saturated solutions", Phil. Mag. 33, 379-481 (1867).
- 3) D. Bernoulli, Hydrodynamica, sive de viribus et motibus fluidorum comentarii, (Strasbourg, 1738).
- 4) D. Freed and W.F. Walker, "Notes on the history of cavitation", in Cavitation and Multiphase Flow Forum -- 1984, ed. J. W. Hoyt, 1-7 (1984).
- 5) Lord Rayleigh, "On the pressure developed in a liquid during the collapse of a spherical cavity", Phil. Mag. 34, 94-98 (1917).
- 6) F. G. Blake, "The tensile strength of liquids: A review of the literature", Tech. Memo No. 9 Harvard Acoustics Research Laboratory (1949).
- 7) E. Klein, "Some background history of ultrasonics", J. Acoust. Soc. Am., 20, 601-604, 1948.
- 8) M. Kornfeld and L. Suvorov, "On the destructive action of cavitation", J. Appl. Phys. 15, 495-506 (1944).
- 9) L. J. Briggs, "Limiting negative pressure of water", J. Appl. Phys. 21, 721-722 (1950).
- 10) R. B. Dean, "The formation of bubbles", J. Appl. Phys. 15, 446-451 (1944).
- 11) E. N. Harvey, et. al., "Bubble formation in animals", J. Cell. Comp. Physiol., 24, 1-22 (1944).
- 12) H. B. Briggs, J. B. Johnson, and W. P. Mason, "Properties of liquids at high sound pressure", J. Acous. Soc. Am. 19, 664-677 (1947).
- 13) F. Seitz, "On the theory of the bubble chamber", Phys. Fluids 1, 2-13 (1958).

- 14) D. Lieberman, "Radiation-induced cavitation", Phys. Fluids 2, 466-468 (1959).
- 15) F. Fox and K. Kerzfeld, "Gas bubbles with organic skin as cavitation nuclei", J. Acoust. Soc. Am. 26, 984-989 (1954).
- 16) M. Strasberg, "Onset of ultrasonic cavitation in tap water", J. Acoust. Soc. Am. 31, 163-176 (1959).
- 17) W. Connolly and F. Fox, "Ultrasonic cavitation thresholds in water", J. Acoust. Soc. Am. 26, 843-848 (1954).
- 18) W. Galloway, "An experimental study of acoustically induced cavitation in liquids", J. Acoust. Soc. Am. 26, 849-857 (1954).
- 19) D. Sette and F. Wanderlingh, "Nucleation by cosmic rays in ultrasonic cavitation", Phys. Rev. 125, 409-417 (1962).
- 20) V. Akulichev, "Hydration of ions and the cavitation resistance of water", Sov. Phys. Acoust. 12, 144-149 (1966).
- 21) M. Greenspan and C. Tschiegg, "Radiation-induced acoustic cavitation; apparatus and some results", J. Res. Nat. Bur. Stds. 71C, 299-312 (1967).
- 22) R. Apfel, "The role of impurities in cavitation-threshold determination", J. Acoust. Soc. Am. 48, 1179-1186 (1970).
- 23) R. Apfel, "Vapor nucleation at a liquid-liquid interface", J. Chem Phys. 54, 62-63 (1971).
- 24) L. Crum, "Tensile strength of water", Nature 278, 148-149 (1979).
- 25) R. Winterton, "Nucleation of boiling and cavitation", J. Phys. D: Appl. Phys. 10, 2041-2056 (1977).
- 26) D. Yount, "Skins of varying permeability: A stabilization mechanism for gas cavitation nuclei", J. Acoust. Soc. Am., 65, 1429-1439 (1979).
- 27) M. Sirotyuk, "Stabilization of gas bubbles in water", Sov. Phys. Acoust. 16, 237-240, (1970).
- 28) D. Yount, "On the evolution, generation, and regeneration of gas cavitation nuclei", J. Acoust. Soc. Am. 71, 1473-1481 (1982).

- 29) J. W. Gibbs, The Scientific Papers of J. W. Gibbs Vol. I, 237 (Dover, New York, 1961).
- 30) P. Epstein and M. Plesset, "On the stability of gas bubbles in liquid-gas solutions", J. Chem. Phys. 18, 1505-1509 (1950).
- 31) T. Alty, "The cataphoresis of gas bubbles in water", Proc. Roy. Soc. A. 106, 315-340 (1924).
- 32) T. Alty, "The origin of electrical charge on small particles in water", Proc. Roy. Soc. A. 112, 235-251 (1926).
- 33) K. F. Herzfeld, Comment, Proc. First Sympos. Naval Hydrodynamics, ed. F.S. Sherman, 319-320 (1957).
- 34) L. A. Crum, "Nucleation and stabilization of microbubbles in liquids", Appl. Sci. Res. 38, 101-115 (1982).
- 35) R. E. Apfel, "Acoustic cavitation prediction", J. Acoust. Soc. Am. 69, 1624-1633 (1981).
- 36) H. G. Glynn, "Physics of acoustic cavitation in liquids", Physical Acoustics, ed. W. P. Mason, 1B, 57-172 (Academic, New York, 1964).
- 37) F. G. Blake, "The onset of cavitation in liquids. I", Tech. Memo No. 12 Harvard Acoustics Research Laboratory (1949).
- 38) A. Prosperetti, "Bubble phenomena in sound fields", To be published in Ultrasonics.
- 39) R. E. Apfel, "Acoustic Cavitation", in Ultrasonics, Methods of Experimental Physics 19, ed. P. Edmonds, (Academic, New York, 1981).
- 40) D. Bergeman and F. Van Voorst Vader, "Effect of surfactants on contact angles of nonpolar solids", J. Colloid and Interface Sci. 42, 467-472 (1973).
- 41) E. W. Washburn, ed., International Critical Tables Vol. III, 257 (McGraw-Hill, New York, 1928).
- 42) R. C. Weast, ed., Handbook of Chemistry and Physics 56th Edition, page F-43 (CRC Press, Cleveland, 1975)
- 43) D. Eisenberg and W. Kauzmann, The Structure and Properties of Water. 61-62 (Oxford, Oxford, 1969).

- 44) D. E. Yount, E. W. Gillary, and D. C. Hoffman, "Microscopic study of bubble formation nuclei", in Underwater Physiology VIII: Proceedings of the Eighth Symposium on Underwater Physiology (to be published).
- 45) R. A. Roy, A. A. Atchley, L. A. Crum, J. B. Fowlkes, and J. R. Reidy, "A precise technique for the measurement of acoustic cavitation thresholds and some preliminary results", accepted for publication in J. Acoust. Soc. Am.
- 46) C. Seghal, R. G. Sutherland, and R. E. Verrall, "Optical spectra of sonoluminescence from transient and stable cavitation in water saturated with various gases", J. Chem. Phys. 84, 388-395 (1980).

Appendix

Experimental Determination of the Variation of the Acoustic Cavitation Threshold as a Function of Dissolved Ion Concentration

A-1 Introduction

In this appendix the experimental aspects of the measurement of the acoustic cavitation threshold of water as a function of the dissolved ion concentration of the water will be discussed. This discussion will be presented in four parts: the purpose of the experiment, the experimental apparatus, the experimental procedure, and the results of the experiment. The conclusions drawn from the experiment were presented in section 4-2.

A-2 Purpose of the Experiment

One purpose of the experiment was to attempt to verify the results of Akulichev's experiment²⁰ since his results are the only strong evidence for the existence of an ionically stabilized nucleus. In addition, our apparatus made it possible to extend the range of his measurements to lower ion concentrations. This range of concentrations (below 1 mmol/l) had not previously been investigated, and yet, the behavior of the threshold at low concentrations is a strong test of the ionic skin hypothesis.

A-3 Experimental Apparatus

The apparatus used in making these measurements was developed over

a period of several years by our research group. It is designed to be versatile so that it can be used to make threshold measurements for a wide range of fluid conditions. Since the system is described in some detail elsewhere,⁴⁵ only a brief description will be given here.

The apparatus is composed of two major groups: the sample preparation system and the data acquisition system. The sample preparation system is shown schematically in figure 20a. A typical sample preparation takes place as follows. Prefiltered distilled water is introduced into the reservoir. The water is pumped from the reservoir and may be passed through either the organic removal column or the ionic removal column, or both. The organic removal column is a Barnstead Organic Removal Cartridge (part number D8904) and lowers the concentration of long chain organic molecules to less than one part per million. The ionic removal column is a Barnstead Ultrapure Cartridge (part number D8902) and produces water with a conductivity of less than one micromho and a pH of between 6.8 and 7.2. The specific conductance of the water is measured with a Cole Parmer conductivity meter (model number R-1491-20). The resolution of the meter is 0.1 micromho and the accuracy is 0.2 micromho. The water then passes through an in-line teflon filter to remove solid contaminants. The filter size can be chosen to suit the requirements of the experiment. After the filter, the water circulates through a spherical quartz flask in which the acoustic field is produced, and then back to the reservoir. Except when passing through the organic and ionic removal columns, the water is in contact with either teflon, glass or quartz. In this way, the

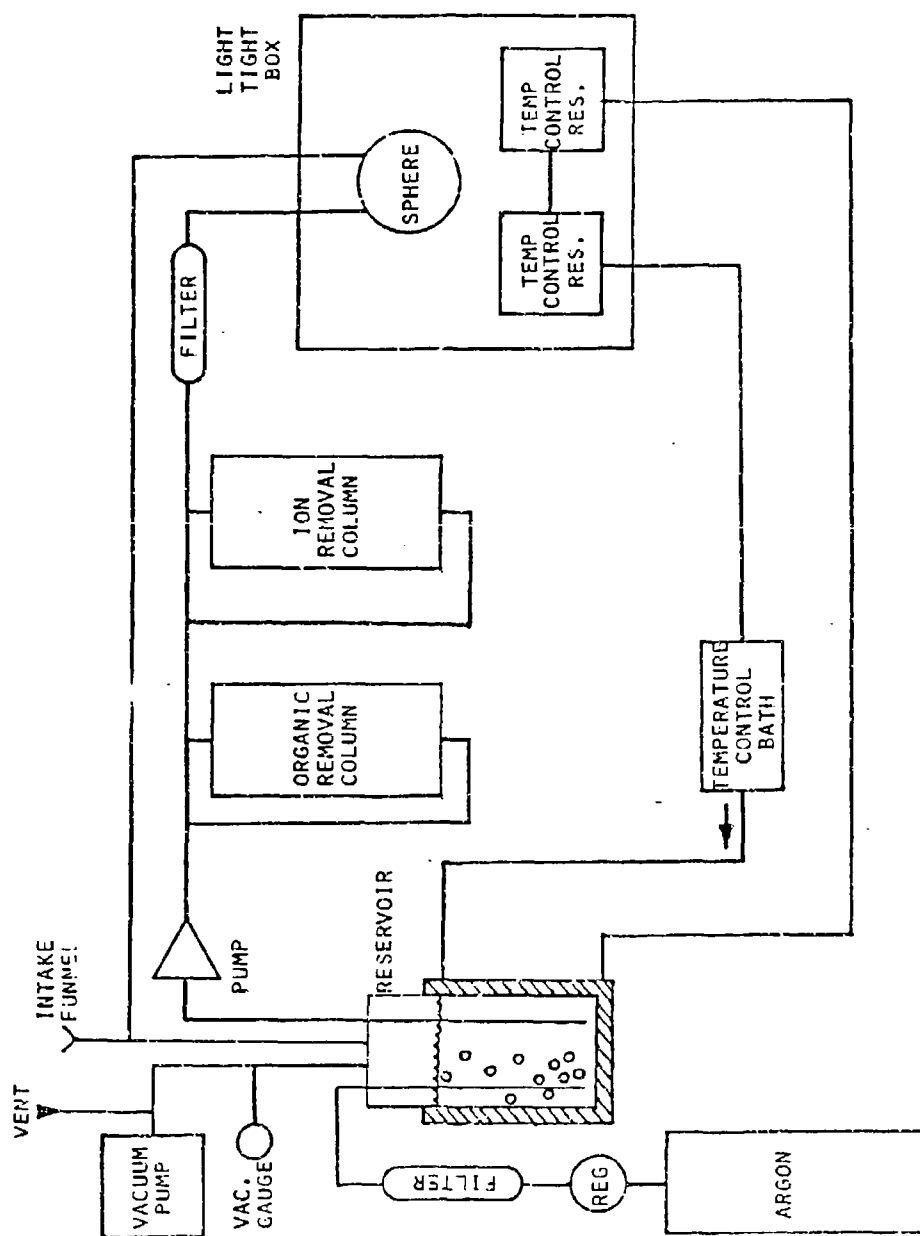


Figure 20a. Schematic diagram of the sample preparation system.

possibility of contamination of the sample is reduced. The capacity of the system is about two liters.

The gas content of the system is controlled in the following manner. The glass reservoir is evacuated to a specified pressure. A gas (usually argon) is bubbled through the liquid in the reservoir as the liquid is circulated. The agitation, so produced, aids in both removing the dissolved air and saturating the liquid with the gas at the specified pressure. Before entering the reservoir, the gas is passed through a filter to prevent the introduction of solid contaminants.

The quartz flask is enclosed in a light tight box which contains two large liquid heat sinks. The heat sinks are maintained at a constant temperature to aid in controlling the temperature of the sample during the data acquisition phase. Also, the reservoir is surrounded by a cooling jacket which is used to adjust the temperature of the sample. The temperatures of the sample and the heat sinks are monitored with thermistors.

The data acquisition system is depicted schematically in figure 20b. The acoustic field is generated by two cylindrical PZT transducers cemented onto the sides of the quartz flask. They are driven by the amplified signal of the oscillator in a resonant mode near 60 kHz. The resonance frequency is determined by monitoring the output of a pill transducer (which is also cemented on the side of the flask) on an oscilloscope. The amplitude of the driving signal is modulated by a ramp voltage, the value of which is displayed on a strip chart recorder. A current probe monitors the transducer current and the

output is displayed on an oscilloscope.

The driving amplitude is increased until a cavitation event is detected. Two methods of detection were employed. The first is audio detection. Vaporous cavitation events are almost always associated with a loud audible "click" that is produced by a collapsing cavity. Thus, cavitation can be detected by the operator who monitors the system through a headphone set. A second type of detection scheme relies upon the production of sonoluminescence. Sonoluminescence is an emission of light associated with cavitation events in liquids. Its origin is not clearly understood, but recent experimental evidence indicates that it is associated with the deexcitation and radiative recombination of chemical species formed during the collapse of a bubble.⁴⁶ This emission is detected with a photomultiplier tube mounted underneath the flask. The photomultiplier signal is processed by a noise reduction system to reduce the occurrence of false triggers. When the detector senses that sonoluminescence has been produced, it resets the ramp voltage and the system is quiescent for a predetermined time before the ramping phase is reinitiated. During the quiescent period the sound field in the flask is generally attenuated by 60 dB below the level associated with a ramp voltage of zero. The ramping/quiescent cycle is repeated until the desired number of data points are taken.

A-4 Experimental Procedure

The discussion to follow is a step-by-step description of the procedure used to acquire a typical set of data. An effort was made to

follow the same procedure as closely as possible for each set of data. This discussion will be divided into two sections: one for the sample preparation and the other for data acquisition.

A-4.1 Procedure for Sample Preparation

The water used for these measurements was acquired from a bulk source of distilled water and stored in a 25 liter plastic bottle. In an effort to eliminate the effect of any variation of the properties of the distilled water obtained from this source at different times, the measurements for a given ionic compound were all made with water obtained at the same time. The water used for measurement of the cavitation threshold at a given concentration was all drawn from the storage bottle at the same time, and after being prefiltered through a teflon filter, was stored in individual 1 liter teflon PFA bottles. The pore size of the filter was chosen to be the same as that of the in-line filter.

The ionic concentration of a sample was adjusted by adding a specified volume of a 0.40 molar stock aqueous solution of the compound. The stock solution was made by adding a known amount of the compound (laboratory grade) to one liter of filtered distilled water having a specific conductance of less than one micromho/cm. The concentration of the stock solution was calculated from the measured value of the specific conductance. The conversion was made according to the relationship

$$C_i = \frac{1000}{\Lambda} K \quad (A1)$$

where C_1 is the ionic concentration in moles/l, Λ is the molar conductance in $\text{mho cm}^2 \text{mol}^{-1}$, and K is the specific conductance in mho/cm . Small amounts of the compound were added, if necessary, to bring the concentration of the stock solution to 0.40 molar. The stock solution was kept in a sealed glass flask and stored in a closed cabinet when not needed. A teflon coated magnetic stirring bar was kept in the solution so the solution could be mixed immediately before being introduced into the sample. The preparation of the sample will now be discussed.

Assume that the sample preparation system contains a previously used sample. The old sample is pumped out of the system. After as much of the liquid as possible has been pumped out of the system, the system is pressurized with argon. This pressurization forces out any remaining liquid except for the portion contained within the quartz flask (about 0.75 liters). After the system has been flushed, about 1.75 liters of prefiltered distilled water is introduced into the system. This water is circulated for about 15 minutes, after which time the system is flushed once again. Then, one liter of prefiltered distilled water is put into the system. This water along with that remaining in the flask is the water used for the next data run.

Circulation is started and the water is routed through the organic and ionic removal columns. The deionization process is continued for thirty minutes at which time the water is routed so as to bypass the columns. (However, whenever the water is circulating, it passes through

the in-line filter.) Three small samples of the deionized water (about 5 ml each) are removed from the system. The conductance of these samples is measured and must be less than 1.5 micromho/cm in order for the preparation phase to progress farther. In every instance the samples always met this requirement after thirty minutes of deionization. In most cases the average specific conductance was less than 1.0 micromho/cm. At this point the stock solution is added. In order to keep the system volume approximately constant for all measurements, an additional amount of water equal to the volume of solution to be added was removed from the system. The solution is then introduced. Throughout this process the water has been continuously circulated.

After the solution has been introduced, the degassing phase begins. The absolute pressure during degassing was maintained at 0.30 bar, and therefore, the dissolved gas pressure of argon in the water was 0.30 bar. As described in reference 45, the system has been calibrated against actual measurements of gas content made with a Van Slyke apparatus. The degassing/argon saturation phase is accompanied by a temperature control phase. At the end of the degassing phase, the temperature of the sample is about 23.15°C. Circulation is stopped and the system is returned to atmospheric pressure. Three more samples are drawn for the purpose of determining the dissolved ion concentration and surface tension of the sample. The system is allowed to rest for one hour. This rest period accomplishes two things. It allows any large bubbles produced by the circulation and agitation to dissolve, or

stabilize, or rise to the surface of the liquid. It also allows the temperature of the system to stabilize. At the end of the rest period the temperature of the sample in the quartz flask is $23.00 \pm 0.10^{\circ}\text{C}$. During the data acquisition phase, the temperature of the sample is maintained at $23.00 \pm 0.20^{\circ}\text{C}$. If the temperature of the sample falls outside this range, data acquisition is stopped. The data acquisition phase will be described next.

A-4.2 Procedure for Data Acquisition

Near the end of the one hour rest phase, the acoustic signal generation system is calibrated (described in detail in reference 43). At the end of the rest period the data acquisition phase begins. The ramp is initiated. When the operator audibly detects that a transient cavitation event has occurred, the drive speed of the stripchart recorder is increased. In this way the "audible" cavitation threshold is noted. If the audible event is not accompanied by sonoluminescence, the ramp continues until sonoluminescence is detected. When it is, the ramp voltage is reset, the chart speed is reduced, and the system is quiescent for a five minute period. This quiescent phase is necessary to allow the temperature of the sample to stabilize and any remnants of the cavitation event to dissolve. This procedure is repeated until either 15 data points are taken or the temperature of the system fails to return to within 0.20°C of 23.00°C after the quiescent period.

The stripchart voltages are converted to pressure amplitudes according to the following relationship

$$P_A = 0.91 + 2.87 V_s \text{ bar} \quad (A2)$$

where V_s is the stripchart voltage corresponding to the cavitation event. (The origin of this relationship is described in reference 43.) Using this relationship two cavitation thresholds are obtained: an audible threshold and a sonoluminescence threshold. The results of these measurements are presented in the following section.

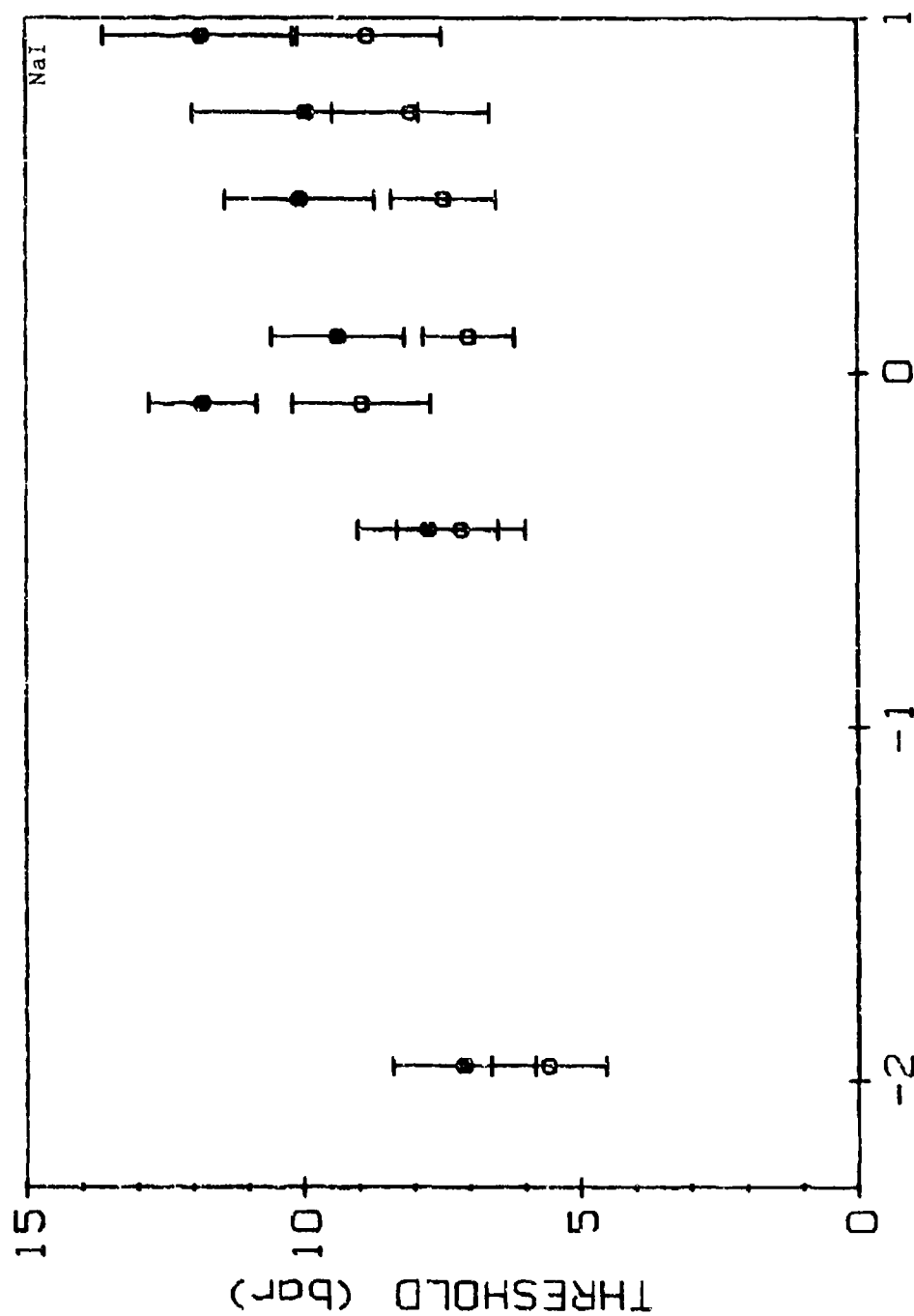
A-5 Results of the Experiment

Six different compounds were used for the measurements: NaF, NaCl, NaI, KCl, KI, and KOH. The audible threshold as a function of concentration for KI and NaI were presented in figures 18a and 18b. The data were normalized to the threshold at the lowest concentration to facilitate comparison among various data sets. The value of the threshold at the lowest concentration is typically about 4.5 ± 1 bar; such variations are, unfortunately, typical in cavitation threshold measurements. The normalization is justifiable since it is the variation in the threshold that is sought and not the absolute value. The error bars in figures 18a and 18b represent plus-or-minus one standard deviation.

The lowest value of the concentration was determined in the following manner. The sample was prepared in the usual way except that no ionic solution was introduced. That is, the threshold of the deionized water was measured. The deionized water had a non-zero specific conductance, typically about 1 micromho/cm. In order to assign a concentration to this deionized sample, it was assumed that the non-

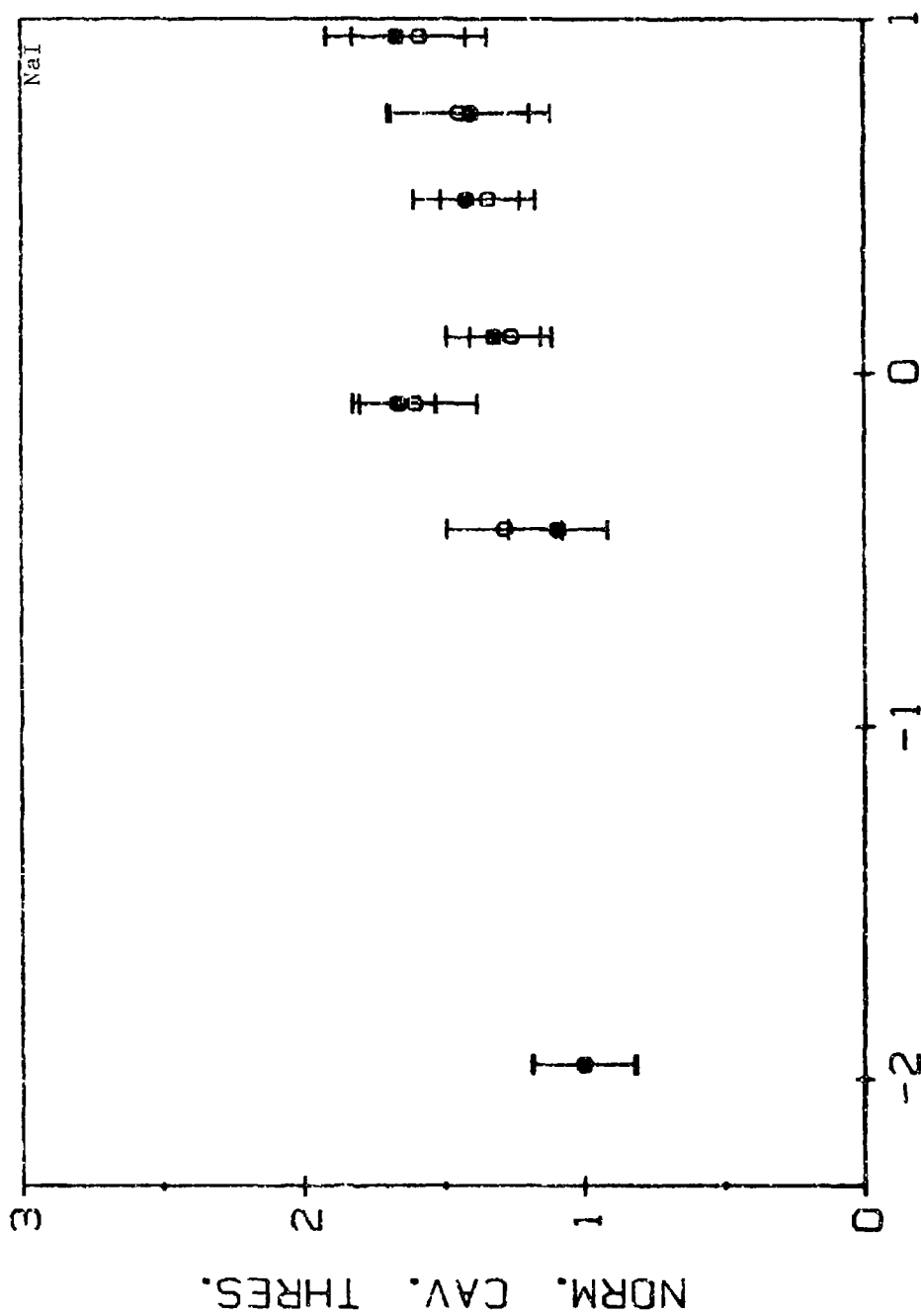
zero conductance was due to the presence of whatever compound was under investigation at that time. This is probably not a valid assumption, but a better method was not apparent. Therefore, the values of the lowest concentrations are to be considered as upper limits. The actual concentration of the specific compound under investigation is probably much less than the assigned value.

As stated above our apparatus made it possible to measure both an audible and sonoluminescence threshold. In figure 21a, both the audible and sonoluminescence threshold are plotted as a function of ion concentration. In every instance, the audible threshold is lower than the sonoluminescence threshold. This trend was present in all six compounds tested. However, the variation with ion concentration was the same for each threshold as shown in figure 21b. That is, when the thresholds are normalized the difference between them is negligible. This trend was also apparent in all six compounds. From this discussion it may be concluded that for measurements of the variation of the transient cavitation threshold, either of the thresholds are applicable. Emphasis has been placed on the words "variation" and "transient". The absolute threshold does not appear to be the same for both cases. Measurements made with single photon counters⁴⁶ indicate that a clear-cut threshold for sonoluminescence emission from stable (gaseous) cavities may not exist. That is, pulsating gas-filled bubbles may emit light even when the pressure amplitude of the applied acoustic field is extremely small. However, when transient cavitation occurs, usually, no



LOG ION CONC. (mmol/l)

Figure 21a. Graph of the cavitation threshold versus the log of the dissolved ion concentration for NaI. The sonoluminescence threshold is denoted by the solid circles and the audible threshold is denoted by the open circles.



LOG ION CONC. (mmol/l)

Figure 2lb. Graph of the normalized cavitation threshold versus the log of the dissolved ion concentration for NaI. The sonoluminescence threshold is denoted by the solid circles and the audible threshold is denoted by the open circles.

one does exist for transient cavitation. The conclusions drawn from this experiment are discussed in chapter 4.

BIOGRAPHICAL SKETCH OF THE AUTHOR

Anthony Armstrong Atchley was born in Lebanon, Tennessee on June 23, 1957, the son of Mr. and Mrs. Kenneth L. Atchley. He attended Castle Heights Military Academy, graduating in May, 1975. He received a B.A. in physics from the University of the South in May, 1979. He continued his studies at the New Mexico Institute of Mining and Technology, receiving an M.S. in physics in May of 1982.

Anthony is a member of Sigma Pi Sigma, Phi Kappa Phi, The American Physical Society, and The Acoustical Society of America. He was selected as the Acoustical Society of America's F. V. Hunt Fellow for 1985. He enjoys racquetball, canoeing, photography and carpentry. He also very much enjoys his teaching duties.

He plans to pursue a career in research and teaching and has accepted a position at the Naval Postgraduate School in Monterey, California. Anthony will take a leave of absence from the NPS to continue cavitation research at Yale University as the Hunt Fellow.

His permanent address is box 851, Smyrna, Tennessee 37167.

January 1985

REPORTS DISTRIBUTION LIST FOR ONR PHYSICS DIVISION OFFICE
UNCLASSIFIED CONTRACTS

Director 3 copies
Defense Advanced Research Projects Agency
Attn: Technical Library
1400 Wilson Blvd.
Arlington, VA 22209

Office of Naval Research 3 copies
Physics Division Office (Code 412)
800 North Quincy Street
Arlington, VA 22217

Office of Naval Research 1 copy
Director, Technology (Code 200)
800 North Quincy Street
Arlington, VA 22217

Naval Research Laboratory 1 copy
Department of the Navy
Attn: Technical Library
Washington, DC 20375

Office of the Director of Defense 1 copy
Research and Engineering
Information Office Library Branch
The Pentagon
Washington, DC 20301

U. S. Army Research Office 1 copy
Box 1211
Research Triangle Park
North Carolina 27709

Defense Technical Information Center 12 copies
Cameron Station
Alexandria, VA 22314

Commanding Officer 1 copy
Office of Naval Research Western Detachment Office
1030 East Green Street
Pasadena, CA 91101

Commanding Officer 1 copy
Office of Naval Research
Eastern/Central Detachment Office
495 Summer Street
Boston, MA 02210

Naval Postgraduate School
Technical Library (Code 0212)
Monterey, CA 93940

1 copy

Commanding Officer
Naval Ocean Research & Development Activity
Technical Library
NSTL Station, Mississippi 39529

1 copy

Naval Explosive Ordnance Disposal Facility
Technical Library
Indian Head, Maryland 20640

1 copy

Naval Ship Research and Development Center
Central Library (Code L42 and L43)
Bethesda, Maryland 20084

1 copy